Silesian University of Technology
Faculty of Mechanical Engineering
Department of Fundamentals of Machinery Design

Doctoral dissertation

Optimisation of Unmanned Aerial Vehicle of Unlimited Flight Endurance

MSc, Eng. Kamil Zenowicz

Supervisor:
Prof. Wojciech Skarka, PhD, DSc, Eng.

Gliwice, 2023

Contents

1. Introduction

Unmanned Aerial Vehicles (UAVs) are an increasing part of air traffic. Today, UAV applications are very diverse. They are used, for example, for traffic observation, air condition monitoring, railway traction condition monitoring, filming, racing, and various types of military purposes [1] [2].

Wide application directly affects the very rapid development of the branch of aviation related to unmanned aerial vehicles, regardless of whether they are multirotor structures, standard fixed-wing structures or other types of structures. The possibilities for the development of unmanned aerial vehicles are practically unlimited. One of the determinants that approximates the choice of the appropriate structure is the task for which the designed drone will be used.

Unmanned aerial vehicles are structures that do not need to be piloted by a person on board. Due to this, they are not subject to the limitations of the human body and flight comfort. This can directly translate into greater accelerations, higher overload, a smaller turning radius, higher flight speeds, and greater or unlimited flight endurance.

The constant development of unmanned aerial vehicles makes it necessary to develop regulations regarding their use, regulations regarding the place and time of flight, better and better methods of control and data transmission, and, as in this work, the development of design and optimisation methodology.

1.1. UAV division and law regulations

Due to the large number of newly developed structures, various laws in various countries and the European Union Aviation Safety Agency (EASA) were forced to develop new regulations and guidelines for unmanned aerial vehicles [3] [4]. Data on the calculation methodology of such aircraft are not clearly defined due to the huge variety of designs. Due to this fact, each type of newly created type of unmanned aerial vehicle requires a separate development of calculation, analysis, testing, and control methodology. Developed based on EASA requirements, the requirements for Unmanned Aerial Vehicles (UAVs) presented by the Civil Aviation Authority (CAA) have been presented depending on weight, size, and type of structure [5].

Unmanned Aerial Vehicle operations are divided into three main categories:

- **Open category** – is a low-risk category, which means that there is no need to submit declarations or obtain permission from the Civil Aviation Authority. In this category, operations can be performed within the visual range of the pilot or with the help of an observer (VLOS, Visual Line of Sight), with drones weighing less than 25 kg at a distance of not more than 120 metres from the nearest point of the Earth's surface. Registration in the CAA system is required for UAS (Unmanned Aerial System) operators who have drones weighing more than 250g or are equipped with a data collection sensor (for example, a camera).
- **Specific Category -** It is intended for medium-risk operations with flight characteristics outside the 'open' category. The operation will require the verification and, in some cases, the consent of the Civil Aviation Authority. When performing operations in a special category, operators must be registered in the Unmanned Aerial System in the Civil Aviation Authority system. In the special category, UAS operations can be performed after the selected variant is met:
  - Submit a declaration of operation in accordance with the standard scenario (STS) or the National Standard Scenario (NSTS);
  - Obtaining authorisation for operations in a special category;
  - Obtaining the CAA certificate.
- **Certified Category-** is a high-risk category, operations require UAV certification under Regulation (EU) 2019/945. Where appropriate, if required by the competent authority based on a risk assessment, operator certification and remote pilot licencing may also be required. Operations shall be classified in the certified category only if the following conditions are met:

o Over assemblies of people;
o Involves the transport of passengers;
o It involves the transport of hazardous materials, which in the event of an accident may pose a high risk to third parties.

Unmanned aerial vehicle division can be done due to many parameters. Agostino and his team in their work [6], presented a division according to the weight, range, and duration of the flight, cruising altitude, and loads acting on the wings. The parameters they adopted when determining the distribution are presented in Table (Tab. 1).

Tab 11 UAVs by Agostino [6]

Classification by Weight		
Designation	**Weight Range**	**Example**
Super Heavy	>2000 kg	Global Hawk
Heavy	200 – 2000 kg	A-160
Medium	50 – 200 kg	Raven
Light	5 – 50 kg	RPO Midget
Micro	<5 [kg]	Dragon Eye
Range and Endurance			
Category	**Endurance**	**Range**	**Example**
High	>24 hours	>1500 km	Predator B
Medium	5 – 24 hours	100 – 400 km	Silver Fox
Low	< 5 hours	< 100 km	Pointer
Classification by Maximum Altitude		
Category	**Max Altitude**	**Example**
Low	< 1000 m	Pointer
Medium	1000 – 10000 m	Finder
High	> 10000 m	Darkstar
Classification by Wing Loading		
Category	**Wing loading kg/m2**	**Example**
Low	<50	Seeker
Medium	50-100	X -45
High	>100	Global Hawk

Taking into account the constructions developed and averaging their capabilities, it can be concluded that all have different purposes. The results of the analysis of existing solutions and examples of flight parameters are presented in Table (Tab 2).

Tab 2 The main types of unmanned aerial vehicles

UAV type	Multicopters	Fixed-wing	A hybrid of several solutions
Maximum flight altitude	7 km (Autel Evo 2) [7]	22,6 km (Zephyr S HAPS) [8]	7 km (CW-25) [9]
Maximum flight speed	140 km/h (DJI FPV) [10]	740 km/h (WOLFHOUND) [11]	220 km/h (Nuuva V300) [12]
Maximum payload	1587 kg (Black Knight Transformer) [13]	1588 kg (WOLFHOUND) [11]	300 kg (Nuuva V300) [12]
Maximum flight endurance	13h 4min (Skyfront) [14]	623h 57min (Zephyr S HAPS) [8]	17h (AV2 Pelican VTOL/HTOL) [15]
Ability to suspend in the air	Yes	No	Yes

Based on the table presented, it is possible to conclude that each of the structures is adapted to the appropriate type of mission. The selection of the appropriate design solution depends, among other things, on the planned flight duration, the planned flight altitude, or the size of the possible additional weight placed on the drone.

1.2. Problem of HALE UAV flight

Solar-powered UAVs demonstrate their superiority in civil and military applications. Due to the availability of solar energy and the constant increase in the efficiency of photovoltaic panels in recent years, more and more unmanned aerial vehicle (UAV) structures are equipped with this energy harvesting system. These are usually high-endurance aircraft at stratospheric altitudes (HALE). High flight altitude means a larger viewing area and greater air clarity during flight. Fewer elements that scatter sunlight increase the efficiency of photovoltaic panels, resulting in a longer flight duration. As Berry proved in his work [16] solar-powered flight is fully feasible. During the design of the described aircraft, he mainly focused on the traditional design processes of solar-powered aircrafts. Bailey and Bower [17] generally discussed the method of determining the parameters of the components and presented and analysed a solar-powered platform designed to perform stratospheric flights for the mission they proposed. Brandt and Gilliam [18] studied the energy performance of a solar-powered flying wing, tandem wing, and airship due to the energy balance based on the shape of the wing. The above works prove the possibility of long-term flights at high altitudes. Romeo, Frulla, Cestino, and Corsino [19] [20], carried out research activities on HALE platforms with a high wing extension, to achieve a continuous flight of several months at northern latitudes of 36° ~ 45° at an altitude of 15~20 km. Noth [21] developed a conceptual design methodology with considerable flexibility of the design that successfully achieved a running time of 27 hours. The solar-powered Sky-Sailor flew over the summer solstice at 44° north latitude in 2008.

In the history of stratospheric flights of solar-powered aircraft, the HALE UAV Zephyr 7 reached a record altitude of 21,562 m above sea level on July 23, 2010 [22]. Its photovoltaic modules are conventionally mounted horizontally only on a geometrically adapted main carrier panel to accommodate a large number of panels. With the conceptual parameters of the Helios flying wing prototype (HP01), Noll and his team [23] demonstrate that the described UAV achieves constant flight in zones of low to medium latitudes throughout the year. Despite the use of a high aspect ratio wing and a large main wing area, it is clear that the HP01 was unable to maintain level flight at high altitudes and latitudes during the winter months. This is due to the fact that both the average elevation angle of the Sun and the length of the day around winter decrease with increasing latitude, leading to a decrease in solar flux projected onto the horizontal surface, that is, the wing, during the day [24] [25]. All described structures are based on the main load-bearing panel with a high elongation coefficient, and thus high flexibility. For structural and strength reasons, this parameter cannot be increased without affecting the flight capabilities of the designed structure. Noting the problem of insolation and being inspired by the possibilities of tracking the position of the sun by ground systems, Chang, Zhou Wang, and Xu [26] propose and prove the possibility of target positioning and flight direction to increase the amount of energy obtained from the panels without the need to increase the surface of the main wing.

The following work presents research carried out in the field of design development and optimisation of the structure of the main wing of the Twin Stratos unmanned aerial vehicle. One of the assumptions adopted when designing the drone is to enable unlimited flight endurance and reach very high flight altitudes. Achieving these goals will enable the use of the drone as a pseudo-satellite measurement and research platform. Another design assumption is the use of a highly flexible structure of the designed aircraft. The issues related to the design of highly flexible structures were

presented by Schor [27]. It shows the effect of increasing the lift coefficient and wing elongation on subsequent deformations during the use of the HALE "NASA Helios" [28].

1.3. HALE UAV constructions and their application

One of the most popular UAV designs is the fixed-wing design. It is a structure with a layout that is used in the case of aircraft. Due to the lack of a crew, it does not have to be so extensive on the fuselage part.

Objects designed to fly at very high altitudes usually have fixed wings. The ability to reach very high flight altitudes by these aircrafts and their extended flight endurance resulted in the creation of the High Altitude Long Endurance (HALE) aircraft group. Aircraft of this type reach stratospheric altitudes, which means that the flight altitude of this type of aircraft exceeds 14 kilometres above sea level.

Compared to other flying objects, HALE UAVs are not often designed or built structures. This is related to the problem of designing aircrafts with significant wing extension. Objects of this type are assumed to be disproportionately light in relation to the supporting surface. The large bearing surface and the low weight of the object also impose an electric type of power supply. This type of power supply causes another problem related to the accumulation of energy and the weight of the battery. To reduce the additional load in the form of batteries, long endurance UAVs are equipped with photovoltaic panels that charge the batteries placed on board. Examples of design data are shown in table (Tab. 3).

Tab 3 Presentation of the existing Long Endurance UAVs

Name	X-HALE [29]	Helios Platform (HELIPLAT) [30]	Sky-sailor [31]	SoLong [32]	Airbus Zephyr 7	NASA Helios [33]	Units
Wing span	8	73	3.2	4.75	22.5	75.3	[m]
Chord	0,2	2,41	0.25	3.16	1,9	2.4	[m]
Platform area	1.6	176	0.8	1.5	43,6	180,7	[m2]
Aspect Ratio	40	33	12.9	15	11.6	30.9	[-]
Max Gross Takeoff Weight	11.1	815	2.6	12.6	53	929	[kg]
Lenght of aircraft	1.01	7	1.8	2.2	No data	5	[m]
Number of motors	5	8	1	1	2	14	[-]
Speed range	10-19	14-38	7-11	12.2-22.5	No data	8.5-12.1	$\left[\frac{m}{s}\right]$
Endurance	45 minutes	26 days	27 hours	48 hours	14 days	14 hours	[-]
Power/Weight	25.5	10.2	~10	63.5	No data	22.6	$\left[\frac{W}{kg}\right]$
Altitude	No data	17 -20	5.5	8	21	29.5	[km]

On the basis of the platforms presented above, it can be seen that they all have a high Aspect Ratio (AR) in common. This parameter is determined on the basis of the dependence of the span of the main wing and its area. As can be seen, the chord of the main wing of the above objects is usually determined on the basis of a multiple of the size of the photovoltaic panel mounted on the upper surface of the wing. The most popular high-AR aircraft that do not reach such extreme altitudes are gliders. These structures have very high aerodynamic perfection. Therefore, the conclusion is that modern HALE UAV

structures are designed with great emphasis on high aerodynamic perfection, maximising the area of photovoltaic panels in the main wing and weight reduction.

1.4.The purpose of research

The purpose of the research described in this dissertation is to develop a numerical model, analysis methodology, and optimisation methodology for an unmanned, electrically powered stratospheric aircraft with unlimited flight endurance, and then to perform aerodynamic and strength analyses to optimise the structure of the main wing of the presented HALE UAV.

1.5. Research problem

The number of unmanned aerial vehicles in airspace is constantly increasing. The drone production market, the possibility of using drones, and additional equipment elements is constantly developing and growing. The development for the market of a given part of the industry causes an increase in the demand for the optimisation of various types of parameters, construction, or production. One of the possibilities is optimisation in terms of reducing drone production costs. Usually, the solution is to unify the components and the production method itself. However, faulty optimisation assumptions cannot be adopted because they may result in the failure to achieve the assumed parameters of the optimised object. Not achieved planned flight parameters, selection of components with too high efficiency for the assumed design, and thus a reduction in the possibilities related to the endurance of the flight due to the increased demand for energy. The last and most serious mistake, from the point of view of UAV design and construction, is a construction-related problem, that is, an unnecessary increase in weight.

By specifying the appropriate analysis methodology and correctly specifying the optimisation function, variables, and optimised value, the objectives in the form of volatile capabilities of the structure can be achieved while maintaining acceptable construction parameters.

Thesis:

Using the structure design process involving the use of generative models and simulation of subsystems, structures, and the developed optimisation methodology, it is possible to perform a partially automated optimisation of an unmanned aerial vehicle with a highly flexible structure that can achieve unusual flight endurance and flight altitude parameters.

The Twin Stratos 17 object optimised in the presented doctoral thesis is a demonstrator aimed at confirming the endurance of the flight of the analysed structure. The presented research and the analysis methodology must be adapted during the optimisation process of the larger Twin Stratos 12 facility, whose purpose is to confirm the possibility of reaching stratospheric flight altitudes.

Unmanned aerial vehicles of the HALE UAV type undoubtedly have the potential to become the future of telecommunications, climate change observation, visual detection, surveillance, and other applications for which satellite systems are currently used. The goal of researchers exploring the subject of designing, optimising, and building such ships is to make these structures able to stay in flight as long as possible and not to fail, which is favoured by extreme weather conditions prevailing at very high flight altitudes.

In summary, HALE platforms have the following advantages over satellites [34]:

- There is no need to place UAVs in orbit based on rocket systems.
- Landing is always possible.
- Possibility of storing various types of cargo on board, depending on the mission.
- During its life cycle, the HALE platform can be used for many types of missions.
- No need to install additional covers.
- The distance from the ground is significantly lower.

- Low weight and cost of production.

Disadvantages of HALE platforms compared to conventional satellites:

- The satellite, depending on its orbit, can reach any point on the Earth in a maximum of 24 hours. The HALE platform will never be able to achieve such a result.
- Due to the high speed of the satellites, typically 7,000 m/s (25,200 km/h), they can quickly cover very large areas. If the entire globe is of interest, there is no better method of observation.
- Satellites do not penetrate the airspace of the country and can take pictures without violating the sovereign rights of the country (UN Agreement on Open Skies).
- The satellite must not injure a person or hit a passenger plane.

The advantages of Solar HALE platforms over standard aircraft are:

- They don't need fuel.
- They are environmentally friendly ("zero emissions").
- They can stay in the air for long or indefinite periods.
- It can operate at high altitudes above normal air traffic.
- They are much more independent of the weather.

The main problem with solar-assisted electric HALEs is high-altitude operations, which require a main wing with a high aspect ratio. Due to the large span, the forces acting on a given wing also increase. This causes flight speed limitations as a result of the possibility of negative aeroelastic phenomena. The payload of the solar HALE is limited by the need to use battery packs that provide an energy buffer that allows a safe landing in the event of loss of power generated by photovoltaic panels. The use of a large number of battery packs also increases the weight of the designed structure.

This dissertation presents examples of applications of HALE unmanned aerial vehicles, along with an optimised research object in the form of a HALE UAV developed by SkyTech eLab in cooperation with the Silesian University of Technology.

It is possible that this methodology will also be developed or form the basis for the development of an accurate methodology for the design of similar HALE UAVs.

2. Subject of research

HALE UAV's are aircraft whose cruising speeds are usually not high, and the most impressive is the possible flight altitude. These are mainly stratospheric aircraft that fly at altitudes exceeding 15 kilometres above sea level. Flying at such an altitude is a huge design and production challenge. Any design imperfection or manufacturing deviation may result in immediate in-flight destruction of the UAV. Frulla and Cestino in their work [35] present the process of designing, building a model, and testing the HALE UAV. The methodology presented in their article defines the importance of the accuracy at each stage of work related to such a structure.

The goal of optimising HALE UAVs is usually to obtain a platform suited to a specific task in terms of internal structure layout, weight reduction, or other key parameter adjustment. These parameters are optimised by predetermined boundary conditions in the form of a function of the bending moment (M_b), mass of the designed aircraft (M_a), wing surface area (S), flight conditions at the assumed altitude, available thrust (P_a) during flight at maximum speed (V_{max}), or the flight parameters at the stall speed (V_{stall}) for the optimised UAV.

Due to the working environment of HALE UAV type vessels, the optimisation task is extremely complex and requires precise determination of the optimised parameters, boundary values, variable values, and the purpose of the optimisation itself. Each optimisation process requires the determination of the research object and all the assumptions necessary to select the best parameters for a given objective function.

2.1. Description of the designed UAV

The Twin Stratos project assumes the use of the main carrier wing as an element that generates the appropriate force to maintain the aircraft during flight and as an element that connects the two fuselages on which the pulling engines are placed. The fuselages are also connected by a tail using the "A" layout. The main design assumption for the UAV under consideration is elongated, with the aim of unlimited flight endurance and high achievable flight altitudes. To obtain the assumed parameters, the model is optimised in terms of maintaining the appropriate stability of the structure in certain critical flight conditions, reducing weight, reducing flight resistance, increasing lift, increasing the ability to accumulate energy generated by the Sun, and reducing power consumption during the flight.

One of the most important elements of the design is the use of movable control surfaces only in the tail part (applied for patent). The main wing should not be equipped with an additional control apparatus. This will allow to reduce the weight of the main wing itself and use a highly flexible and thus slimmed down wing structure along its entire length. These conceptual assumptions became the basis for the development of the model visible in the visualisation presented below.
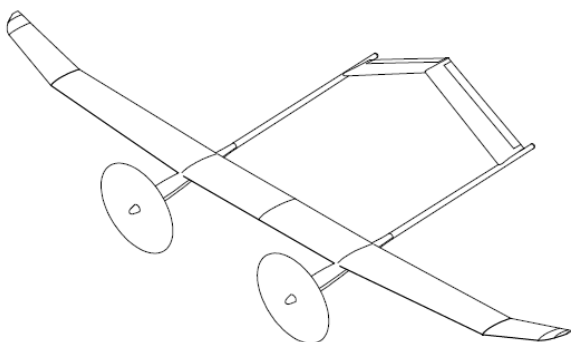
Figure 1 first sketch of the Twin Stratos UAV

Research related to the study of unmanned aerial vehicles led scientists working at SkyTech eLab to develop the Twin Stratos 1:1 UAV concept (Fig. 1). The concept was developed with the creation of two UAV Twin Stratos scales. These were 1:8 scales (changed to 1:7 for design reasons), 1:2 and 1:1, i.e. the target HALE UAV Twin Stratos.

The funding obtained from the programme of international Polish-Norwegian projects allowed the refinement of two smaller concepts of the Twin Stratos drone. The methodology and the process of designing and optimising the presented UAV Twin Stratos structure are presented in the following work. The following doctoral dissertation presents the development of a methodology for designing, analysing, and optimising the main wing of an unlimited flight endurance unmanned aerial vehicle

based on the HALE UAV - Twin Stratos project developed by SkyTech eLab (Fig. 2). The tested aircraft structure is equipped with a symmetrical arrangement of two fuselages offset from the plane of symmetry, a tail wing with the "A" arrangement used connecting the tail beams of the fuselages, and a symmetrical main carrying wing placed on the front part of the fuselages.

Figure 2 Visualisation of UAV Twin Stratos

As part of the research work, a team of scientists and designers developed and built a family of unmanned aerial vehicles called Twin Stratos (TS), which are adapted for continuous flights.

As part of the work related to the Twin Stratos project, the following scale-up versions were created, which will be used to test and verify individual subsystems, as well as to carry out the planned research missions:

- TwinStratos 110 (TS110) scale 1:10 - UAV verifying the overall design and the simplified control system;
- TwinStratos 17 (TS17) scale 1:7 – as a replacement for TwinStratos 18 on the 1:8 scale, UAV allowing verification of the power system, energy consumption simulation model, and technology;
- Twin Stratos 12 (TS12) scale 1:2 – UAV allowing verification of flight parameters and performance range in operating mode, designed for service use and scientific research;
- Twin Stratos 11 (TS11) scale 1:1 - UAV target intended for research and implementation of commercial services.

These constructions would have the task of confirming certain parameters during flight tests and performing assumed missions [36]. The prototype of the developed TS17 is shown in the photo (Fig. 3).

Figure 3 Photo of Twin Stratos 1:7

2.2. The origins and possibility of using the Twin Stratos research platform

The ability to fly at high altitudes ensures the high efficiency of photovoltaic panels due to the lack of obstacles that disperse sunlight [36]. The use of a sophisticated mission planning scheme and an intelligent control system capable of correcting the course in real time to maintain the greatest possible insolation of the panels and use natural air currents allows for a significant increase in the possibility of obtaining solar energy and reducing its consumption while maintaining the flight altitude. The installation of photovoltaic cells on all of the upper surfaces can provide additional power. The

generation of additional energy can be continuously maintained for several months a year, provided the flight is at a given latitude. However, this may result in an increased risk of electronics damage and unnecessary weight gain. However, since the aircraft must generate as low aerodynamic drag as possible, the panels should not be mounted in such a way as to impede flight by increasing drag or disrupting the flow around the main load bearing members. Therefore, flight planning must take into account the position of the Sun during the 24-hour day of operation.

The study of the high layers of the atmosphere will answer many questions about the currently occurring climate anomalies. Unfortunately, only a few of the aircraft currently produced have flight capabilities that allow them to perform the required measurements. Due to the above problem, in 2019 a consortium was established as part of the "Long-Endurance UAV for assessing atmospheric pollution profiles" project. The team, which included scientists from SkyTech eLab company, the Silesian University of Technology, the University of Warsaw, and the NORCE - NORUT research unit, set the goal of developing the concept of the research platform, its construction, and conducting air quality profiling tests. The main objectives of the project [37]:

- Achieving energy self-sufficiency or at least extended flight time.
- Development of a high-strength airframe supporting structure to achieve the appropriate functional parameters.
- Obtain the appropriate load capacity while drastically minimising the weight of the load-bearing structures.
- Development of functional UAV systems that allow maximum use of specific flight parameters, variability at high altitudes, and low cruising speed.
- Development of various types of sensors that allow measurements of atmospheric pollution during both the day and at night.
- Development of a high-strength airframe supporting structure to achieve the appropriate functional parameters.

Preliminary analyses of the planned research platform Twin Stratos allowed to propose applications for which it can be used. The possibilities related to the lifting capacity of additional equipment, a specific flight speed range, the possibility of long-term flight at a fixed altitude and the possibility of reaching high ceilings make the tested object can be used, among others, in industries related to:

- Protection and military,
- Telecommunications,
- Observation,
- Surveys of large areas,
- Cultivation supervision,
- Fire control,
- Meteorology,
- Air quality testing,
- Traffic intensity survey.

The application concepts presented above may become the basic tasks of similar UAVs in the future. All of these activities can be classified as three basic aircraft capabilities: telecommunications, observation, and measurement.

2.2.1. Telecommunications capabilities of the Twin Stratos platform

Opportunities for height observation, data transfer, measurement, and analysis of composition of the air are increasingly important in the light of the developing world. The most important example of how crucial the ability to observe from significant heights and the ability to transfer data is the current situation in Ukraine.

Mozaffari and his research team presented the model of using unmanned aerial vehicles as mobile transmission stations [38]. The ability to conduct uninterrupted observation in conjunction with constant transmission of information can introduce a completely new standard of air safety in the monitored area. The use of the drone as a pseudo-satellite or mobile transmission station will allow telecommunications to be delivered to cutoff places when needed (Fig. 4).

Figure 4 Twin Stratos pseudo-satellite use case

The issues related to data transmission and the use of UAVs to improve the operation of mobile networks were presented by Fotouhi and his team [39]. The studies they developed prove the possibility of a significant improvement in the quality of mobile networks in areas where the construction of standard transmission towers is unprofitable, impossible due to the type of terrain, or there is no possibility of providing connections. The described research presents the design of the telecommunications infrastructure using UAVs (Fig. 5).
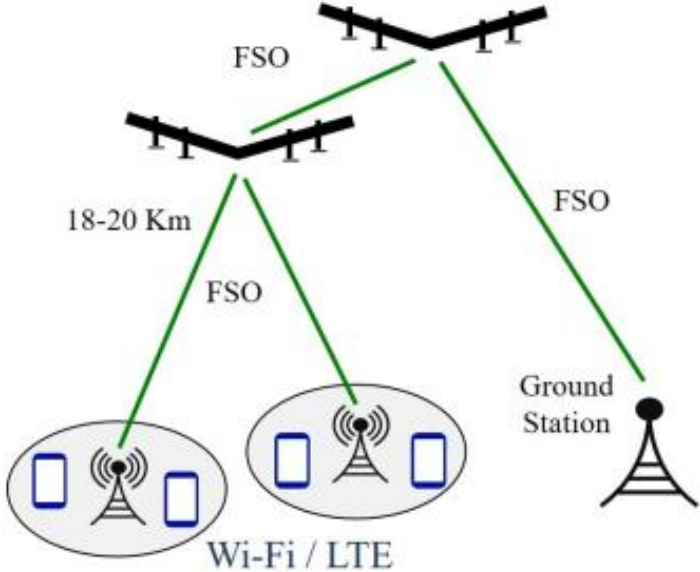
Figure 5 Illustration of the architecture of the Facebook Aquila system [39].

2.2.2. Observation capabilities of the Twin Stratos platform

The main assumptions regarding the capabilities of the Twin Stratos UAV are unlimited flight endurance, lightness, and flexibility of the structure, autonomous flight, and constant communication regarding the collected data. The flight capabilities of the designed structure confirm the ability to perform constant observation. Due to the nature of the observation mission (Fig. 6), it is possible to fly at altitudes from 150 to 20,000 metres above sea level. However, depending on the altitude, it is necessary to select equipment that allows for taking pictures with a resolution appropriate for the planned mission.
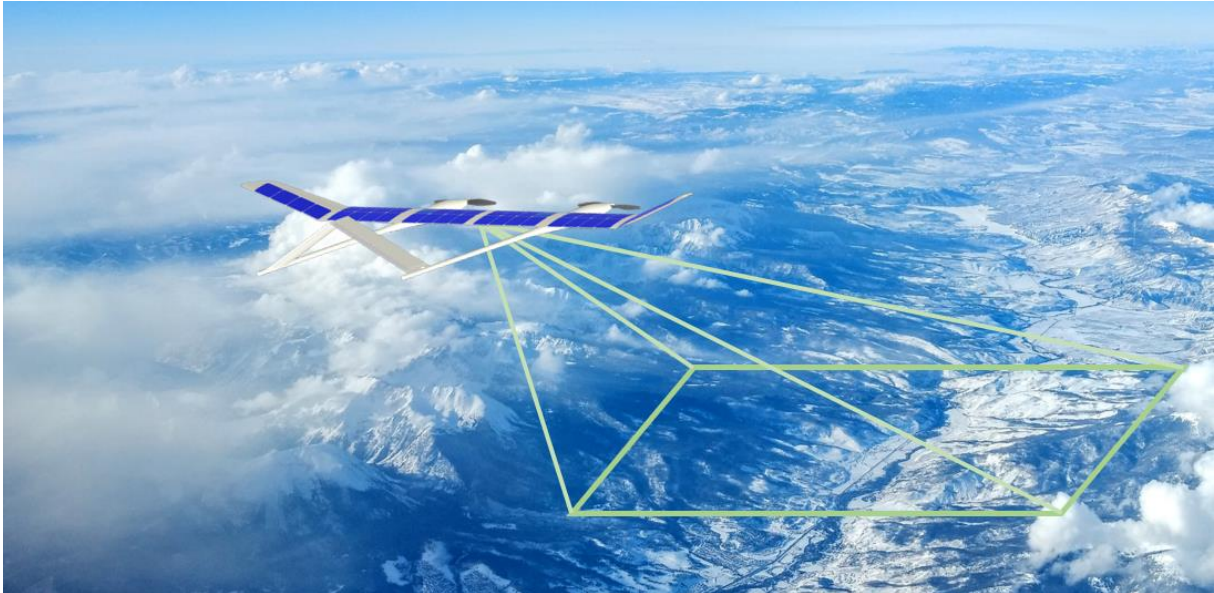
Figure 6 Twin Stratos observation mode

The ability to observe or follow is very important for safety purposes, monitoring the capacity of public roads, and monitoring the quality of water throughout the entire length of rivers. Heintz and his team presented the principle of operation and the application of the UAV [40].

2.2.3. Research and measurement capabilities of the Twin Stratos platform

Due to the possibility of placing additional measurement equipment on the designed UAV, a plan was also developed for air quality testing over a large area. Possibly, low cruising speed allows for accurate research in the assumed area, keeping the flight at a constant height (Fig. 7).

Figure 7 Twin Stratos measuring in a constant altitude mode

It is also possible to perform an analysis of the composition of the air as a function of height (Fig. 8).
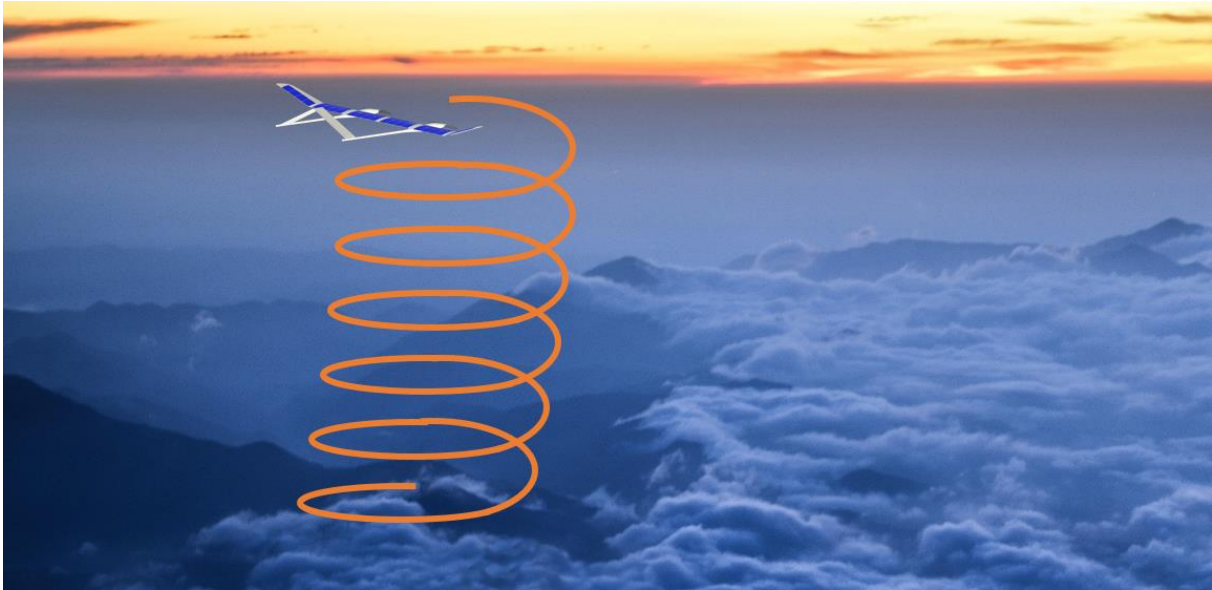
Figure 8 Twin Stratos measuring as a function of altitude

The methodology for observing a given area based on the use of unmanned aerial vehicles is already known. The problem of conducting research in a large area is always to meet the conditions of flight endurance and maintain the assumed flight altitude for a long time. An application of this kind was described by Zheng and his team [41]. The research described in their article is focused on observing vast areas of palm trees. According to the study presented, an observation of this type can warn of the onset of disease in crops at an early stage. When a tree suggests disease or pests, the people involved in the cultivation have the opportunity to prevent the spread of a given danger to the rest of the crop.

2.3. Presentation of the concept of the designed UAV

Due to the small number of companies involved in the construction of similar aircrafts, the methodology for designing unmanned pseudo-satellites has not been clearly defined. The dimensions and geometric parameters of the HALE solar powered UAV configuration are significantly different from those of traditional aircraft. These parameters are determined taking into account the energy obtained and the total weight of the designed HALE UAV [25]. Assuming that all of the energy comes exclusively from photovoltaic modules mounted on the main wings and tail section, it should be noted that these surfaces are strongly coupled with aerodynamic properties. The weight of the panels placed on the structure, photovoltaic modules, and additional equipment related to the given power supply system takes up a large part of the total weight of the designed UAV and thus affects the total energy consumption.

Without taking into account the geometric dimensions of the fuselages, the horizontal and vertical tails, and small areas that disturb the lift force, four characteristic variable parameters can be defined for the wing-tail configuration. They are determined on the basis of the main wing span (b_w), tail span (b_t), main wing chord (c_w), tail chord (c_t), main wing area (S_w) and tail wing area (S_t). Thus, the four characteristic variable parameters for the wing-tail configuration are:

- Aspect Ratio (AR),
- span-to-chord ratio of the main wing (b_w/c_w),
- tail wing chord to main wing chord ratio (c_t/c_w),
- area ratio (S_t/S_w).

Based on the above parameters, it is possible to compare the designed structure with existing solutions. On the basis of the data determined in this way, it is possible to initially determine the parameters of the designed object. On the basis of the comparison of existing HALE UAVs, it is possible

to conclude that the shapes of the tail and main wing should be rectangular or as close to rectangular as possible, with constant chord lengths to facilitate the integration of photovoltaic modules and reduce the complexity during production. All elements of the panels are developed according to assumptions regarding the length and width of the photovoltaic cells placed on them. Based on assumptions regarding safety factors, planned missions, and possible applications, the Twin Stratos concept was developed, presented in the figure (Fig. 9). The chord ratio (ct/cw) was determined on the basis of the design experience of the Chief Designer of SkyTech eLab and the existing coefficients, similar in terms of application and the assumed size of the structure. However, the assumption of flight endurance required the development of a structure with the highest possible coefficient of aerodynamic excellence. For this reason, the shape of the main wing is inspired by glider designs.
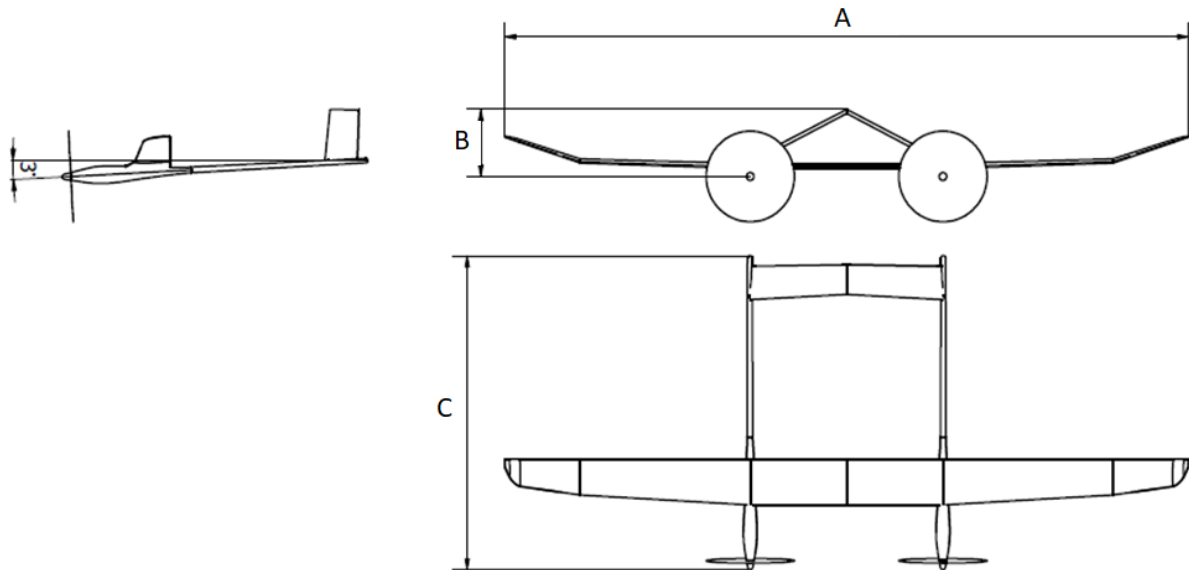
Figure 9 The first concept of the designed UAV

The values of the geometrical parameters of the structures developed in this way are presented in the table (Tab. 4). The results were developed for the three scales considered in the planned Twin Stratos UAV.

Tab 4 Parameters of individual scales of the designed Twin Stratos UAV

Scale	1:8	1:2	1:1	Unit
Mass of aircraft	7,1	30	80	[kg]
Aspect Ratio (AR)	16,91	19,15	17,87	[-]
Wing area	0,55	8,6	34,4	[m²]
Maximum flight altitude	5000	20000	20000	[m]
Maximum flight endurance	12	24	>24	[h]
Maximum payload	2,5	2,5	5	[kg]
Mean aerodynamic chord	0,2	0,8	1,4	[m]
Wingspan	3,0	12,4	24,8	[m]
Tail unit area	0,21	1,2	2,4	[m²]
Lenght of aeroplane [C]	1,4	5,6	11,2	[m]
Hight of tail unit [B]	0,24	1,2	2,4	[m]
Assumed motors power	150	2200	5500	[W]

Geometric analysis of the initial concept of the Twin Stratos 1:8 drone showed a problem with placing the appropriate number of photovoltaic panels. Reducing the number of solar panels would result in a reduction in flight endurance and a significant reduction in flight altitudes. The work aimed at solving the problem resulted in the development of the Twin Stratos 1:7 concept and a change in the geometry of the main wing of the newly created concept. The geometrical parameters developed for both structures are presented in the table (Tab. 5).

Tab 5 Comparison of the TS17 and TS18 parameters

Scale	1:8	1:7	Unit
Take off mass	7,1	9,8	[kg]
Aspect Ratio (AR)	16,91	14,46	[-]
Wing area	0,55	0,70	[m^2]
Maximum celling	5000	5000	[m]
Maximum flight duration	12	24	[h]
Payload	2,5	2,5	[kg]
Middle chord	0,20	0,28	[m]
Wing Span [A]	3,0	3,6	[m]
Tail unit area	0,21	0,25	[m^2]
Lenght of aeroplane [C]	1,4	1,8	[m]
Hight of tail unit [B]	0,24	0,29	[m]
Assumed motors power	150	300	[W]

The initial concepts of the Twin Stratos drone in 1:8 scale (Fig. 10) and Twin Stratos in 1:7 scale (Fig. 11) along with changes in the shape of the wing are shown in the visualisations below. Due to the possibility of increasing the number of panels mounted on the upper surface of the main wing, it was decided not to change the chord of the wing from the line of the fuselages and use stay length of chord until the wingtips. They were designed with a higher cant angle to maintain stability during flight.
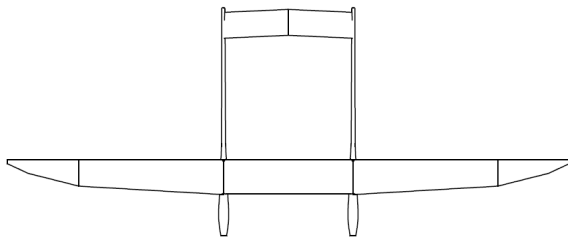
Figure 10 Before main wing modification
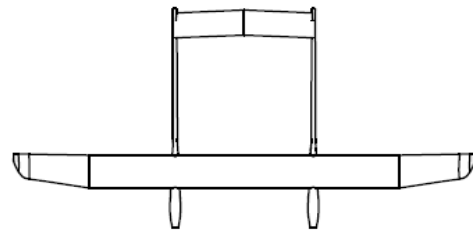
Figure 11 TS17 After main wing modification

Twin Stratos 17 is a demonstrator with limited functionality (Fig. 12). The parameter that has been reduced for the construction of TS17 in relation to TS11 is the altitude of flight. Due to the scale, the amount of power generated by the photovoltaic panels is much lower than in the case of Twin Stratos 1: 1. This is also associated with reduced power and the possibility of mounting additional equipment. Due to the favourable results of the analyses based on the given methodology, they showed the great potential of the structure to perform flights for missions at altitudes of up to 5000 metres above sea level.
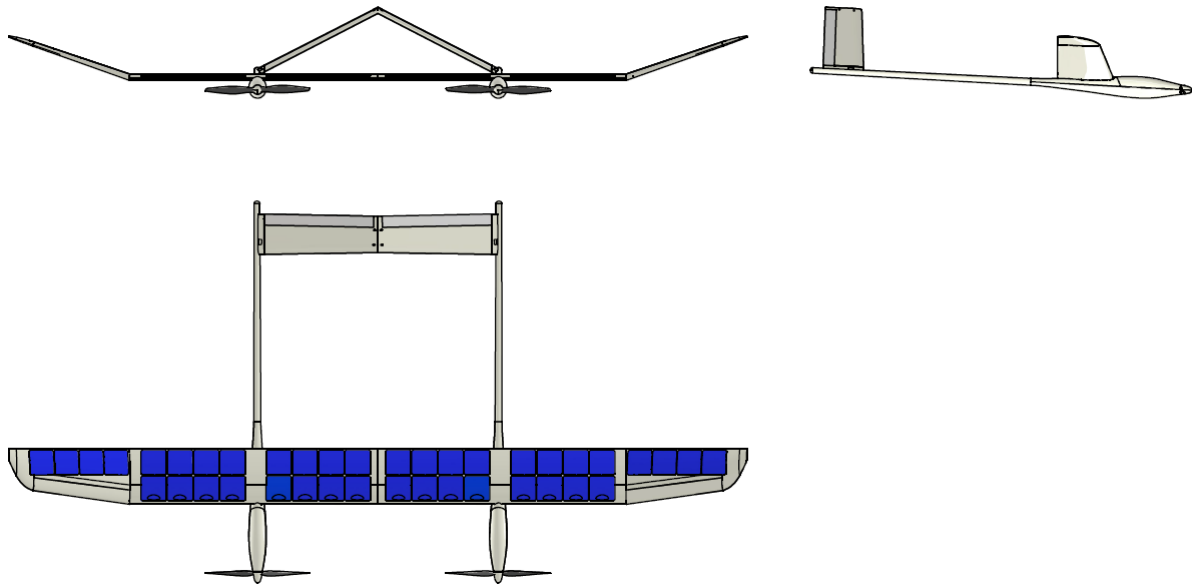
Figure 12 Twin Stratos geometry showcase 1:7 scale

The methodology for the analysis and design of aircrafts with flight capabilities similar to the assumed structure is extremely complicated and requires a multidisciplinary approach to the analysed object. However, there are schemes of action aimed at increasing the accuracy of the analyses carried out and facilitating the design stage itself.

3. Review of the state of the art

HALE UAV aircraft, despite their unusual proportions, are wing structures. Due to this fact, the design and optimisation methodology itself cannot differ significantly from the methodologies used during the analysis of aircraft or gliders. As in the case of standard structures, it is therefore necessary to analyse the parameters:

- air prevailing at cruising altitude,
- masses and their influence on the location of the centre of gravity,
- geometric, determined by the shape of the analysed structure,
- aerodynamic forces acting on the analysed structure and load distribution,
- structural, material, and strength,
- propulsion system used in the project.

Each of the above points defines parameters that can be determined on existing methodologies for performing analyses. The main problem with regard to HALE UAV analysis is to determine which of the existing methods will be the best parameters to determine the given in the designed structure.

3.1. Methods of air parameter identification at the analysis flight altitude

Testing the flight capability of the designed aircraft usually begins by determining the air parameters prevailing at sea level and at the assumed cruising altitude. In the case of ordinary aeroplanes, gliders, and other structures flying at low altitudes, the influence of changes in pressure, temperature, air density, and the decrease in the value of gravitational acceleration are values that affect flight to a small extent. The influence of the parameters given increases when the designed object is to reach very high altitudes, as is the case with the HALE UAV aircraft [42]. Parameters prevailing at required altitudes can be determined:

- By performing a test flight and obtaining measurement data from another aircraft or radiosonde equipped with measurement equipment. To obtain information on the air parameters at the tested altitude, a flight is carried out in an aircraft equipped with the appropriate measuring equipment. Analysis with a radiosonde lifted by a balloon filled with hydrogen or helium works similarly [43].
- Through satellite meteorological observations from space orbits.
- Data obtained from satellites make it possible to determine the state of the atmosphere throughout the world, which is particularly useful in relation to space above the oceans [43]
- Through analytical models – simulating the behaviour of air parameters based on data from sensors, radars, and satellites. An example is Computational Fluid Dynamics (CFD) analysis, which uses numerical methods to analyse fluid flows [44].
- Literature methods - comparative, i.e., historical. Determination of parameters based on comparative tabular data [42].

3.2. Methodology of determining mass parameters

The purpose of mass analyses is to determine the size of the mass and the location of the centre of gravity of all elements of the structure and equipment of the flying object. For aircraft equipped with propulsion systems powered by liquid fuels, it is necessary to perform analyses for an empty system, i.e. without fuel, without additional payload, and for a full system, i.e., one in which the maximum take-off weight is reached. The most important result obtained during a given analysis is the determination of the inertia parameters of the analysed structure and its balancing [45].

3.2.1. Aeroplane balance based on analytical calculations of forces and moments

The method of the centre of gravity location consists of summing up the masses of individual elements of the structure and equipment of the aircraft and then integrating the given values with respect to the entire aircraft. The inertia analysis method consists of calculating the moment of inertia of each element of the aircraft relative to its own centre of gravity, and then determining the moment of inertia relative to the location of the centre of gravity of the entire aircraft and summing up these moments. The literature assumes the location of the centre of gravity (CG) of the analysed aircraft in 30-35% of the mean aerodynamic chord (MAC) [46]. The purpose of this assumption is to maintain the longitudinal stability of the designed aircraft.

3.2.2. Based on numerical methods

Accurate mapping of the analysed structure using modern Computer Aided Design (CAD) methods allows determining mass parameters with considerable accuracy. Modelling taking into account the type of materials used and their properties allows for the development of a digital twin. The model in such a state can be used not only to accurately determine the location of the centre of gravity, but also to determine the moments of inertia in relation to any selected point of the coordinate system in an automatic manner. The principle of determining the value data is the same as in the case of the analytical method, while the calculations carried out using the CAD environment are incomparably faster. There is also no need to determine the appropriate system of equations that describe all distances, because they are automatically determined by adding the appropriate solid taking into account the parameters of the mass in a given place of the model [47].

The issue of determining the mass parameters of the designed aircraft using computer methods is complex due to the coupling of the current generation of the model and the obtaining of the results. The live preview of the positioning of components results in a more accurate determination of the location due to the view of the place where the component is to be placed. The advantage of other methods is the ability to determine the connections between electronic components, which allows to determine the length of the required wires and helps to avoid errors related to the arrangement of components at a distance that makes assembly difficult or generates the need to use unnecessarily long wires.

3.2.3. The method of balancing an existing flying object

The use of a given method requires a ready-made aircraft. The aircraft should be placed on platforms that measure the pressure at given points, and then the measurement points should be applied to the projection of the analysed aircraft in the plane determined by the measurement platforms. The advantage of the method is the high precision in determining the mass of the entire analysed structure and the location of the centre of gravity. The determination of inertia moments with respect to the location of the centre of gravity, longitudinal and transverse stability is performed on the basis of analytical calculations in the same way as in subsection 3.2.1 "Aeroplane balance based on analytical calculations of forces and " [47] [48].

3.3. Currently used methods for determining load distribution and aerodynamic parameters

Analysis of load distribution and aerodynamic parameters is crucial for designing and testing aircraft performance [49]. Analyses of this type make it possible to determine the dynamic characteristics of the UAV, which describe the dependence of changes in aerodynamic forces and moments depending on the angle of attack, steering angle and air flow around the tested object. The geometrical parameters and aerofoils used in the designed structure are directly related to the performance achieved and the aerodynamic efficiency. Striving to achieve the highest possible coefficient of

aerodynamic excellence allows to extend the endurance of the flight and increase the achievable flight altitude [50]. Parameters can be determined on the basis of the following analysis methodologies:

3.3.1. Analytical methods

- The Schrenk method considers the average lift per unit of span between the wing height and the elliptical height distribution. The model of the Schrenk method is presented graphically in the figure (Fig. 13) [51].
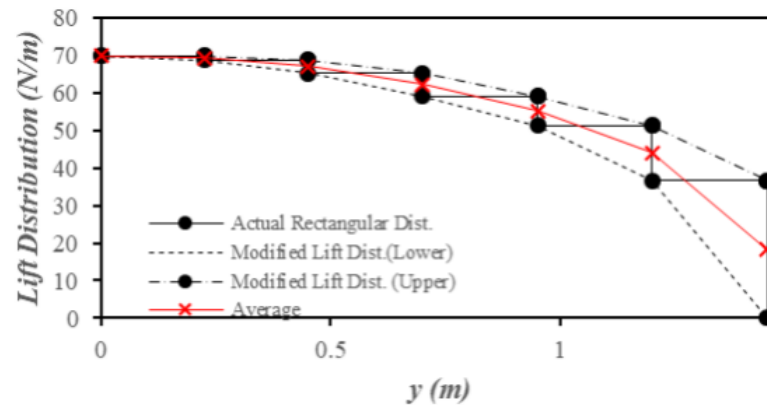
Figure 13 Actual lift distribution of the CFD and modified results to achieve an elliptical lift distribution profile [51].

According to Soemaryanto and Rosid [51], the results obtained during a given analysis are characterized by high accuracy and an error not exceeding 2% in relation to the analysis of patches without the tip. The wing ending elements get much less accurate results with error values of 24%.

3.3.2. Numerical methods

Turbulent flows are inherently unstable and their accurate simulation requires enormous computational power. For this reason, the most common engineering approach is to try to solve the time-averaged Navier-Stokes equations (the so-called RANS - Reynolds-Averaged Navier-Stokes equations). Since the N-S equations are nonlinear [52], each averaging process generates additional unknowns, which are associated with averages (the so-called closure problem). To determine the exact results of the flow analysis, it is necessary to select the appropriate computational solver to determine the turbulence. Typically, the selection is made on the geometry being studied and the planned flow rates:

- None (Laminar) – The model does not take into account the turbulence of the flows tested.
- K-Epsilon turbulence model ($k - \epsilon$) – Turbulence Model that introduces new variables, k - so-called kinetic energy of turbulence and ϵ - energy dissipation. Both variables form the so-called turbulent viscosity (μt), which is designed to model the apparent increase in viscosity associated with the existence of additional fluctuations [53].
- Generalised k-Omega ($k - \omega$) - The GEKO model was developed to consolidate the advantages of the many available RANS two-equation models based on spinal viscosity into one unified general purpose model that covers a wide range of flow conditions and applications [54].
- Shear Stress Transport- a model that combines the advantages of the $k - \epsilon$ model and the $k - \omega$ model and introduces an additional term limiting the overproduction of turbulence kinetic energy in areas of strong positive pressure gradients (stagnation points, areas of boundary layer detachment) [55].
- BSL EARSM - The model based on the EARSM-BSL combination (Explicit Algebraic Reynolds Stress Models – Baseline model) [56], is obtained by extending the standard models with two equations. They are based on the Reynolds stress transport equations and offer a non-linear relationship between the Reynolds stresses and the rotation and strain rate tensors. Many

flow phenomena can be included in the model without solving the transport equations due to the presence of higher-order terms [57]. To avoid being forced to use additional terms in the BSL formula, a slight recalibration of the Wallin and Johansson formula was performed [58].

3.3.3. Experimental analysis

The method depends on the size of the tested object. In the case of extremely large objects, consisting of the appropriate scaling of the tested object and preparing it for tunnel aerodynamic analysis. In the case of small objects, that is, when the object can fit inside a wind tunnel, it is attached in a way that allows the generated lift and drag to be measured. Data are usually presented as a function of the force value of the flow velocity within the tunnel [59].

3.4. Methods of analysis of aircraft propeller propulsion systems

The efficiency of the propulsion system is one of the basic parameters for determining the flight characteristics of the designed structure. Dependencies of aircraft thrust selection are determined on the basis of their weight and comparative parameters in the form of historical data. In the case of unmanned aerial vehicles, the dependence is usually described in the form of a percentage dependence on the mass of the designed structure.

3.4.1. Analytical calculations

Tests carried out on the basis of calculations based on assumed theoretical data. In the case of propeller systems, analytical analyses are based on the rotational speed, pitch of the tested propeller, diameter of the propeller, and parameters of the medium in which it rotates. The calculation is carried out in a manner similar to the main wing. The main difference is the change in velocity along the span of the analysed surface due to the rotational speed and distance from the axis of rotation. Typically, blade element models are developed for an axial-flight propeller (the axis of rotation is parallel to the direction of the free air stream) that has straight blades. The blades are divided into small elements in the radial direction. It is assumed that each element behaves as a two-dimensional wing. Another assumption is the lack of interaction between adjacent elements. The validity of this assumption has been confirmed [60]. Analytical methods also assume the slip value, which is related to the efficiency of the propeller system. This parameter is an estimate, and accurate determination of its value usually requires bench tests [61].

3.4.2. Experimental analyses

The tests consist of the direct examination of a given drive system. Due to this, it is possible to obtain information on the actual operating conditions of the drive system. Tests are generally conducted on specially prepared dynamometers or by placing the test aircraft on a platform that allows measurement to be performed [62]. This method allows to determine the occurrence of abnormalities in the operation of the drive system with the greatest precision [63].

3.4.3. Numerical analyses

Numerical simulations allow for relatively accurate analysis of driveline behaviour under specific conditions and help design more efficient and reliable systems. The accuracy of the analysis depends to a large extent on the adopted boundary conditions, the type of mesh, and the correctness of the preparation of the analysed models. CFD-based analysis usually uses Moving Reference Frame (MRF). The analysis performed in this way is defined and illustrated in the figure (Fig. 14). The analysis area is divided into a global stationary domain and a divided rotating region, called a rotating domain. The rotating domain is defined by a smaller cylinder that completely covers the blades and the hub [64].

Flow analyses require the determination of the appropriate turbulence solver. They are identical to those presented in Subsection 3.3.2 "Numerical methods".
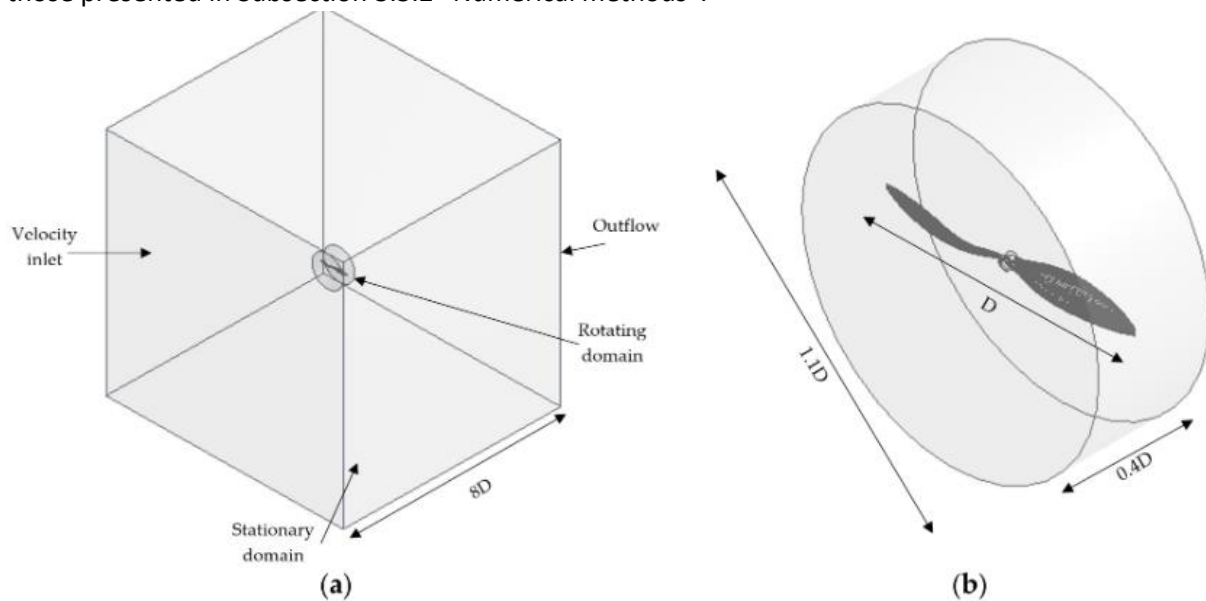
Figure 14 Flow domain and boundary conditions. (a) Stationary domain and boundary conditions. The boundary conditions include an inlet, outlet, stationary domain, and rotating domain; (b) Rotating domain [64].
Where: D – propeller diameter

Tests of propeller propulsion systems can only be considered by static determination of thrust. It is also important in terms of the operation of the system to determine the dynamic phenomena such as vibrations caused by the unbalance of the propeller. The problem is more complicated, the more non-linear the structure of the tested propeller is. Composite propellers are characterised by a non-linear arrangement of fibres, which can cause unbalance. The problems of modelling composite elements rotating on the basis of a high-speed rotor shaft were presented by Dąbrowski, Dziurdź and Deuszkiewicz [65].

3.5. The method of structural, material, and strength analysis

Real aircraft structures consist of many elements, generally arranged in an irregular manner. These components are usually continuous and, therefore, theoretically have an infinite number of degrees of freedom and redundancy. Thus analysis is only possible when the real structure is replaced by an idealised approximation or model. However, there is a correlation between increasing the simplification that introduces idealisation and a lower inaccuracy of the analyses. In aircraft design, where structural weight is of the utmost importance, accurate knowledge of component loads and stresses is essential. At some stage of the design, they should be determined as precisely as possible. This accuracy can only be achieved by considering an idealised structure that closely reflects the real structure. Standard methods of structural analysis are insufficient to deal with the necessary degree of complexity of such structures. It was this situation that led to the development of matrix analysis methods at the turn of the 1940s and 1950s, and at the same time to the use of computers in calculations. Matrix methods are ideally suited to express structural theory and theory in appropriate form and for numerical computer solutions [66].

3.5.1. Analytical calculations

Many structural problems are statically determinate; in other words, support reactions and systems of internal forces can be found by simple statics where the number of unknowns is equal to the number of equilibrium equations available. In cases where the number of unknowns exceeds the possible

number of equilibrium equations, for example, a supported cantilever beam, other methods of analysis are required. The methods fall into two categories and are based on two important concepts;

- Principle of numerical work. It is the most basic and powerful tool available for the analysis of statically indeterminate structures and has the advantage of being able to deal with conditions other than those of elasticity.
- The strain energy principle can provide approximate solutions to complex problems for which exact solutions do not exist.

In some cases, the two methods are equivalent because although the governing equations differ, the equations themselves are identical. Both methods were thoroughly described by Megson [66].

3.5.2. Numerical simulations

Computer techniques are widely used in modern structural analysis. These include flexibility and stiffness methods. However, the formulation of the stiffness matrix for elements of a complex structure is based on one of the approaches presented in the subsection 3.5.1. "Analytical calculations", so knowing and understanding their use is beneficial [66].

3.5.3. Experimental analyses

Due to the large number of aircraft components, experimental tests of components, materials, and systems used in the analysed structure are usually performed. The tests can be divided into bench tests and flight tests:

- Bench tests will therefore take into account:
  - Material tests, such as strength tests of materials used in the components of the designed aircraft,
  - Structural tests of the designed ship's structure to determine critical strength values,
  - Dynamic tests and modal analyses.
- Flight tests enable analysis:
  - Deformations that occur during flight under certain conditions.

4. Methodology of analysis and optimisation of the considered structure
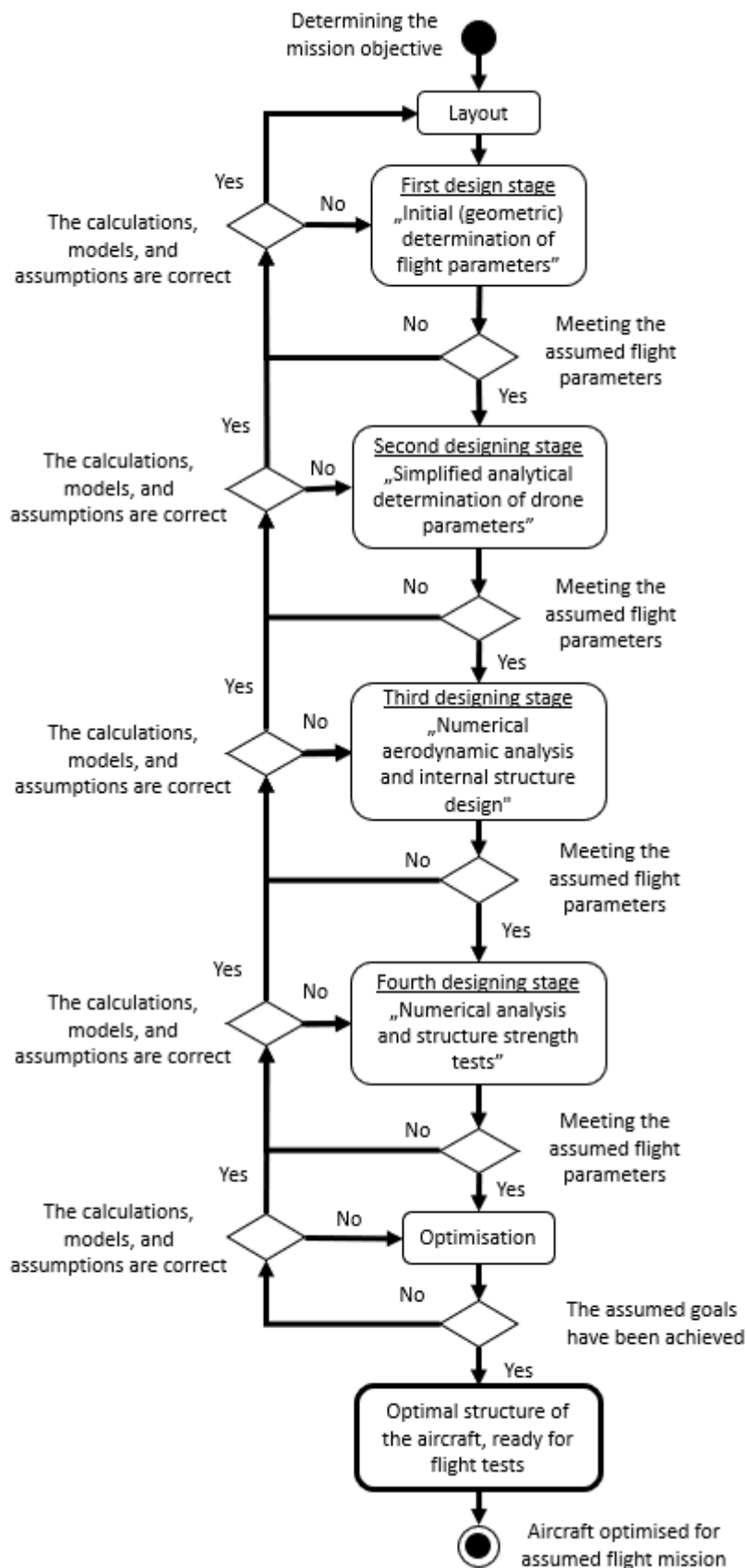
Figure 15 A simplified optimisation path of the designed and analysed UAV Twin Stratos

The HALE UAV design and optimisation path should not differ significantly from the design paths of small utility aircraft or gliders. The principle of staying in the air, the types of drives used, and the type of control during flight are the same solutions that have been used in the above constructions for many years. Due to the limitations of the energy balance and mass balance, it is necessary to determine the correct design methodology and optimisation for the given requirements of the designed structure. Based on chapter 3. "Review of the state of the art" the path adopted during the work related to the analysis of the HALE UAV Twin Stratos 1:7 was developed. The developed path for obtaining the optimal structure is presented in the form of a set of design stages, taking into account feedback in the event that incorrect construction assumptions are made for the analyses being made at the previous stage. The construction development and optimisation methodology is presented in a simplified way in the picture (Fig. 15). Each of the stages presented is responsible for another type of analysis developed there.

Due to this assumption, the optimisation results obtained during the fourth design stage have a direct impact on the initial assumptions, analytical calculations, and all previous

work steps. Any nonconformances and construction problems must be eliminated in order to obtain the final optimal design.

Each of the design stages presented in the figure is responsible for the given types of analyses and determines the sequence of performed works.

4.1. The first designing stage

At this stage of the research, the main layout of the designed UAV was defined, its application, and the initial values of speed and altitude at which it was to move were determined. This stage includes the following assumptions, and the following analyses are performed:

- Development of the shape concept and geometric assumptions,
- Approximate sizes of bearing and control surfaces,
- Determining the type of drive,
- Approximate values of the flight speed and mass parameters.

The set of parameters developed in this way allows for the first analytical calculations and optimisation of the geometry of the analysed object.

4.1.1. Development of the shape concept and geometric assumptions

The concept of the designed aircraft was based on the 1:1 scale Twin Stratos platform developed earlier by SkyTech eLab. The object of research in the form of Twin Stratos in the scale of 1:7 has been reduced accordingly. Due to the determination of the scale, all elements of the drone were determined on the basis of the scale. This resulted in the development of the drone geometry of the analysed (Fig. 16).
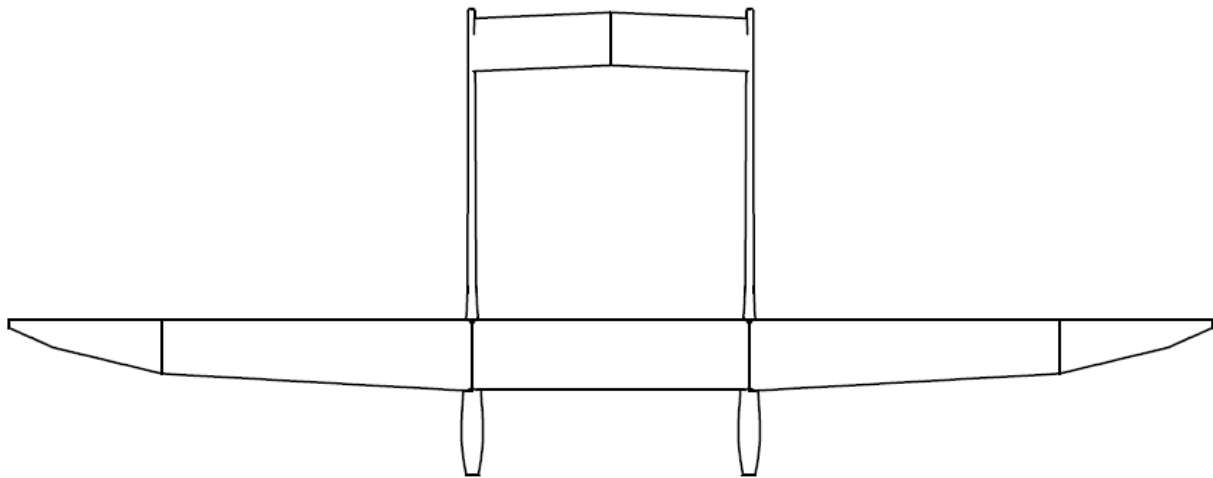
Figure 16 The first concept of the TS 17

Due to the geometric parameters of the 1:1 Twin Stratos project, it was possible to initially determine the distance between the fuselages, the main wing span, the main wing outline, tail parameters, and control surfaces. Scaling, however, turns out to be problematic. It is possible to reduce all dimensions geometrically, taking into account the assumed scale, but it is not possible to change the minimum thickness of the composite layer, the air density in which the scaled model is to move, or the electronic components necessary to control, navigate, or even drive the UAV.

Due to these problems, it was concluded that the UAV Twin Stratos 17, which will be a confirmation of the correct operation of a larger structure, must become a platform aimed at checking the correct operation of most electronic systems. The principles of control, propulsion, and communication have not changed. However, as presented in the following part of the work, the outline of the main wing, the aerofoils used there, the location of additional stiffening composite layers, and many other

elements affecting the balance, stiffness, and behaviour of the structure during flight have been completely changed.

4.1.2. Determination of wing and control surfaces

The surfaces of the analysed structure were presented in the form of a rectangular projection on a plane defined by the span and chord of the main load-bearing panel. Then, on the basis of the view obtained in this way, the surface parameters of the main wing and the tail section were determined. The surface area of the main wing was determined by dividing a given aerofoil into simple geometric figures, which were presented in the form of orthogonal projections on planes determined by chords and spans of given parts. The sum of the given surface areas determined the surface area of the main aerofoil.

The surface area of the tail part, by the system used in the analysed structure, was presented in the form of a rectangular projection on the plane of symmetry and the plane perpendicular to it. Thanks to this procedure, the surface area of the vertical and horizontal stabiliser was determined.

4.1.3. Propulsion system determination

Flight endurance assumptions, an understanding of existing aircraft, and reference to Twin Stratos main design intent allowed the aircraft's propulsion type to be determined. The parameters assumed force the use of a renewable energy source. Due to this, the only possible system is the electric power supply with an additional photovoltaic system that charges the batteries installed in the HALE UAV during flight.

The type of power supply also forces the use of a propulsion system in the form of electric motors in combination with propellers generating thrust, allowing for the achievement of the assumed mission parameters.

4.1.4. Determination of initial flight speeds and mass parameters

With data of the lifting surface and the type of power supply for the propulsion system, it is possible to determine the approximate flight parameters and mass parameters based on existing structures. The multitude of existing structures allows the estimation of these data on the geometrical parameters of a given structure and the assumed maximum flight altitude.

4.2. The second designing stage

The stage of designing and optimising the shape introduces the first confirmation of the assumptions adopted in the form of the results of analytical calculations. At this stage, all adopted aerodynamic coefficients, exact sizes of individual surfaces, assumptions regarding rudder deflections, and the impact of weather conditions on the ability to fly at particular altitudes are determined. In this loop, the following analyses are performed, and the given parameters are defined:

- Air parameters at the considered flight altitudes,
- Mass distribution and the location of the centre of gravity,
- Analysis of longitudinal and transverse stability,
- Determination of moments of inertia and controllability,
- Analysis of geometric parameters,
- Analysis of aerodynamic parameters,
- Aerodynamic load distribution analysis,
- Analysis and optimisation of the drive system.

4.2.1. Determination of air parameters depending on flight altitude

Flight capability and parameters related to load capacity and speed are functions of air density and temperature, therefore it is necessary to include a thermodynamic model in the design methodology. The atmosphere at stratospheric altitudes is much thinner, leaving less air flowing around the wings to generate lift, drag from the propellers to generate thrust, and convection properties are very important for dissipating excess heat. For both the propulsion system and for aircraft equipped with photovoltaic panels, overheating components related to energy acquisition or thrust generation can be disastrous for an unmanned aerial vehicle. Durisch, Urban, and Smestag [67] show that the total irradiance slightly affects the efficiency of Si cell photovoltaic modules, which is consistent with the range of irradiance in the stratosphere. However, experimental data on Si cell photovoltaic modules [67] [68]show that the surface temperature of the photovoltaic modules shows a linear relationship with the absorption efficiency. The issue of temperature removal from working solar panels is not the main problem presented and solved in this work, and only its occurrence has been signalled. The most important problem related to the high altitude at which HALE UAV aircraft operate is the change in air density, which has a huge impact on the thrust generated by propeller propulsion systems and on the lift generated by the main wings. Due to the high accuracy of the calculations, the change in the gravitational acceleration value depending on the flight altitude was taken into account.

As in the case of the calculations presented by Chang and his team [26] , in the case of the presented HALE UAV Twin Stratos, the weights of individual components were taken into account, and the location of the centre of gravity and all aerodynamic forces were determined for the heights considered with a jump of one thousand metres. Due to changes in air density, not only the lift force, but also the aerodynamic drag generated by the aircraft decreased. The method adopted to determine air parameters depending on height was based on the methodology presented and described in reports by NASA [69].

4.2.2. Mass distribution and the gravity centre location

Centre of gravity tests are usually identical regardless of the type of aircraft being designed. The methodology defined by Stafiej in his work on glider design [70] can be successfully used to conduct UAV mass analyses of UAVs.

The proposed methodology assumes the determination of masses based on :

- Preparation of a profile drawing of the tested object,
- Determination of a reference system that does not overlap a given contour,
- Description of all assumed masses based on the assumed frame of reference.

The elements are described in the form of a table, where each of them is assigned the value of its own mass, position from the X axis (horizontal, along the axis of the aircraft), Y (horizontal, along the main wing span), and Z (vertical) axis (Fig. 17). The presentation of the parameters in the form of a table makes it easier to determine the sum of all masses and further analyses of inertia.
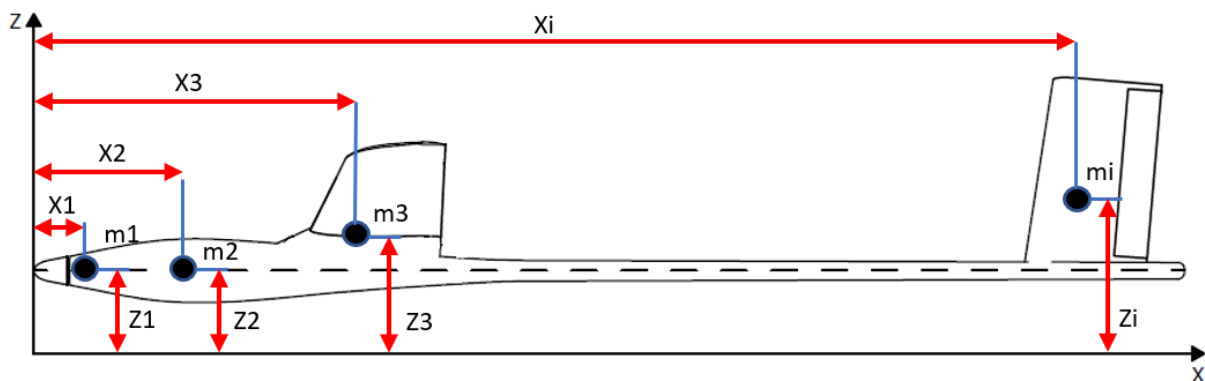
Figure 17 The coordinate system adopted for the analysis

29

The determination of the location of the centre of gravity is based on a system of equations that takes into account the masses and distances from the origin of the coordinate system. The weight of the tested system is determined on the basis of the sum of the weights of all component elements (Q_i), which are multipliers of the masses of each element (m_i) and gravitational acceleration (g):

$$Q_i = m_i \cdot g \tag{4.1}$$

The resultant distances from all axes of the coordinate system are determined by the following dependencies:

$$X_{cg} = \frac{\sum_{i=1}^{n} m_i \cdot g \cdot x_i}{\sum_{i=1}^{n} m_i \cdot x_i} = \frac{\sum_{i=1}^{n} m_i \cdot x_i}{\sum_{i=1}^{n} m_i}$$

$$Y_{cg} = \frac{\sum_{i=1}^{n} m_i \cdot g \cdot y_i}{\sum_{i=1}^{n} m_i \cdot y_i} = \frac{\sum_{i=1}^{n} m_i \cdot y_i}{\sum_{i=1}^{n} m_i} \tag{4.2}$$

$$Z_{cg} = \frac{\sum_{i=1}^{n} m_i \cdot g \cdot z_i}{\sum_{i=1}^{n} m_i \cdot z_i} = \frac{\sum_{i=1}^{n} m_i \cdot z_i}{\sum_{i=1}^{n} m_i}$$

Due to the planned use of electric power supply and additional load in the form of a fixed measuring system, the analysed structure does not require re-analysis of the location of the centre of gravity. However, this can be done by an analysis that does not take into account the load on the measuring apparatus.

In the case of analysis of fixed-wing aircraft, it is important to determine the location of the determined centre of gravity in relation to the mean aerodynamic chord. This is usually expressed as a percentage of the mean length of the reference chord. For this purpose, the location of the centre of gravity along the direction of the mean aerodynamic chord (MAC) is determined and its length is subtracted.

$$X_{l0} = X_{cg} - X_{MAC} \tag{4.3}$$

Then, after presenting the length of the MAC as "l_0", the percentage position of the centre of gravity was obtained in the form [%MAC].

$$\overline{X_{l_0}} = \frac{X_{l_0}}{l_0} \cdot 100 \tag{4.4}$$

4.2.3. Determination of moments of inertia and controllability

During calculating dynamic loads, it is necessary to know the moments of inertia of the analysed object with respect to three perpendicular axes passing through its centre of gravity (Fig. 18). They are marked with capital letters "X", "Y", "Z".
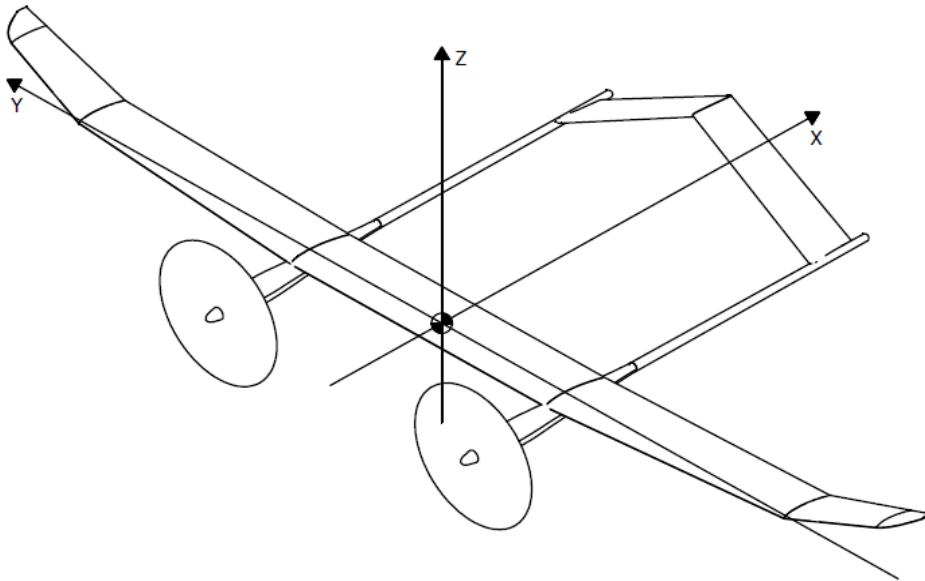
Figure 18 The coordinate system of the centre of gravity of the analysed object

The new coordinate system passing through the centre of gravity of the analysed object is shifted relative to the previously adopted system with the values Xcg, Ycg and Zcg determined on the basis of Equations 4.2.

Determining the moments of inertia relative to the new coordinate system requires redetermining the position of each element relative to the axes passing through the centre of gravity. Due to this, the distances of the mass 'm$_i$' from the new axles are:

$X_i - X_0$ — along the 'X' axis,
$Y_i - Y_0$ — along the 'Y' axis,
$Z_i - Z_0$ — along the "Z" axis.

Assuming the location of the gravity centre in the plane of symmetry, the value y$_0$=0 can be assumed. Due to the layout of the analysed aircraft, a decision was made not to adopt such a simplification. Due to this, the distances of individual masses from the axis of the system, expressed in the form of mass coordinates, are:

$$
\begin{aligned}
R_{X_i} &= \sqrt{(y_i - y_0)^2 + (z_i - z_0)^2} \\
R_{Y_i} &= \sqrt{(x_i - x_0)^2 + (z_i - z_0)^2} \\
R_{Z_i} &= \sqrt{(x_i - x_0)^2 + (y_i - y_0)^2}
\end{aligned}
\qquad (4.5)
$$

Based on the distances and mass parameters, it is possible to finally determine the inertia parameters of the tested object. They are determined in relation to three axes, and the equations are as follows:

$$
\begin{aligned}
J_X &= \sum_{i=1}^{n} \left(m_i \cdot R_{X_i}^2 + J_{0xi} \right) \\
J_Y &= \sum_{i=1}^{n} \left(m_i \cdot R_{Y_i}^2 + J_{0yi} \right) \\
J_Z &= \sum_{i=1}^{n} \left(m_i \cdot R_{Z_i}^2 + J_{0zi} \right)
\end{aligned}
\qquad (4.6)
$$

It should be remembered that each of the elements of the tested aircraft has its own values of inertia parameters based on the shape and own weight. These values have been included in the above equations (4.6), in the form of the values of the components J_{0x}, J_{0y} and J_{0z}.

4.2.4. Geometric parameters analysis

Geometric parameters are determined for a given structure. For the object analysis of the tested in the form of HALE UAV Twin Stratos 1:7, this analysis was divided into a wing, a part concerning the main wing and a part concerning the tail part.

4.2.4.1. Main wing analysis

As in the case of other parts, the geometrical parameters of the main wing are a function of the contour. A generally accepted simplification is the division of the wing in the plane of symmetry of the aircraft. The wing geometry is described by the following parameters:

„b" – wing span,

„l" – chord, defined as a function of span $l_y = f(y)$

„S" – the surface of the main wing. It is referred to as a dependency (3.7):

$$S = 2 \cdot \int_0^{\frac{b}{2}} l_y dy \tag{4.7}$$

„λ" – elongation, given by the equation:

$$\lambda = \frac{b^2}{S} \tag{4.8}$$

"l₀" – mean aerodynamic chord (MAC):

$$l_0 = \frac{2}{S} \int_0^{\frac{b}{2}} l_y^2 dy \tag{4.9}$$

„y$_{l0}$" – the distance of the mean aerodynamic chord from the plane of symmetry of the test object. It is defined by the equation:

$$y_{l0} = \frac{2}{S} \int_0^{\frac{b}{2}} l_y \cdot y \cdot dy \tag{4.10}$$

Accurate determination of the aerofoil parameters also requires determining the geometry of the leading edge determined by offsetting the leading edge from the straight line perpendicular to the plane of symmetry of the analysed wing and passing through the leading edge of the chord "ly₁" by the distance "X$_c$". The offset value X$_c$ is determined based on equation (4.11), and the parameter "d" is the offset from the previously determined perpendicular to the plane of symmetry by the last chord of the trapezoidal part of the wing:

$$X_c = \frac{2 \cdot d}{b} \cdot y \tag{4.11}$$

The lift of the wing is determined by the chord angle "θ" between the plane and the horizontal plane. The horizontal plane is determined by the intersection of the plane of symmetry and the plane of the chords. The line formed at the intersection of these planes determines the plane perpendicular to the plane of symmetry and is a reference used to determine the sheer of the analysed wing. The angle of slope is determined by the relation (4.12). The "H" parameter is the distance of the last chord of the analysed wing from the previously determined reference plane:

$$X_c = ar\,ctg\frac{2 \cdot H}{b} \tag{4.12}$$

4.2.4.2. Tail unit analysis

The aircraft controls usually consist of two wings, a vertical stabiliser, and a horizontal stabiliser. There are many types of geometry of these elements and their arrangement in relation to each other and the plane of symmetry. Usually the shape of these elements is based on a rectangle or a form similar to a trapezoid. Calculations based on the geometry of such systems give very good results on the controllability parameters of the analysed objects.

The geometrical parameters of the tail height are identical to those of the trapezoidal wing, the only difference being the division between the control surface and the stabiliser defined by "depth".

$$\tau_H = \frac{l_{Htuc}}{l_{Htu}}$$

(4.13)

Where:

l_{Htu} – rudder chord, from the axis of rotation to the trailing edge

l_{Htuc} – horizontal tail chord

The depth is defined in the section of the mean reference chord of the tail unit. The geometric quantities characterising the tail height are distinguished by the "Htu" index, while the quantities relating to the stabiliser are distinguished by the "Htuc" index.

The tail height arm is the distance between the point lying in 25% of the mean reference chord of the tail height (a.c.)H and the centre of gravity of the analysed object (Fig. 19).
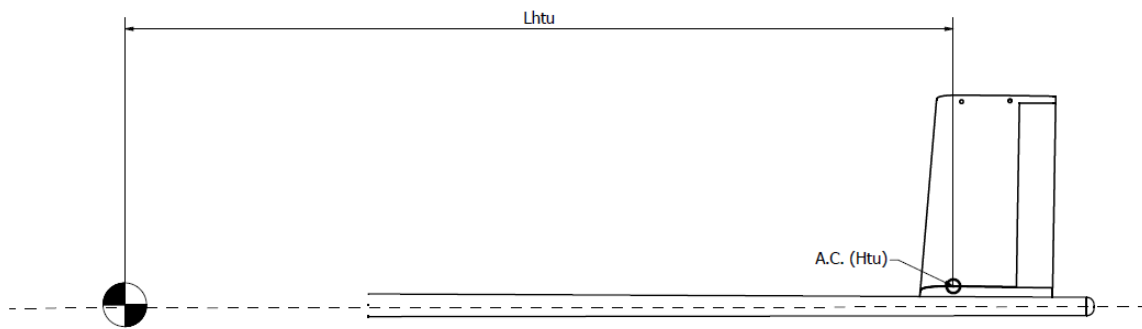
Figure 19 Elevator arm

The actual outline of the tail is replaced with a trapezoid matched to the shape of the tail (Fig. 20), so that the lower edge of the trapezoid rests on the fuselage axis plane, and the upper one runs through the average line of the top of the tail.
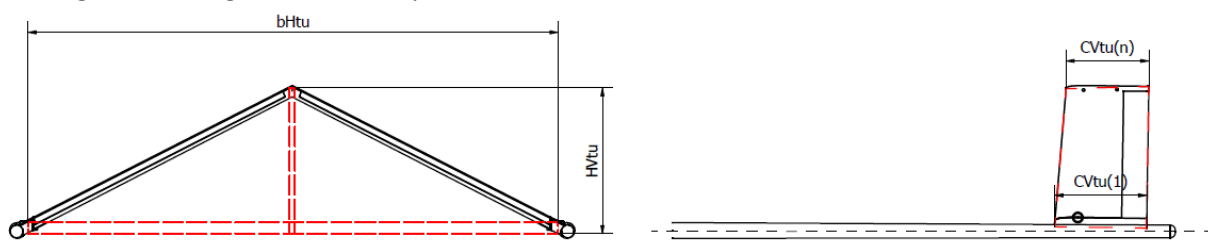
Figure 20 Directional tail outline

The calculation methodology used to determine the geometrical dimensions of the vertical stabiliser itself is the same as in the case of the horizontal stabilizer. The main differences are based on nomenclature. Parameters related to the vertical stabiliser of the tail part are usually marked with the "Vtu", while the values referring to the rudder itself are marked with "Vtuc".

The tail arm is the distance between the point lying in 25% of the mean reference chord of the tail A.C. (Vtu) and the centre of gravity of the analysed aircraft (Fig. 21).
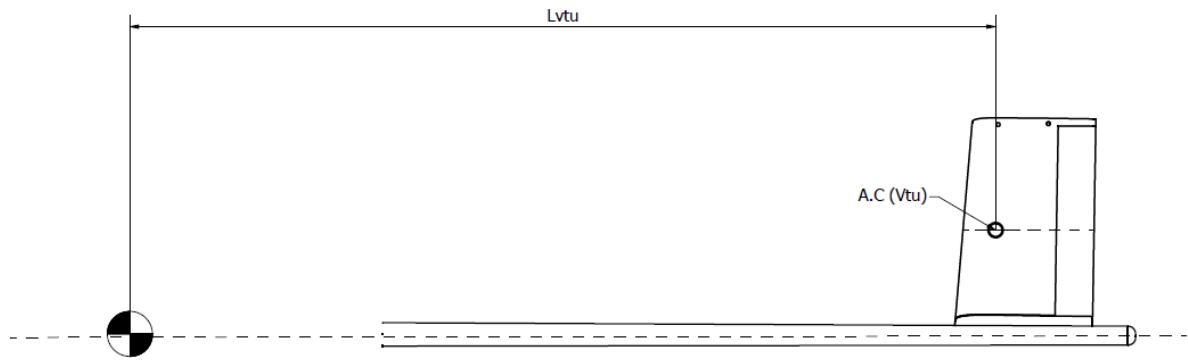
Figure 21 Rudder arm

4.2.5. Aerodynamic parameters analysis

The wing aerofoil determines the performance and flight characteristics of the designed aircraft. The selection of the aerofoil is made according to criteria depending on the type of application, various ones corresponding to the goal set by the constructor. The most common criteria are:

- Lift coefficient for the critical angle of attack,
- The value of the drag coefficient in the ranges of angles of attack of interest to the constructor,
- Gentle course of the stall,
- Symmetry or almost symmetry of the aerofoil characteristics for positive and negative angles of attack.

The wing can have a uniform aerofoil along the span of the entire wing or a variable one. Changing the aerofoil of an aircraft wing, i.e. mixing, can be done in various ways. The most common ways of mixing aerofoils are shown in the figure (Fig. 22). The diagonal line defines the multiplier with which the parameters of a given aerofoil affect a given part of the aircraft wing. The dashed lines indicate the boundaries of the aerofoil blending.

The aerodynamic properties of an aerofoil are usually determined based on analyses performed in a real wind tunnel. Due to the increasing computing power of computers and the development of numerical methods, the analysis of newly developed aerofoils and entire wings is performed through analysis in a digital environment. In both cases of analysis, the results are provided in the aerofoil catalogues in the form of graphs of aerodynamic coefficients as a function of the angle of attack. The analyses are performed with a constant Reynolds number and the variable is the angle of attack of the tested wing. The Reynolds number is determined from Equation 4.14:

Figure 22 Aerofoil mixing methods

$$Re = \frac{v \cdot l}{V}$$

(4.14)

Where:

V – velocity of fluid flow,

l – aerofoil chord length,

v – kinematic viscosity coefficient of the fluid. For air $v = 14{,}53 \cdot 10^{-6} \left[\frac{m^2}{s}\right]$

34

The exact methodology for determining the parameters of the mixed wing was presented by Stafiej [70]. In his work, he presents a detailed methodology for the analysis of wing aerofoils and the application of results based on gliders.

4.2.6. Aerodynamic load distribution analysis

Deformation analyses, strength analyses and structural stability analyses require determination of critical forces acting on the tested wing.

4.2.6.1. Load distribution along the chord

The quantities allowing to determine the pressure distributions along the chord are:
- Wing aerodynamic coefficients,
- The flight speed "V" is associated with the angle of attack "α", causing dynamic pressure. This parameter is described by Equation 4.15. Parameter ρ in presented equations is fluid density.

$$q = \frac{1}{2} \cdot \rho \cdot V^2 \tag{4.15}$$

The distribution of pressures on the nonbroken aerofoil (Fig. 23) located at the given angle of attack "α", the characteristic pressures are:

$$p_0 = (11 \cdot Cl - 60 \cdot Cm) \cdot \frac{1}{8} \cdot q \tag{4.16}$$

$$h_0 = (25 \cdot Cl - 300 \cdot Cm) \cdot \frac{1}{8} \cdot q \tag{4.17}$$

Where:

Cl - coefficient of lift force, force normal to the bearing surface,

Cm – moment coefficient relative to a point at 25% of the chord of the aerofoil.
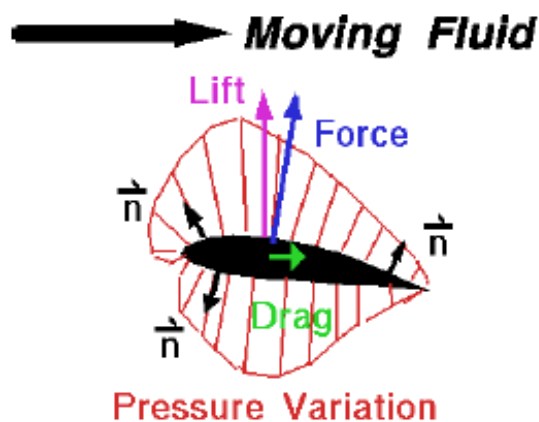
Figure 23 Pressure distribution along the chord of the wing (n – moving fluid) [71]

4.2.6.1. Load distribution along the wing span

There are various analytical methods for calculating the lift distribution of the coefficient along the wing span. With modern computer software, the calculation of the lift distribution along the span of the analysed wing is not difficult. However, for quick initial information needed by the constructor, it is good to resort to the empirical Schrenk's method, which gives an error in relation to analytical methods so small that it is not significant in technical applications. Therefore, the algorithms of this method are discussed here.

This methodology is correct both for determining the normal distribution of the wing with a constant and variable aerofoil. For the angle of attack of the wing "α „the magnitude of the lift coefficient in the cross section "i" of the wing is:

$$Cl_i = \frac{1}{2} \cdot \frac{Cl}{d\alpha} \cdot \alpha \cdot \left[1 + \frac{4S}{\pi b l_i} \sqrt{1 - \left(\frac{2y_i}{b}\right)^2} \right]$$ (4.18)

To perform the calculation tabularly, the wing should be mentally divided into "n" calculation segments (i = 1,2 .....n). Each segment (Fig. 24) is characterised by the chord in the middle of the segment "l_i" and the width of the segment "Δy_i".
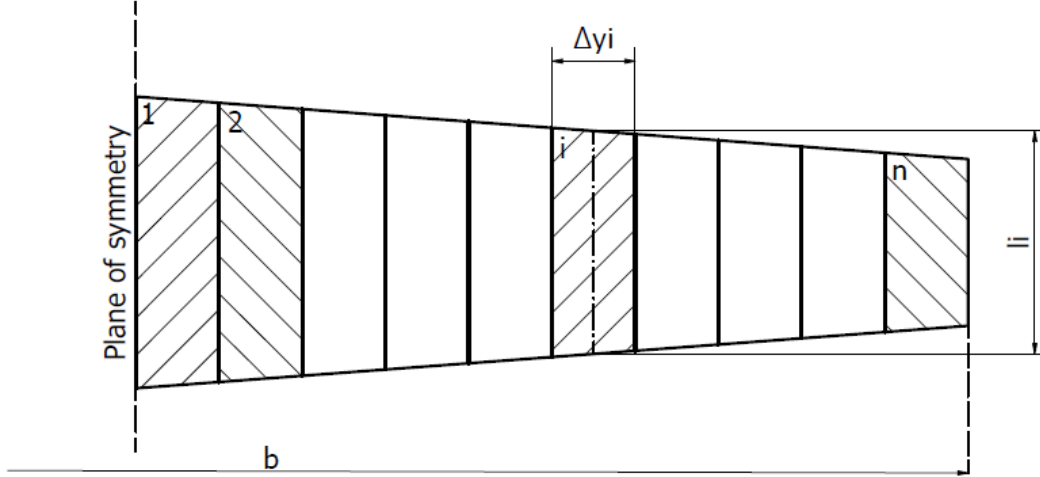
Figure 24 Mental division of the wing into segments

During the analysis, it is necessary to determine the values of the constants used in the calculations. They should be determined on the basis of equations 4.19 and 4.20:

$$A_1 = \frac{1}{2} \cdot \frac{Cl}{d\alpha} \cdot \alpha$$ (4.19)

$$A_2 = \frac{4S}{\pi b}$$ (4.20)

In the case of a variable aerofoil along the span, the average slope value is determined. It is determined on the basis of equation 4.21:

$$\left(\frac{dCl}{d\alpha}\right)_{mean} = \frac{2}{S} \sum_{i=1}^{n} \left(\frac{dCl}{d\alpha}\right)_i \cdot l_i \cdot \Delta y_i$$ (4.21)

Then the size of the lift coefficient is determined on the basis of the relationship 4.22:

$$Cl_i = \frac{1}{2} \left(\frac{dCl}{d\alpha}\right)_{mean} \cdot \alpha \cdot \left[\frac{\left(\frac{dCl}{d\alpha}\right)_i}{\left(\frac{dCl}{d\alpha}\right)_{mean}} + \frac{4S}{\pi b l_i} \cdot \sqrt{1 - \left(\frac{2y_i}{b}\right)^2} \right]$$ (4.22)

Determine the value of the constant using equation 4.23:

$$A_3 = \frac{1}{2} \cdot \left(\frac{Cl}{d\alpha}\right)_{mean} \cdot \alpha$$ (4.23)

4.2.7. Stability analysis

Stability is the ability of the system to restore a state of equilibrium from which the system has been lost. Static stability tells whether a system tends to return to equilibrium, while dynamic stability determines how the system returns to equilibrium over time. The stability analysis of the tested object was divided into two parts:

4.2.7.1. Longitudinal stability

The pitching moment coefficient (Cm) of the fuselage relative to the MAC of the point located at 25% of the wing depends on the wing wedge angle α_z relative to the zero line of the fuselage capacity. If the designed aircraft results of the tunnel tests are not available, it should be assumed that the line of

36

zero load capacity of the fuselage is a straight line connecting the tip of the fuselage nose with a point lying in the middle of the height of the fuselage at the end [70].

To determine the pitching moment of the entire analysed object, it is necessary to determine the value and position of the resultant tangential force consisting of the analysis of all aerodynamically significant elements of the tested structure. In other words, the values of the drag and lift forces generated by the main wing, tail unit, and fuselage, and their exact location should be determined (Fig. 25). On their basis, the resultant is determined.
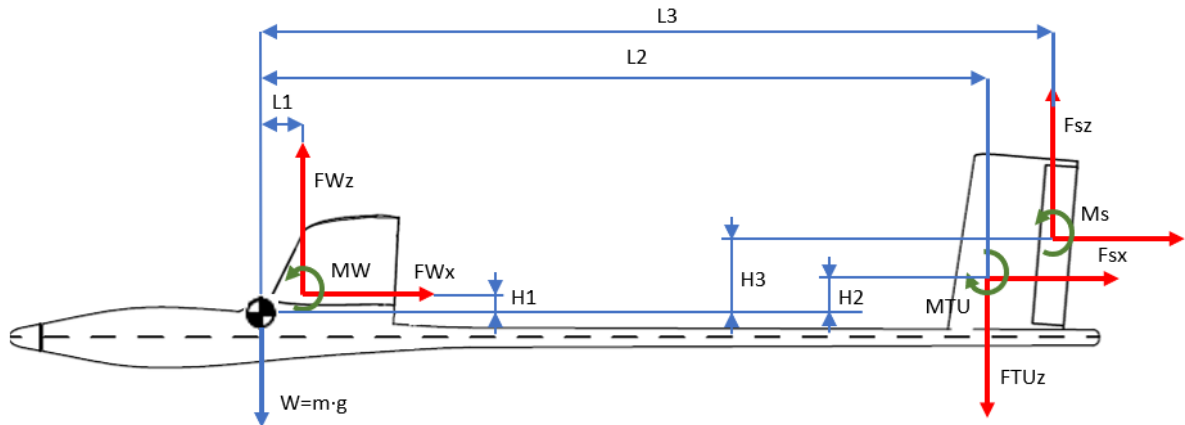
Figure 25 Forces acting on the UAV analysed

Where: FWz - lift of the wing, FWx – drag of the wing, MW – wing pitching moment, FTUz – lift of tail unit, FTUx – drag of tail unit, MTU – tail unit pitching moment, Fsz – lift of elevator, Fsx – drag of elevator, Ms – pitching moment of elevator, L1 – main wing aerodynamic centre to gravity centre distance along "x" axis, H1 - main wing aerodynamic centre to gravity centre distance along "z" axis, L2 – tail unit aerodynamic centre to gravity centre distance along "x" axis, H2 – tail unit aerodynamic centre to gravity centre distance along "z" axis, L3 – elevator aerodynamic centre to gravity centre distance along "x" axis, H3 - elevator aerodynamic centre to gravity centre distance along "z" axis,

The developed system of forces allows for precise determination of the pitching moment of the tested object.The determination of the moment itself is based on analytical techniques for solving the stresses of linear systems in the place of attachment is the aerodynamic centre of the analysed object.

The analysis was based on the Clebsch method, which consists of the analytical solution of a heterogeneous differential equation of a bent beam with appropriate boundary conditions and a properly set external load distribution [72].

The state of equilibrium of the UAV around the lateral axis (longitudinal stability) occurs in an isolated form, while the state of equilibrium around the vertical axis (lateral stability) and the longitudinal axis (rolling stability) are related and do not occur separately. Therefore, this complex state of equilibrium is called transverse equilibrium.

The issue of lateral stability requires analysis only for unconventional systems. In the case of conventional structures, the symmetry of the UAV relative to the vertical plane passing through its longitudinal axis automatically creates favourable conditions for proper lateral stability. For this reason, lateral stability calculations are not usually performed.

The correctness of the "lateral" characteristics of the analysed object is checked during flight tests, and only when they show any irregularities, the designer must take countermeasures, individual for each case of instability.

4.2.8. Propulsion system analysis

The propulsion system usually consists of three parts (engine and its control electronics, propeller), usually does not include a transmission due to the necessary reliability in long-term operation and extreme conditions. The sum of the weight of the drive system is proportional to the maximum continuous power on the drive shaft, referred to as (Pp)max, and inversely proportional to the power to weight ratio of the designed drone, referred to as Sigma(p). While resting flight is the main

requirement for flight, greater power for take-off, climb, and flight into stratospheric winds and low-altitude turbulence must be taken into account. Generally, the ratio of maximum continuous shaft power to shaft power in level flight, called μ(p), is about 2 to 3.

Due to the results, the minimum thrust that should be generated for the level flight was determined. The optimal thrust was also determined to allow performing all assumed manoeuvres and ensure an appropriate safety factor. Calculations, however, allow only theoretical values to be determined. The value generated during the propeller calculation is based on the pitch and does not take into account the slip occurring during the rotation of the propeller. Slip greatly reduces the amount of thrust generated. This relationship is shown in the graphic (Fig. 26).
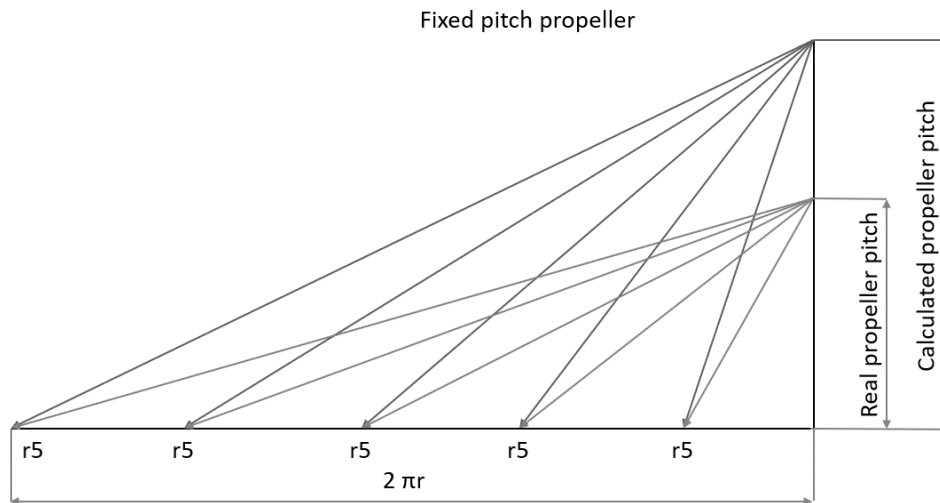
Figure 26 Difference between theoretical and actual thrust for the tested propeller radius (r)

At this stage of the analysis, theoretical research is insufficient to determine the value of the thrust that is achievable by the designed drive system. The string value was analysed under laboratory conditions. The drive system itself can also be optimised. Usually, tests and optimisation of drive systems are performed on specially prepared stands in the form of a measuring stand.

The main purpose of using the measuring stand is the possibility of performing various analyses of the drive system due to the design and production stage of the UAV analysed. The types of testing and optimisation of the electric drive system can be divided into:

- Analysis of the generated propeller thrust,
- Optimisation to reduce energy consumption,
- Analyses to adjust the drive parameters to the requirements of the structure,
- Drive system failure analysis.

4.3. The third designing stage

At this stage, the initial layer thicknesses of the materials used are developed, stiffeners are planned, the internal structure, and other parameters related to the preparation of the designed UAV for production are determined. At this stage, the designed UAV is mapped as a digital twin of a non-existent structure.

The key for a given stage is the correct determination of the parameters of the materials used in the prepared model, the types of connections between the individual elements of the structure, and the introduction of simplifications for stiffening points that often occur during modelling. At a given stage of the analysis, the following parameters are determined and tests are performed:

- Mapping of the external structure of the analysed UAV,
- Numerical Aerodynamic Analyses,
- Determination and modelling of the initial internal structure,

- Determining the materials of individual components,
- Mass analysis, determining the location of the centre of gravity of the designed UAV for various planned configurations.

4.3.1. Development of the external structure of the analysed aircraft and numerical aerodynamic analysis

Depending on the type of software used, it is possible to determine the geometry of the tested aircraft on the basis of the following:

- Flat surfaces - taking into account load bearing parameters and resistance adopted for the analysis of aerofoils and shapes (Fig. 27). The problem with this method is the need to determine the parameters using another method and then enter them into the computing environment. Programmes based on this method include the MatLab AeroFlex extension, developed by Riberio and his team [73].
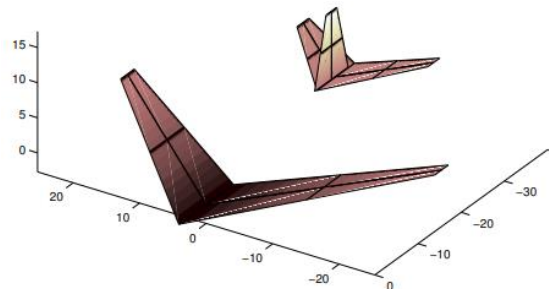
Figure 27 Example of aeroplane modelled in AeroFlex [71]

- Solids - taking into account the shape of the main load-bearing elements connected with each other by geometric relationships. A method that allows to generate a simplified model of the analysed structure and determine the aerodynamic parameters of the modelled parts (Fig. 28). Due to the inability to model aircraft with fuselages located offset relative to the plane of symmetry, the XFLR5 programme was included in this group [74].
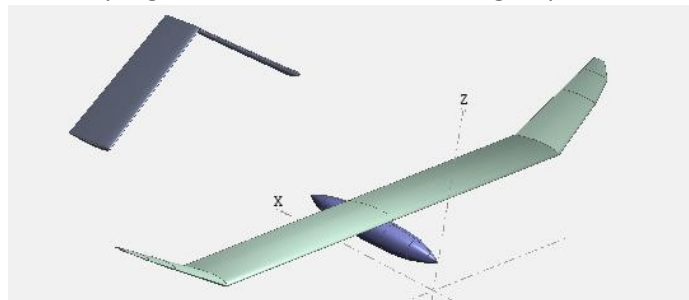
Figure 28 Example of aeroplane modelled in XFLR5

- Accurate geometric model - including all elements of the external outline of the analysed object. Aerodynamic analyses of this type can be carried out using many programmes. The number of possible environments is growing, taking into account the fact that the preparation of the model of the analysed object does not have to be done in the programme that performs the analysis. Analysed solids can usually be imported. Ansys is an example of an environment that allows model preparation and analysis (Fig. 29).
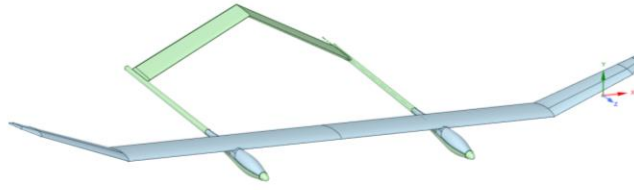
In the case of the analysed Twin Stratos 1:7 structure, all three types of software presented were used at a given stage of the analysis to compare the results and determine the degree of correctness.

The computational fluid dynamics (CFD) tool ANSYS-Fluent, which solves problems according to the finite volume method, is used to compare the CL and CD results obtained by the aerodynamic analysis tool. Langtry and Menter developed a new correlation-based flow model to simulate the transition from laminar to turbulent flow [75]. The model is based on two equations of motion. One equation is for the flow start criterion, and the other is for discontinuity. To validate this model, examples of cases that have been studied, such as a three-dimensional flap, a two-dimensional aerofoil and a transonic wing, are given. The transient CFD simulation was found to be very consistent with the experimental results. In the previously mentioned publication, Langtry and Menter compared the following turbulence models for flow over NACA4415 for Re 120000 with experimental results: Spalart-Allmaras, K–ω SST, intermittency SST, k–kl–ω and γ–Re_θ SST [76]. According to the results, only γ-Re_θ SST provided reliable results for low and high α values. Lanzafame and his team developed a three-dimensional CFD model of a horizontally axis wind turbine to predict the performance of a wind turbine [77]. K–ω SST and γ–Re_θ SST were compared with the experimental data. According to the result, the γ-Re_θ SST captured the trend of the aerodynamic coefficients, while the K-ω SST overestimated the Cl values and underestimated the Cd values. Aerodynamic analyses in each of the above cases are performed on the basis of the parameters of the medium in which the analysed object is to move. These parameters are usually selected on the basis of libraries of parameters contained in the given programmes. It is important to select a solver that affects the correctness of the analysis results. The selection is based on the Reynolds number and the types of solver are presented in section 3.3.2 "Numerical methods" of the dissertation.

4.3.2. Determination of the type of internal structure and preliminary acceptance of materials

The type of aircraft structure depends mainly on the application and flight parameters of the designed object. In the case of the analysed TS17 structure, a decision was made to use a self-supporting structure of the main wing skin with the use of one main spar ensuring adequate transverse stiffness of the wing.

The visualisation (Fig. 30) shows the initial assumptions regarding the thickness of the materials used and the location of individual structural elements. As can be seen, the construction was based on a single-chamber caisson closed with a "C" profile.
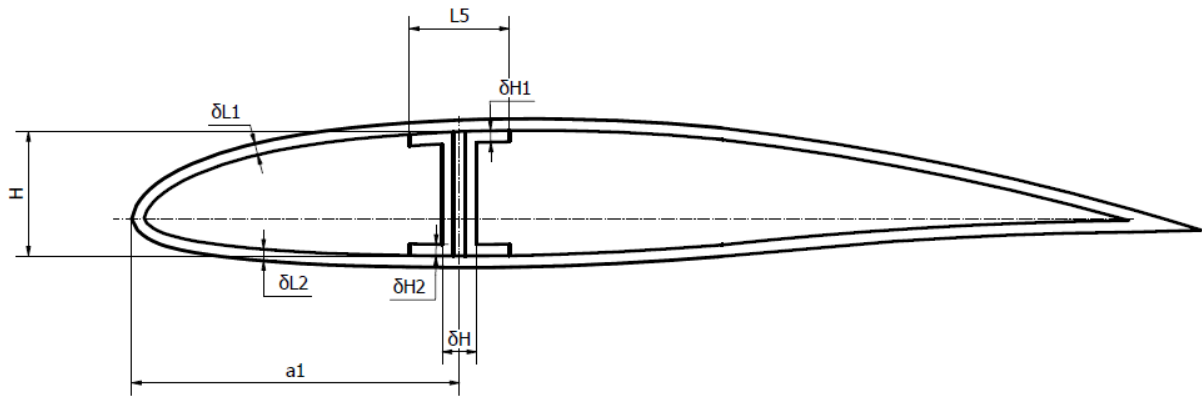
Figure 30 Visualization of structural elements within the wing

Where: H – Main wing spar height [mm], a1 – Distance of main wing spar to the leading edge of the wing [mm], L5 – Main wing spar width [mm], δH – The width of the main spar wall [mm], δH1 – Component 1 thickness of wing spar [mm], δH2 – Component 2 thickness of wing spar [mm], δL1 – The thickness of the upper wing skin [mm], δL2 – The thickness of the lower wing skin [mm]

4.3.3. Numerical mass analysis

Mass analysis enables the correct balance of the aircraft. This task is to ensure controllability and stability during flight. Numerical mass analysis is usually based on the generation of an accurate model of all elements of the internal structure and the use of density parameters of previously selected materials. It is also necessary to map the mass parameters of all components placed in the analysed object. This mapping can be done by replacing exact component models with approximate solids with mass parameters of real objects. This type of approach accelerates the work related to the design and analysis itself.

4.3.4. Numerical strength analysis

Analyses based on structural models and aerodynamic analyses prepared in previous stages of design. Strength analysis can be performed based on linear, surface, or solid models. As in the case of numerical aerodynamic analyses, each of the methods has a direct impact on the labour intensity of the analyses, the time of the analyses themselves, and the quality of the results obtained.

In the case of analyses related to the HALE UAV, the decision was made to use surface models to which the parameters of the materials from which the given components were made. The appropriate determination of the connections between given components and the correct assignment of loads are necessary to ensure the accuracy of the results.

4.3.5. Determination of optimisation parameters of the analysed structure

The main problem of the UAV presented is the very large elongation of the main wing. Its span is twice as long as the full length of the aircraft, and in combination with the small reference chord of the designed wing, it can be a simple recipe for negative aeroelastic flutter phenomena. The aircraft will behave differently at an altitude not exceeding one kilometre and differently at altitudes close to stratospheric. This is influenced, among other things, by the winds that occur at different layers of the atmosphere. In order to perform optimisation and tests, a number of assumptions regarding the designed UAV were defined:

- Analysis is performed for three critical flight conditions covering a given speed and angle of attack.
- The analyses are to take into account the temperatures and pressure values prevailing at individual altitudes,
- The external shape of the analysed object is constant for each of the critical states,

41

- Structural changes are limited by the electronic components within the aircraft wing.

4.4. The fourth designing stage and optimisation

The data were adopted after previous analyses and corrections in the three previous design stages. This is the final verification of the correctness of the designed structure. At this stage of the work, all kinds of strength analyses and bench tests are carried out.

A UAV designed, analysed, and optimised in accordance with this scheme should not exhibit previously unforeseen properties. The key to performing any analysis, either analytical or numerical, is the precision in determining the initial data. If a value was adopted during the initial assumptions and in the third designing stage the assumption turned out to be wrong, it is necessary to change the parameter in the place of occurrence and recalculate the values it affects. The following steps are performed at this stage:
- Development of the internal structure of the analysed wing,
- Static analysis of structures in previously determined critical states.

4.4.1. Static structural analysis for specific critical states

Analyses based on previously prepared structural models and aerodynamic analyses. Strength analyses can be performed based on linear, surface or solid models. As in the case of numerical aerodynamic analyses, each of the methods has a direct impact on the labour intensity of the analyses, the time of the analyses themselves and the quality of the results obtained. In the case of analyses related to the presented HALE UAV, a decision was made to use surface models to which the parameters of the materials from which the given components were made were assigned. The appropriate determination of connections between given components and the correct assignment of loads is necessary to ensure the accuracy of the results.

Increasing the accuracy of the analyses carried out requires modal analyses. This allows to perform a convergence test to select the best number of elements. Due to this method of analysis, the accuracy of the mapping of the analysed elements is increased. The methodology related to similar analyses of the wing was presented by Ali and Saeed in their publication [78].

4.4.2. Optimisation of the structure to reduce the weight of the object

The optimisation plan assumes that the mass of the tested structure is as low as possible while maintaining the stiffness and safety parameters. Optimisation process was developed based on the assumptions presented in the figure (Fig. 31).

Due to the complexity of the designed structure described in the work, the main wing of the designed Twin Stratos 17 UAV will be optimised. As shown in the graphic below, the optimisation is mainly based on determining the exact position of the main spar beam of the wing structure and the number of individual layers of composites included in the stiffener of the main spar.
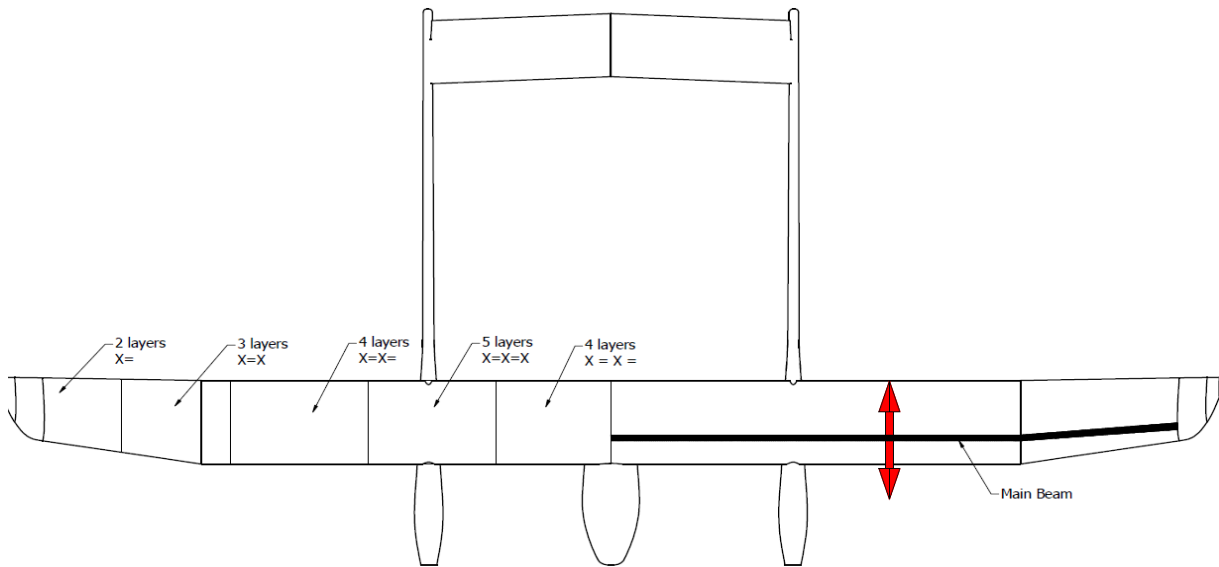
Figure 31 Main assumed elements of the optimised design
Where: X - Laying the composite at an angle of 45° to the wing span, = - Laying the composite along of the wing span

The simplification of work on optimising the UAV Twin Stratos to the form of optimising the main wing is due to the high complexity of the analyses and the lack of comparative data in the form of existing models of the optimised object.

5. Analysis of the developed HALE UAV

To design the structure, conduct analyses, and optimise the main wing of the analysed structure, the methodology developed and presented at this chapter. Subsequently, within the four stages of analysis, the following work was carried out:

- First stage – Initial (geometric) determination of flight parameters:
    - Adoption of initial assumptions, which were determined on the basis of HALE UAV TS11,
    - Determination of the external geometry of the tested object,
    - Estimation of mass parameters and volatile properties based on historical data,
- The second stage - Simplified analytical determination of drone parameters):
    - The exact air parameters prevailing at the planned flight altitudes were determined,
    - Determination of the exact external shape of the analysed object,
    - Accurate aerodynamic characteristics were determined, taking into account the suspension angles and the lift angles of the winglets of the main wing,
    - The distribution of loads along the chord and along the wing span was estimated.
    - The positions of electronic internal components are specified,
    - Determination of the mass and moments of inertia of the analysed structure,
    - The minimum, optimal and maximum flight speeds for each of the considered altitudes were determined,
- Third stage - Numerical aerodynamic analysis and internal structure design:
    - The flight envelope for the designed UAV was determined.
    - Stability parameters in flight for particular flight altitudes were determined.
    - The position of the main wing spar was initially determined,
    - A geometric model was generated in the XFLR5 programme, in which the first numerical aerodynamic analyses were carried out.
- Fourth stage - Numerical analysis and structure strength tests:
    - An exact model of the external structure of the analysed UAV was developed in the Ansys environment ,
    - Aerodynamic analyses were performed, taking into account the entire external shape of the analysed object
    - Structural analysis of the analysed object was performed.

5.1. Results of the analysis performed in the first stage of the analyses

As presented in Chapter 4 "Methodology of analysis and optimisation of the considered structure", the first stage of the analysis aims to determine the exact application of the object analysed. Then, on estimates and historical data, preliminary parameters are determined for the first analyses, which are aimed at confirming the correctness of the adopted assumptions or determining the values that the assumptions should adopt in the next design stages.

The results of the analysis developed at a given stage and related to the TS17 analysis are presented in the following subsections.

5.1.1. Determination of the geometry and initial parameters of the analysed TS17 drone

The geometric data presented in the table (Tab. 6) were developed on the basis of the geometry of the object developed by SkyTech eLab Project Twins Stratos 1:1 and subjected to scaling.

Tab 6 Parameters of UAV TS17

Scale of Twin Stratos	1:7	Unit
Take off mass	9,8	[kg]
Wing area	0,70	[m^2]
Maximum celling	5000	[m]
Aspect Ratio (AR)	16,91	[-]
Maximum flight duration	24	[h]
Payload	2,5	[kg]
Middle chord	0,28	[m]
Wing Span [A]	3,6	[m]
Tail unit area	0,25	[m^2]
Lenght of aeroplane[C]	1,8	[m]
Hight of tail unit [B]	0,29	[m]
Assumed motors power	300	[W]
Propeller revolutions	7000	$\left[\dfrac{rev}{min}\right]$
Propeller diameter	0,4	[m]
Maximum speed	29	$\left[\dfrac{m}{s}\right]$
Stoll speed	11	$\left[\dfrac{m}{s}\right]$
Main Wing aerofoil	Mixed	

The data set prepared in this way was used to make the first sketches of the analysed UAV. Due to the type of drive and power supply specified in the case of the HALE UAV, the decision was made to transfer the given solution to the analysed facility. The result of this activity was the development of preliminary sketches containing photovoltaic panels placed on the upper surface of the main wing (Fig. 32). Based on the determination of the dimensions of the panels mounted on the upper skin of the main load-bearing panel, the possibility of obtaining energy was determined and compared with the energy demand estimated on the basis of similar structures.

A set of geometric data prepared on the basis of the developed concept (Fig. 32) was defined as the initial assumptions used in the analyses presented in the following chapters.
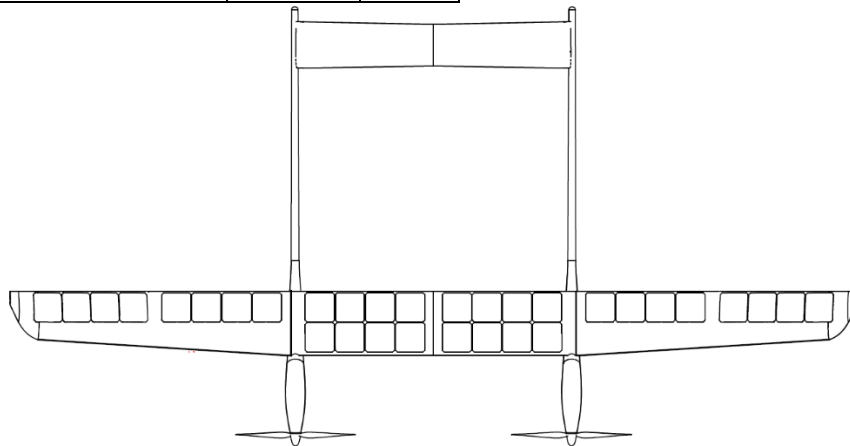
Figure 32 Sketch of the TS17 initial concept

5.2. Results obtained at the second stage of the analysis

The analysis performed at a given stage was based mainly on analytical calculations. The assumption of this stage was to determine the theoretical flight parameters for the developed TS17 concept. The results obtained during the performance of individual analyses at a given stage have been divided and presented in the following subsections.

5.2.1. Determination of air parameters depending on flight altitude

The determination of the flight parameters of the analysed UAV began with the determination of the atmospheric parameters prevailing at individual flight altitudes. Parameters were determined based

on the assumed maximum flight altitude. Due to the adopted safety and system efficiency factors, this altitude has been limited to 5000 metres above sea level.

Due to the need to confirm the safety of the achieved parameters at the assumed altitude, the input data were extended by an additional thousand metres. This increased the number of analyses carried out but confirmed the safety of the parameters achieved. During the analysis, the flight altitude was assumed to be from 0 to 6000 meters above sea level with a step of 1000 meters, and for each of the considered altitudes, the following parameters were determined: pressure at a given altitude, air temperature, gravity acceleration value, air density, the dynamic viscosity of the liquid, and speed of sound. These parameters made it possible to precisely determine the behaviour of the analysed UAV at each of the altitudes considered. This was a key stage due to the selection of appropriate flight speeds and the value of thrust generated by the propellers. These data were determined on the basis of the methodology specified in point 3.1. "Methods of air parameter identification at the analysis flight altitude". The given parameters determined for the individual considered heights are presented in the table (Tab. 7):

Tab 7 Air parameters depending on flight altitude

Air parameters							
Altitude "H" [m]	0	1000	2000	3000	4000	5000	6000
Gravity acceleration "g" $\left[\frac{m}{s^2}\right]$	9,820	9,816	9,813	9,810	9,807	9,804	9,801
Temperature "t" [K°]	293,15	286,65	280,15	273,65	267,15	260,65	254,15
Temperature "t" [C°]	20	13,5	7,0	0,5	-6,0	-12,5	-19,0
Pressure "P" [Pa]	101300	90026	79796	70534	62168	54627	47849
Density "ρ" $\left[\frac{kg}{m^3}\right]$	1,228	1,114	1,009	0,911	0,821	0,738	0,661
Dynamic viscosity "μ" ($\cdot E^{-5}$)	1,750	1,824	1,789	1,754	1,718	1,682	1,647
Speed of sound $\left[\frac{m}{s}\right]$	339,84	336,05	332,22	328,34	324,42	320,44	316,42

5.2.2. Determination of the exact external shape of the analysed UAV and the distribution of aerodynamic loads

To perform analytical optimisations, aerofoils and parameters were adopted on which all calculations were based. They were based on data placed in the "Airfoil Tools" database [79]. The structure is planned to be equipped with a main wing with a mixed aerofoil. This results in additional calculations mixing the parameters of a given part of the wing depending on the distance to the assumed aerofoil. The methodology of aerofoil mixing is presented in the chapter 4.2.5. "Aerodynamic parameters analysis". The places that determine the use of a given aerofoil are shown in the picture (Fig. 33).
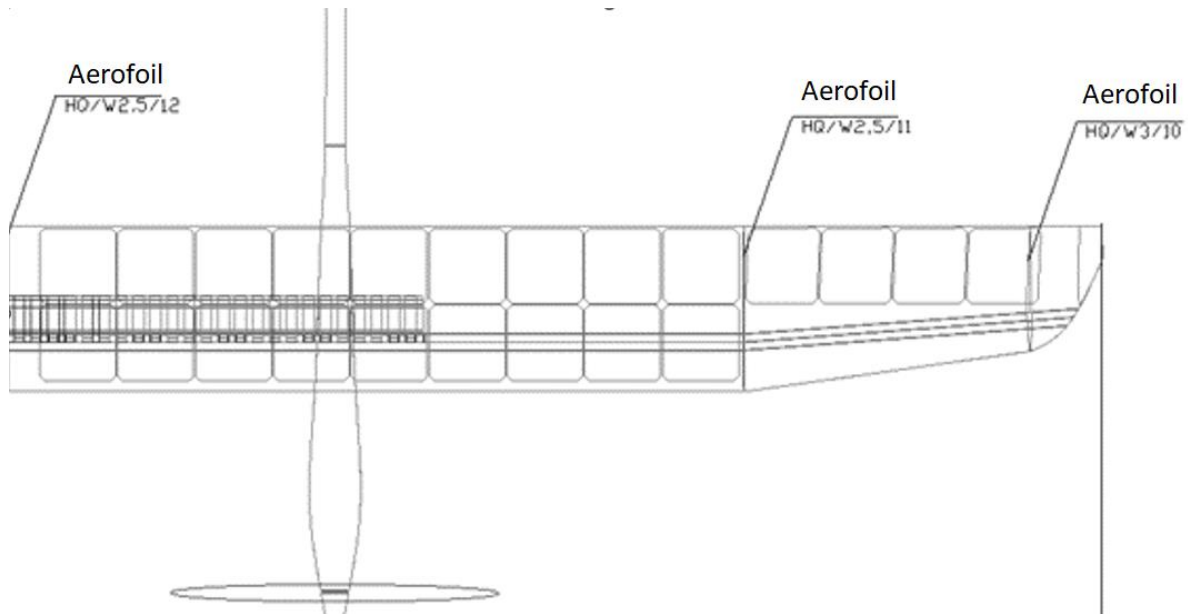
The adopted aerofoils are presented below, together with graphs showing the main aerodynamic parameters in relation to the angle of attack read from a publicly available database of aerofoils. Aerofoil mixing parameters were made during the Schrenk analysis [80]. The parameters of the applied aerofoil as a function of a given variable on the angle of attack are presented in the tables (Tab. 8 – Tab. 11).

Tab 8 HQ 2.5 12 aerofoil shape with parameters
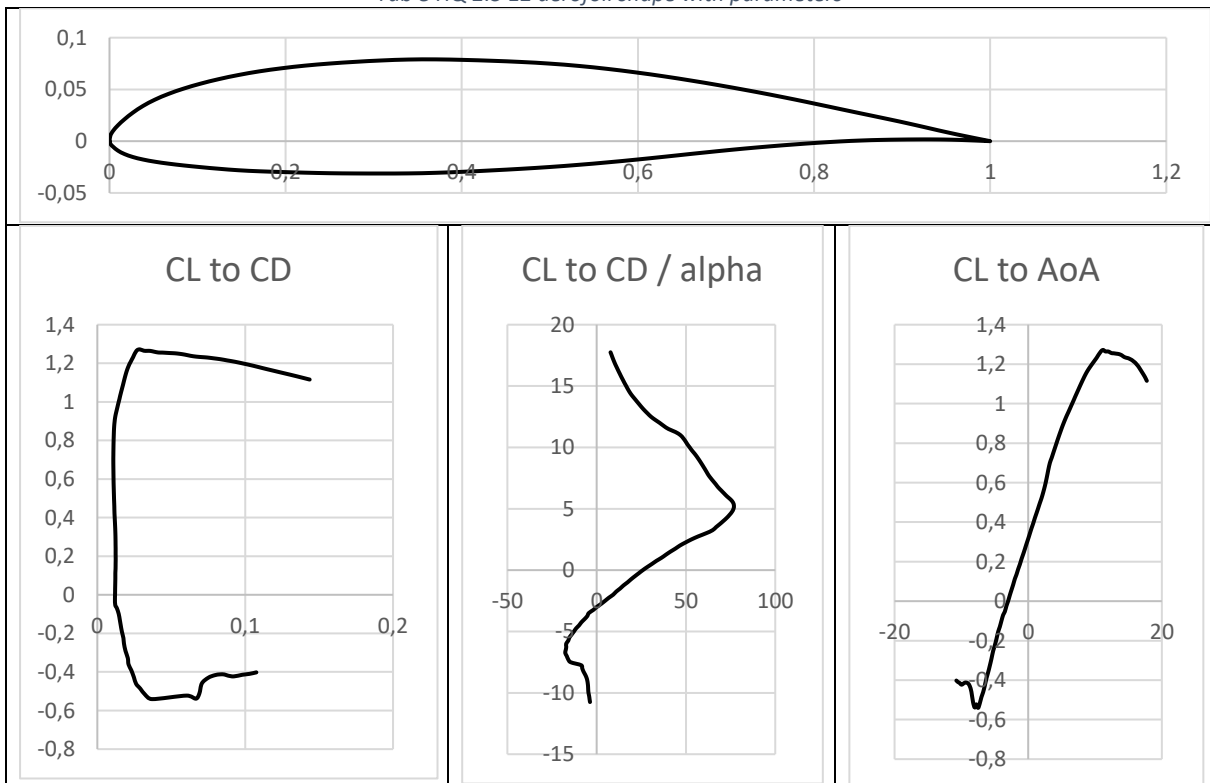
Tab 9 HQ 2.5 aerofoil shape 11 with parameters

CL to CD

CL to CD / alpha

CL to AoA
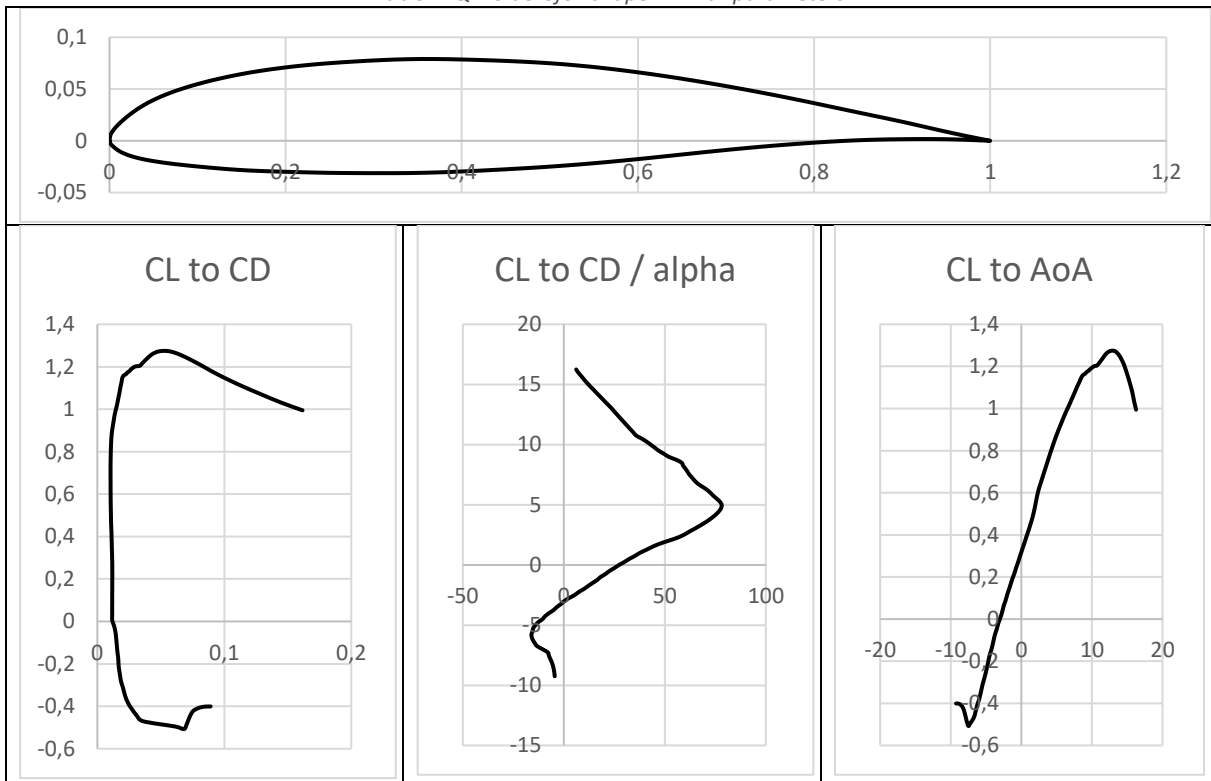
Tab 10 HQ 3.0 10 aerofoil shape with parameters

Cl do Cd

Cl/Cd to AoA

Cl to AoA
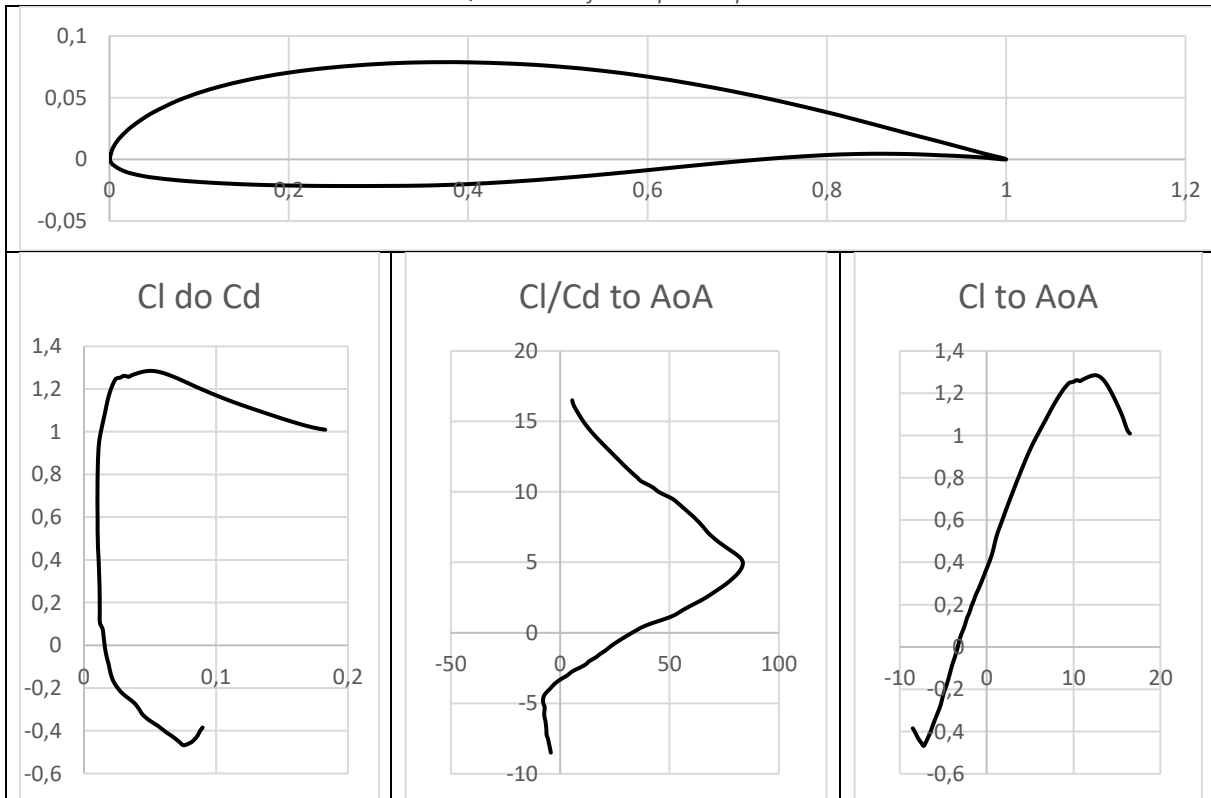
Tab 11 Clark Y aerofoil shape with parameters
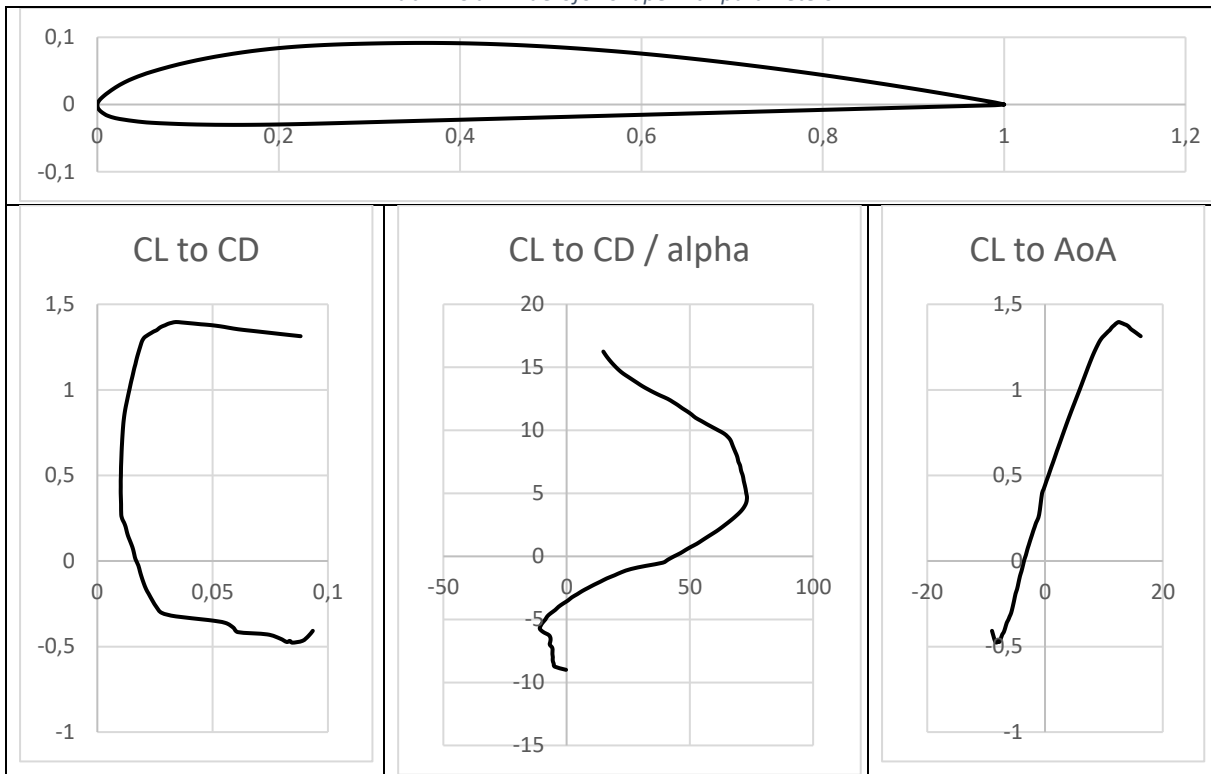
Determination of the coefficients of lift, drag, and pitching moment for the main wing and tail unit was necessary to enable further analysis. In order to perform a thorough analysis of the designed aircraft, the main wing angle, the angle of the tail section, and the UAV angle of attack during level flight were taken into account. The view of the half of the main wing for which the analyses were performed is shown in the photo (Fig. 34).
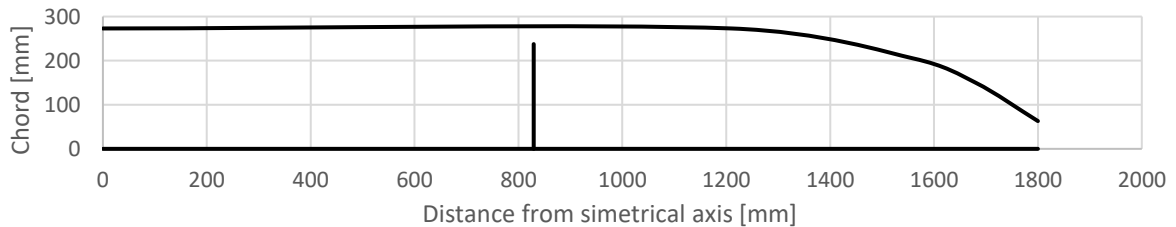
Figure 34 Half of TS17 wing. Top view.

The influence of drag and air flow disturbance through the fuselages was determined on the basis of approximate geometries, suspension angle, and frontal area of a given element relative to the direction of flight.

The distribution of forces that act on the main wing along its length was determined based on the Schrenk approximation [80]. Taking into account the drone fuselages was done by applying a reduction in aerofoil efficiency at the place where the fuselage was attached. This was done based on airbrake efficiency reduction calculations provided by Stafiej [70].

The analysis began by determining the distribution of force coefficients that act on a given section along the length of the wing. Due to the use of a mixed aerofoil on the wing and the complex outline of the main wing, it was necessary to develop a mixing of characteristics. Because the differentiation of the aerodynamic coefficients occurs as a result of different Reynolds numbers in individual cross sections. The mixing of parameters was made on the basis of geometric relationships. Thanks to this procedure, it was possible to demonstrate the continuity of loads acting on the wing, and there was no problem related to the full forces generated by two aerofoils on one of the considered parts.

Due to the lack of additional control surfaces located on the main wing, the pressure distribution along the chord in each of the considered wing elements depended only on the aerofoil parameters or aerofoil mixing and the length of the chord itself. The other parameters of the entire main wing were not changed, and there was no need to determine the parameters of the divided wing.

The mental division of the wing into the analysed element is presented as in the picture below (Fig. 35). Based on these divisions, the forces and moments acting on the wing were determined. Each of the lines dividing the wing defines the analysed chord. The area loading a given chord is half of the designated area on the right and to the left of the line. The last chord of the wing, the tip, is loaded only with half of the area according to the wing span, and the line located in the axis of symmetry is loaded with half of the area according to the wing span. The use of such a simplification made it possible to obtain the load values closest to the real ones.
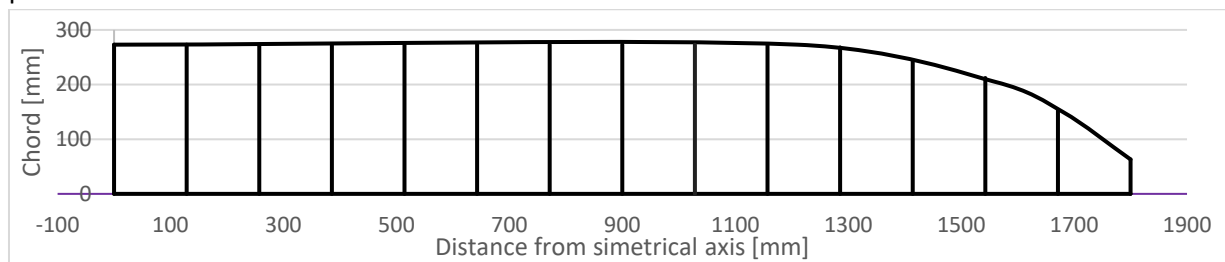
Figure 35 Mental division of the wing into analysed parts

In the place where the fuselage is attached to the considered half of the main wing, it was necessary to introduce an additional factor that reduces the efficiency of the wing itself in a given area. Due to the lack of structurally similar solutions described, a decision was made to use an additional aerodynamic drag coefficient based on the shape of a cylinder and an area equal to the frontal surface of the fuselage itself at the section made in the leading edge of the wing. The coefficient determined in this way acted abruptly, and the non-linearity of the coefficients caused a serious jump in the load values. Due to this problem, a decision was made to soften the impact on the calculations by using a spreading angle (Fig. 35). This is the methodology mainly used when determining the influence of the air brakes on the lift generated by the glider wing during flight.

The load distribution data were validated with XFLR5 (Fig. 36) [74], and SolidWorks (Fig. 37) [81]. In both programmes, the shape of the wing was accurately reproduced, identical flight parameters were selected, and air parameters corresponding to the values adopted during analytical calculations were determined.
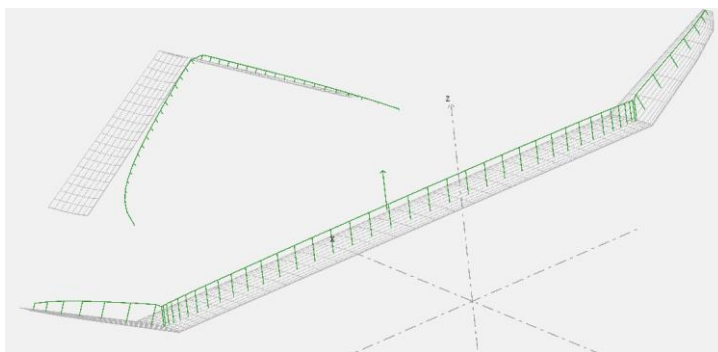
Figure 36 Model developed for analysis in XFLR5
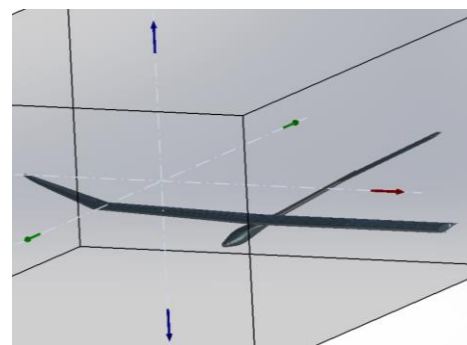
Figure 37 Model developed for analysis in SolidWorks

Both programmes have the ability to determine the parameters of the fluid in which the analyses are performed. Due to the insignificant discrepancy in the results, the values presented in the following were assumed to be correct.

The distribution of forces and moments along the wing span, determined analytically, is shown in the graphic (Fig. 38). The graphs below show the distribution of loads determined for air parameters at sea level. The analysis took into account the loads generated by the fuselages, which was reflected

50

in reducing the loading forces and bending moments in the fixing part. The blue line shows the forces and moments determined for the standard arrangement of the aircraft with a central fuselage, and the orange lines define the load parameters, taking into account the fuselages in specific places.
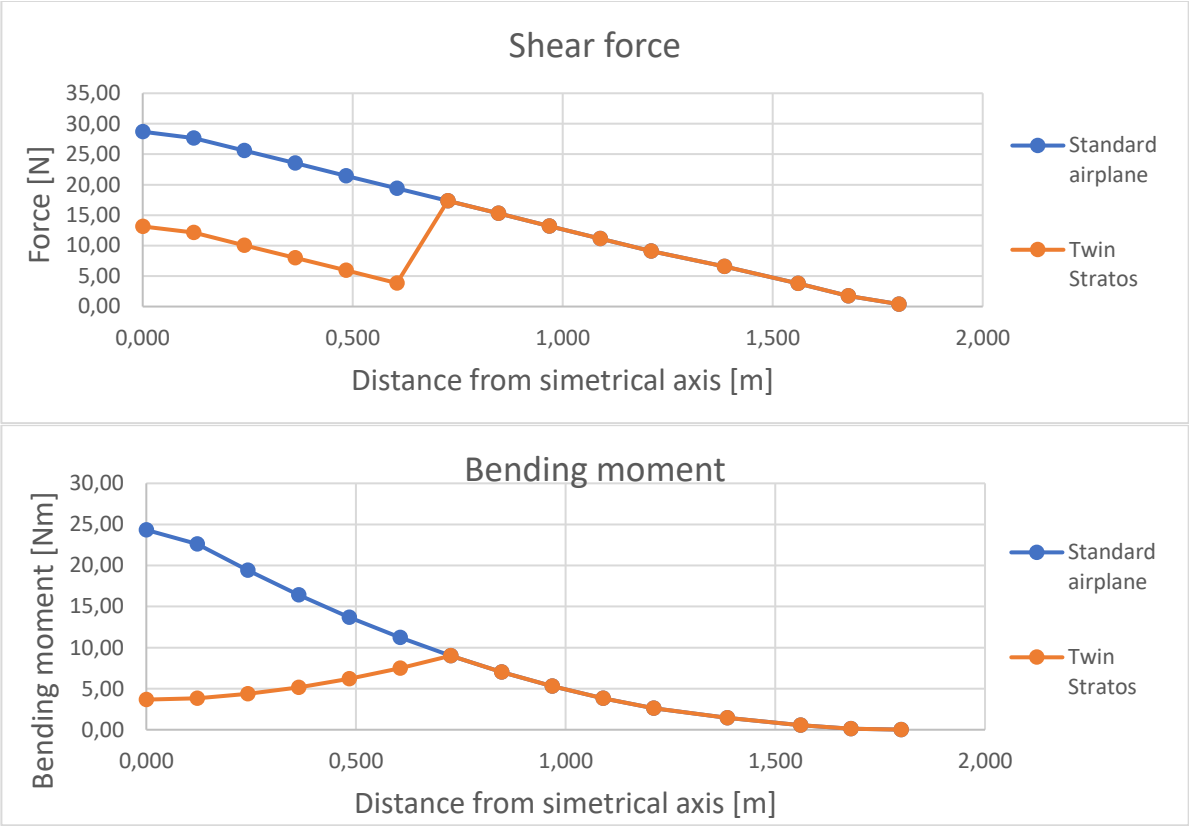
Figure 38 Distribution of loads along the wing

Further stages of work on the construction of the presented UAV Twin Stratos 17 are constantly being improved. Based on this aircraft, the methodology for designing approximate structures and the methodology of approximate determination of flight parameters will be presented.

Loads shown by arrows in the visualisations (Fig. 39 and Fig. 40) reflect the method of wing loading during planned further analyses of the wing. Typically, during similar tests, loads are applied to the structural ribs of the wings. Due to the use of a single-chamber caisson, the loads were distributed according to the distribution adopted during the calculations. This type of distribution allowed for a significant density of fixing points and an increase in the accuracy of mapping the loads acting on the wing during flight in the form of surface operating pressure.
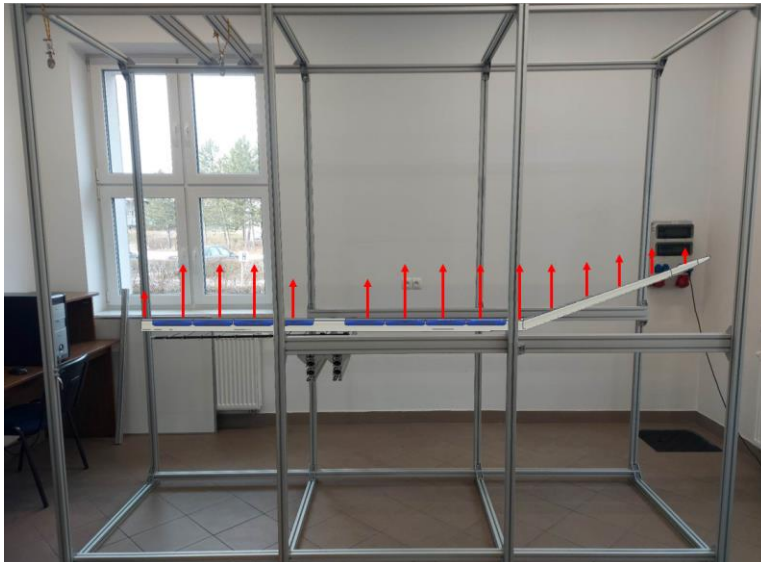
Figure 39 Visualisation of the mounting and loading of the tested wing
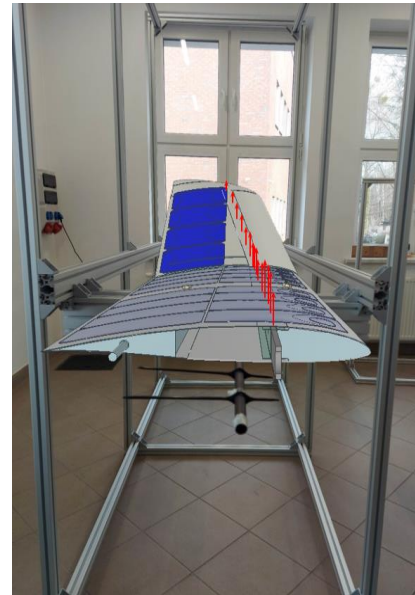
Figure 40 Visualisation of the mounting and loading of the tested wing

The calculations presented in Section 4.2 "The second designing stage" will be used to perform a further detailed analysis of the Twin Stratos 17 UAV. It is planned to assemble a part of the wing in a way that reflects the actual UAV system and apply loads determined in accordance with previous calculations. This type of analysis will confirm the correctness of the designed UAV and the strength capabilities of the designed wing structure. The mapping of the actual system of forces acting on the aircraft wing will be made by the place and method of mounting, applying forces in accordance with the previously determined distribution and placing the wing in a mounting that matches the cross section under consideration. Achieving this type of mapping will be done by:

➢ Fixing the fuselage in place with factory-provided elements,
➢ Applying forces to clamps closely matched to the aerofoil in a given leaf cross section,
➢ Distribution of forces using a system of beams prepared to analyse a given wing loading a given cross-section with an appropriate ratio of force values to neighbouring cross-sections.

Analysis of the TS17 wing will allow determining the wing's response to deflection and twisting during flight. The analysis methodology presented above concerns only a small part of the research carried out during the design, construction, and optimisation of the UAV TS17 structure. Previously conducted analyses were based on determining the thrust values necessary for the analysed structure [82], determining the possibility of occurrence of negative aeroelastic phenomena [83], determination of the efficiency of photovoltaic panels and the quality of cell lamination, determination of controllability for a predesigned structure [84] [85] and generating a digital twin for the analysed structure.

5.2.3. Determination of mass parameters and centre of gravity

Most of the calculations necessary for aircraft analysis require an accurate determination of the centre of gravity of the structure with minimum, maximum, and optimal loads. The area was pre-designated, taking into account all the configurations provided for in the project. A visualisation of a given distribution is shown in the figure (Fig. 41).
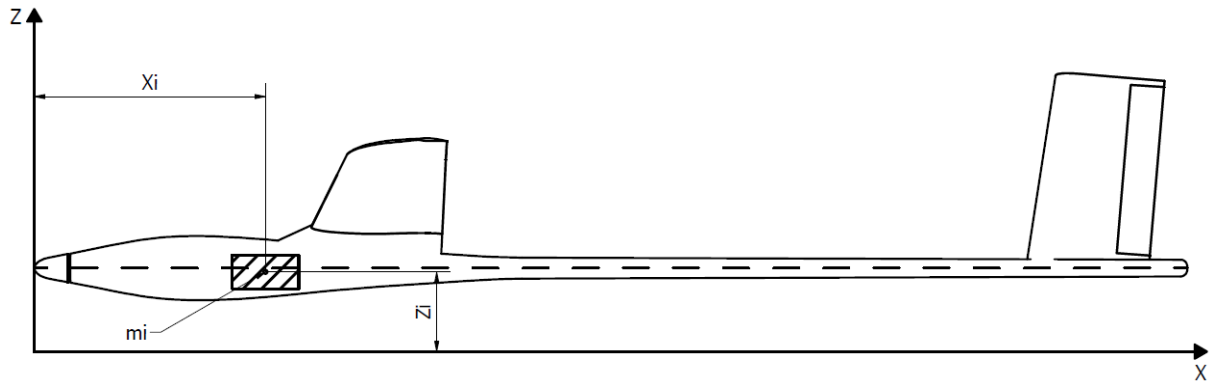
Figure 41 Example component specified relative to the adopted coordinate system
Where: Xi – Distance of the component centre of gravity location from the origin along the "X" axis [mm], Zi – Distance of the component centre of gravity location from the origin along the "Z" axis [mm], mi – Component weight [kg]

The designed drone is supposed to be equipped with additional payload. Based on the separation of the UAV structure itself from the equipment necessary for basic flights, it was necessary to determine the location of the centre of gravity of the structure, not taking into account the measuring equipment. The presented location of the centre of gravity is shown in the graphic below (Fig. 42) does not take into account measuring equipment.
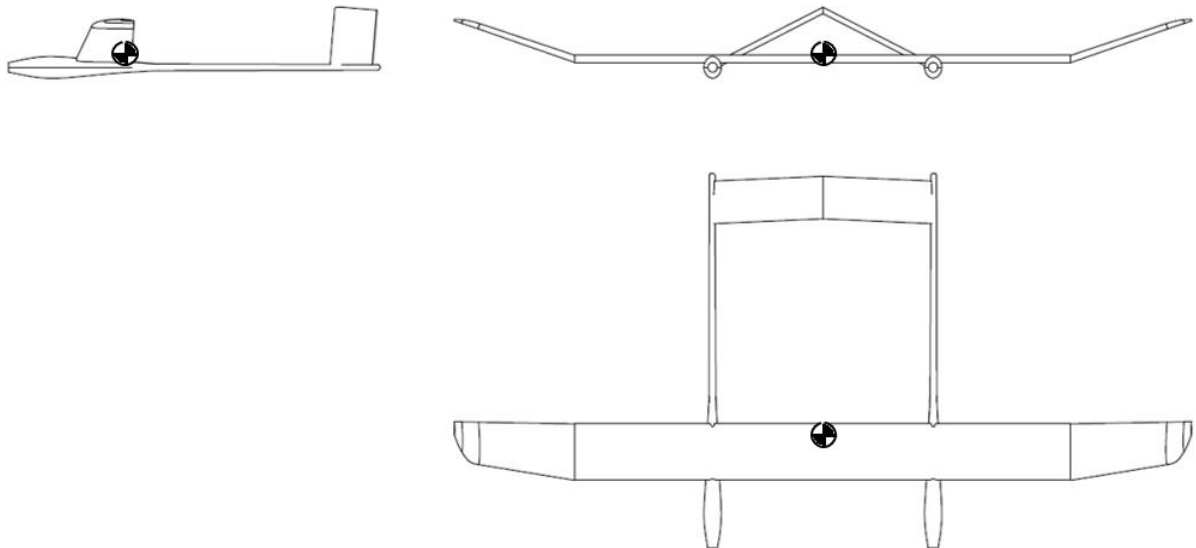
Figure 42 Centre of gravity position without additional load on the measuring head

The specified positions of the centres of masses based on the distribution of the components of the structure and apparatus are given in the table (Tab. 12). The distances from the centre of gravity to the origin of the coordinate system were adopted according to the designation and location of the external system axes in a manner consistent with the figure (Fig. 18) presented in the subsection 4.2.2. "Mass distribution and the gravity centre location".

Tab 12 Determination of the position of the centre of gravity

Distance of the centre of gravity from the origin of the coordinate system			Distance of the centre of gravity from the origin of the coordinate system (system with measuring head)		
Xcg=	0,482	[m]	Xcg=	0,365	[m]
Ycg=	-0,001	[m]	Ycg=	0,000	[m]
Zcg=	0,243	[m]	Zcg=	0,236	[m]

The location of the centre of gravity was based on the assumptions of the location of electronic components. The initial distribution of these components is shown in Figure (Fig. 43). The graphic does not take into account the measuring equipment that would be additional payload.
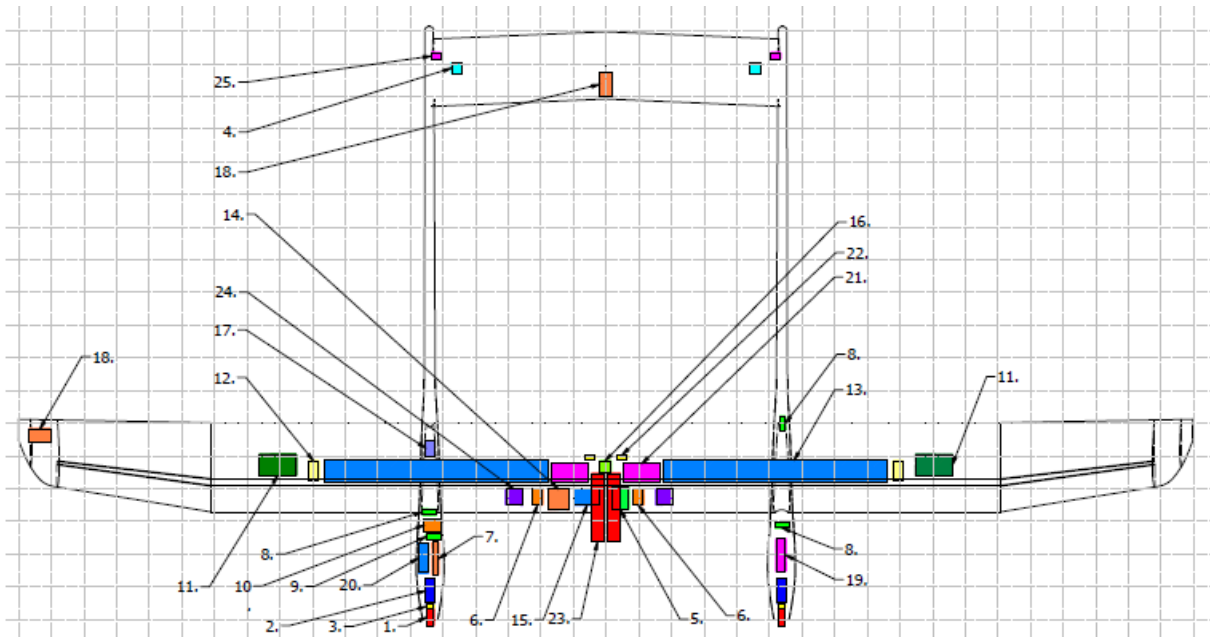
Figure 43 Visualisation of the planned distribution of components of the designed UAV TS17
Where: 1 – Electric motor, 2 – Motor controller, 3 – Encoder, 4 – Servomotor, 5 – Power Distribution Unit, 6 – IDS, 7 – Lights Controller, 8 – DC/DC converter, 9 - DC/DC converter, 10 - Ignition switch, 11 – BSM module, 12 – CAN-UART converter, 13 - Battery pack, 14 - Flight control microcomputer, 15 - Flight controller, 16 – GPS module, 17 - RC remote controller receiver, 18 – FPV camera, 19 – Computer, 20 - Emergency battery, 21 - MPPT converter, 22 - Current sensor, 23 - Computer controlling the measuring apparatus, 24 - Current distributor, 25 - Rudder potentiometer.

The parameters of the location of the centre of gravity determined in this step were also used to determine the total moment of inertia relative to the previously adopted origin of the coordinate system and the later determined centre of gravity. Due to the need to balance the structure unloaded with additional measuring equipment, it is planned to use additional mass in place of the measuring head, which will allow the first flights to be performed without the risk of damaging the measuring equipment and will allow proper alignment of the structure in flight.

With such a set of input data, the model could be discretised to the external form of the aircraft and its centre of mass. This allowed for a significant simplification of further calculations and enabled the determination of further parameters of the analysed UAV.

5.2.4.   Determination of flight parameters of the designed UAV

Knowing the shape, mass, and the previously adopted resistance parameters for the considered structure, the first flight feasibility analyses were performed. First of all, the possibility of flight altitude and the possibility of minimum and maximum speed were studied. The optimum speed parameters related to the climb angle were determined. The optimum speed for the UAV, taking into account only the parameters of the wing, is as shown in the figure below (Fig. 44).
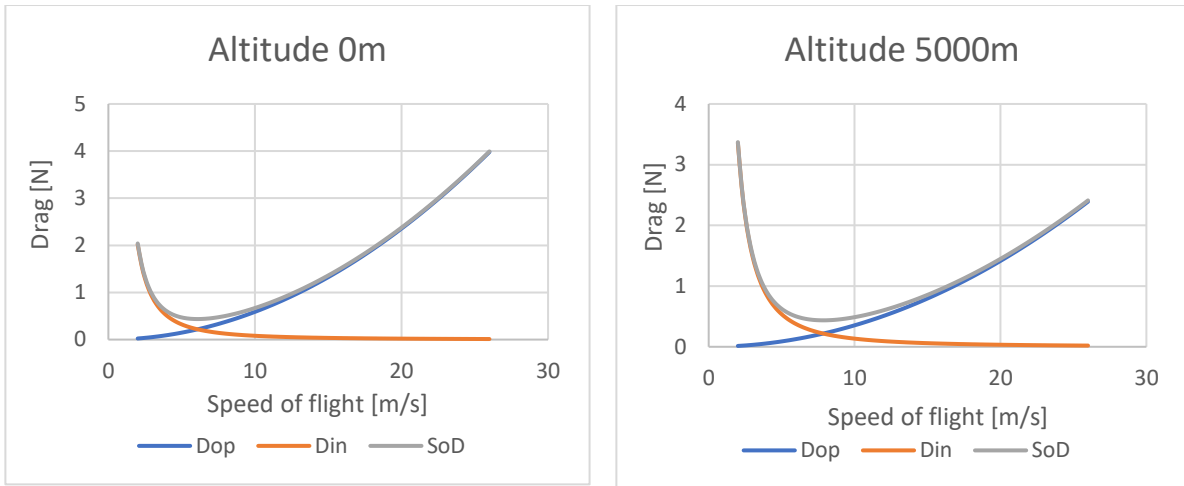
Figure 44 Diagram showing the determination of the optimal speed for UAVs taking into account only the aerodynamic parameters generated by the wing

Where: Dop – Drag of aerofoil, Din – Inducted drag, SoD – Sum of drag,

This is one of the basic analysis performed for the aircraft. The results obtained determine the speeds with which the designed UAV will fly. The optimal speed parameter is usually determined by the drag generated by the structure and the induced drag. The intersection of both lines determines the point of least resistance of the structure and allows one to determine the optimal flight speed.

A more accurate indicator of speed is the so-called bid chart. It includes the functions of minimum speed, maximum speed, angle of maximum rate of climb, and altitude. The developed results for the analysed structure are presented as functions of the above parameters (Fig. 45).
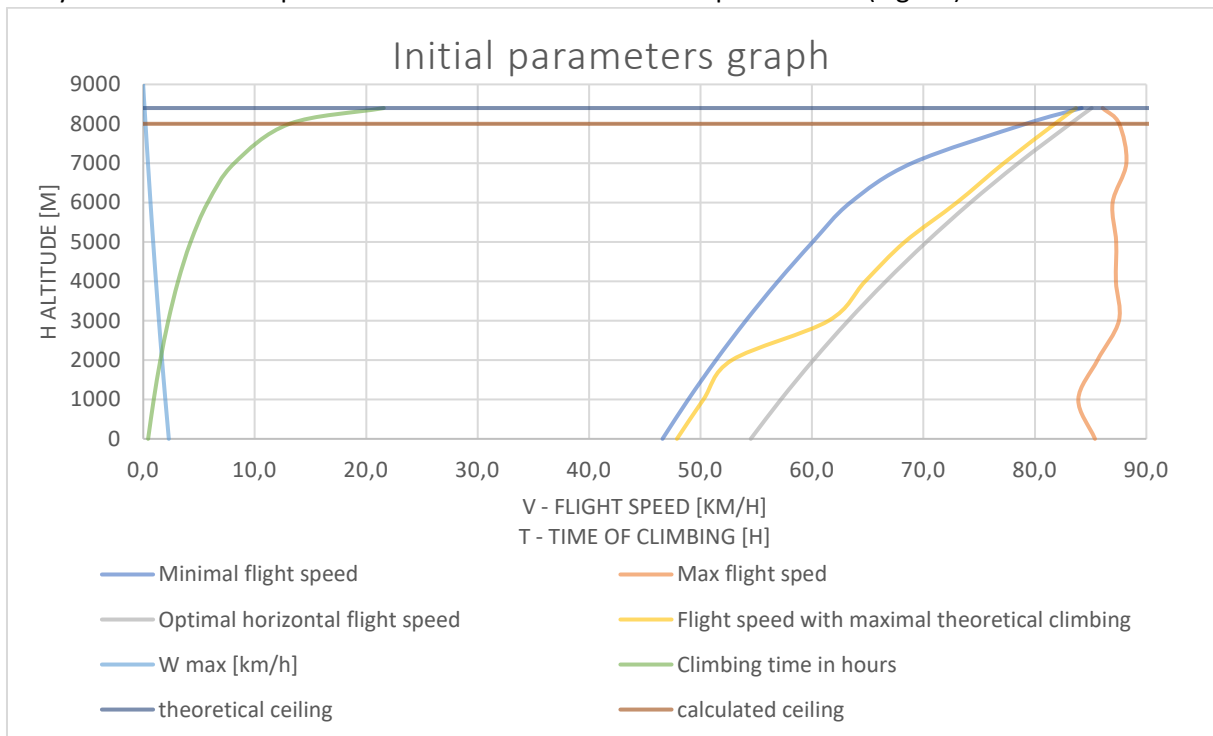
Figure 45 Initial parameters chart

Problems related to determining the parameters of the tail part of the object presented as the research subject are related to the lack of two separate tail units and replacing them with one wing located at an angle to the plane of symmetry of the analysed object.

For this purpose, a substitute system was determined based on the parameters of the analysed tail unit, the geometry of which was presented in the form of a rectangular projection on the plane of symmetry and the plane determined by the line of the fuselages. In this way, the parameters of the substitute tail were determined, whose geometry could be used to determine controllability parameters based on the methodology presented in Section 4.2.4.2 "Tail unit analysis". The values of the substitute parameters specified for a given wing are presented in the table (Tab. 13).

Tab 13 Substitute parameters specified for the tail part

		Horizontal tail unit			Vertical tail unit	
Wing span	bh	1,10	[m]	Hv	0,27	[m]
Wing surface	Sh	0,23	[m^2]	Sv	0,06	[m^2]
Aspect Ratio (AR)	λh	5,26	[-]	λv	1,22	[-]
Mean aerodynamic chord	MACh	0,21	[m]	MACv	0,21	[m]

5.2.5. Examination of the propulsion system parameters for the designed UAV

The analysis data are determined from the developed sample flight plan. The flight plan parameters are shown in the table below. The plan was prepared for the analysis of the propulsion system performed at the stand and assumes such flight elements as take-off, climb, level flight, glide, descent, and landing. The results of the analysis can be extended with accurate diagnostics and the inspection of the efficiency of the control system and the drive system. The results of the primary target values are presented in the table below (Tab. 14).

Tab 14 Flight parameters based on actual plan

System Efficiency Test for a given measuring path						
		Propeller rotational speed	Maneuver start flight altitude	Duration of flight stage		The time from the beginning to the end of the stage	Propeller thrust value
Lp	Stage	[Rew/min]	[m]	[s]	[min]	[min]	[N]
1	Start [ts]	8000	0	0	0,0	0,0	0,0
2	Start [te]	8000	100	145	2,4	2,4	43,4
3	Climbing [ts]	8000	100	0	0,0	2,4	43,4
4	Climbing [te]	8000	2500	4000	66,7	69,1	44,5
5	Horizontal flight [ts]	1500	2500	0	0,0	69,1	4,0
6	Horizontal flight [te]	1500	2500	600	10,0	79,1	3,8
7	Climbing [ts]	8000	2500	0	0,0	79,1	43,9
8	Climbing [te]	8000	5000	5000	83,3	162,4	45,0
9	Horizontal flight [ts]	1500	5000	0	0,0	162,4	5,0
10	Horizontal flight [te]	1500	5000	3600	60,0	222,4	3,5
11	Gliding [ts]	0	5000	0	0,0	222,4	0,5
12	Gliding [te]	0	3500	2000	33,3	255,8	0,0
13	Horizontal flight [ts]	1500	3500	0	0,0	255,8	3,0
14	Horizontal flight [te]	1500	3500	600	10,0	265,8	4,0
15	Gliding [ts]	0	3500	0	0,0	265,8	0,5
16	Gliding [te]	0	1000	3000	50,0	315,8	0,0
17	Descending [ts]	1000	1000	0	0,0	315,8	1,0

18	Descending [te]	1000	100	600	10,0	325,8	2,0
19	Landing [ts]	4000	100	0	0,0	325,8	9,6
20	Landing [te]	4000	0	200	3,3	329,1	10,5

Performing measurements based on the proposed flight plan at the station used to determine the static thrust will allow to check the propulsion system for the actual parameters controlled during the flight. Deviations regarding the rotational speed and times of individual flight stages result from the need to carry out analyses in real conditions and the flight is affected by air parameters such as wind speed, air humidity, and wind direction. The visualisation of the engine rotational speed, flight altitude and the value of the thrust that was generated during the examination of a given flight stage is shown on the chart (Fig. 46).
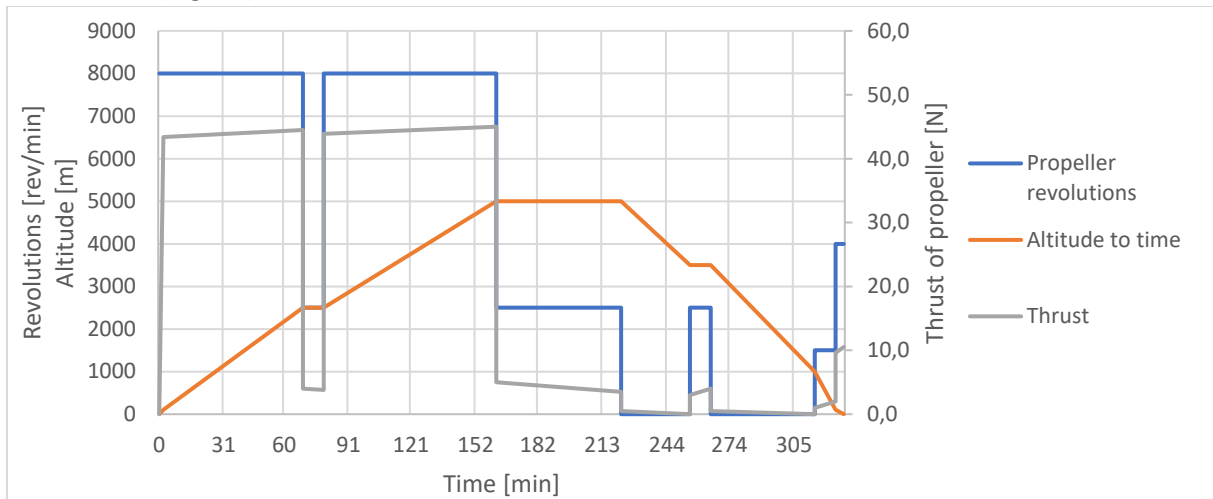
Figure 46 Diagram of the dependence of thrust, height, and rotational speed on time

On the basis of the study, the thrust of the proposed drive system turned out to be sufficient for the designed structure. Changes in the values measured at the start and end points of a given stage may be caused by inertia of the measuring system or an inaccurate determination of the rotational speed in relation to the assumed value.

5.3. Results obtained during the third analysis stage

The results of the analyses presented in this chapter were developed based on the parameters determined at the previous stages of work. The results obtained at a given stage include the following:

- The flight envelope was determined for the designed UAV.
- In-flight stability parameters were determined for particular flight altitudes.
- The location of the main wing spar was initially determined.
- A geometric model was generated in the XFLR5 programme, in which the first numerical aerodynamic analyses were performed.

Typically, the parameters that define the aircraft developed at this stage are sufficient to determine whether the design should be developed or if it should be fundamentally changed. The further development of aircraft structures is based mainly on design work related to individual components of the aircraft or their optimisation.

5.3.1. Development of the flight envelope

Due to the lack of legal requirements for similar flying platforms, safety factors were determined on the basis of regulations for gliders. This allowed the so-called flight envelope [86]. This chart is a map of the angles of attack and flight speeds at which the designed aircraft can move in flight. The envelope is determined for the atmospheric conditions that prevail at sea level. The flight envelope refers to the load factor, defined as the ratio of the aerodynamic force perpendicular to the chord of the wing to its

weight. This envelope represents the allowable load factors in an integrated manner. For given flight conditions, no component should fail or undergo plastic deformation. The loads shown in the envelope can be called permissible loads. To ensure a safety margin, the safety factor for aviation is also adopted, which, in addition to the exceptions specified in the regulations, is 1,5. In the calculations, it was planned to adopt the permissible load factor in accordance with the CS-22 regulations for gliders and motor gliders [87]. In their case, the regulations require, to an extent exceeding the design possibilities. The decision was made to follow the parameters described by Chachurski and Choszczewski [88]. Based on the adopted parameters, the load envelope for the UAV TS17 was developed (Fig 47).
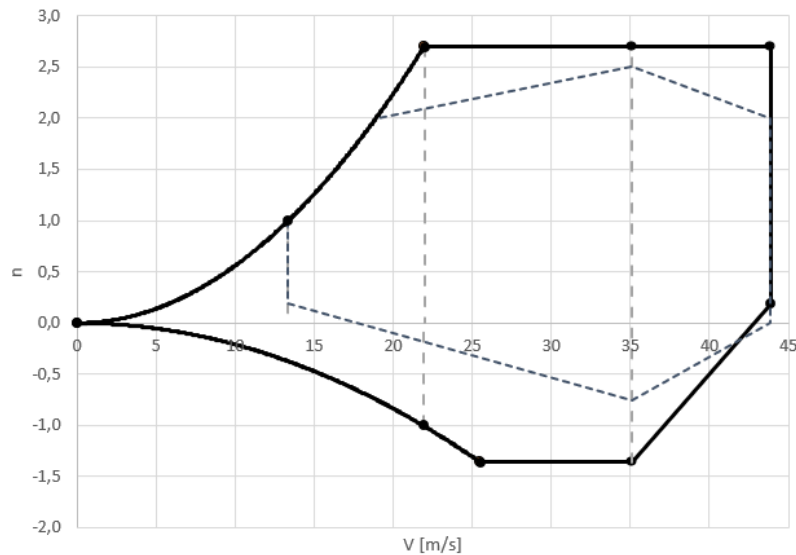
Figure 47 Flight envelope prepared for TS17

5.3.2. Results of numerical aerodynamic analyses

Preliminary analysis made possible to check what kind of parameter values are related to further work. Analyses performed at a given stage of work significantly improve the flight parameters of the analysed UAV. There are many programmes that allow to carry out numerical aerodynamic analyses. More extensive ones allow to determine the parameters of controllability, balance and can help in optimising not only the shape but also the structure of the designed aircraft or UAV.

Numerical tests, compared to experimental tests, allow to verify design assumptions at an early stage of work and avoid the costly process of preparing a model or prototype tested on a test bench. Using the CFD method, it is possible to compare the aerodynamic characteristics and evaluate the stability of the aircraft. Simulation testing is a common tool in aircraft design. They allow, among other things, to determine their aerodynamic properties by determining the external forces acting on them. Typically, these methods are less expensive and often provide data that is difficult to obtain in experimental studies [89].

The XFLR5 programme is a simplified engineering software that allows the determination of aerodynamic parameters, controllability parameters, and stability and stability parameters in the initial stages of aircraft design. Possibilities of analyses carried out in the programme allow for the adoption of any shape and type of aircraft.

XFLR5 is an aerofoil and wing analysis tool. There are four different solvers based on the non-viscous potential flow solution implemented in it. These solvers are based on the following methods:

- Horseshoe vortex lattice method,
- Ring-vortex lattice method,
- the 3-D panel method,
- Non-linear lifting line theory.

58

A solver based on nonlinear lifting-line theory calculates CL and CD results by taking polar wing drag data from Xfoil, which is also implemented in XFLR5. Results are obtained using the default values defined by the solver, except for the iteration number [90].

Software limitations made it necessary to adopt simplifications concerning analyses. The capabilities of the software, however, allow for the analysis of in-flight stability, determining the exact aerodynamic parameters and simulating the drone's response to side gusts.

The modelling of the analysed structure was started by determining the previously adopted aerodynamic aerofoil and mapping them in the programme. This step was done reading the points defining the aerofoils downloaded from the "Airfoil Tools" database [79].

Due to the requirements of the programme, it was necessary to change the location of points in such a way that it was possible to automatically draw aerofoil lines. The requirements specified in the programme manual defined the sequence of points, and the collected points were described from the trailing edge to the leading edge of the aerofoil and again from the trailing edge to the leading edge. Recording points in this way allows to determine the wing aerofoil axis on the basis of which the wing model is later made and the angle relative to the adopted coordinate system (Fig. 48).
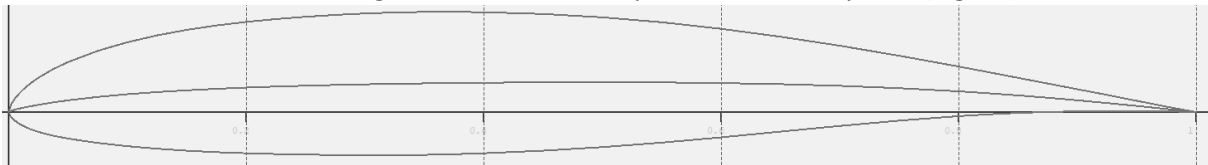
Figure 48 View of the wing aerofoil along with the axis of the wing specified by the programme.

The programme allows to scale a given aerofoil while modelling the analysed shape of the wing. This allows to shorten the time of modelling the aerofoil itself and allows to speed up the analysis. Developing a model requires accurate mapping of the independent parts of the whole. These are the main wing, central fuselage, horizontal stabiliser, and vertical stabiliser. It is possible to model additional wings, fuselages, and other parts. However, it is not possible to build a system that does not use a central fuselage and two fuselages, as in the described Twin Stratos design. Due to this, fuselage modelling was omitted at this stage of the work.

The modelling of the wing began with determining which of the aerofoils defined in the previous stage of work are assigned to which distance from the plane's symmetry axis. The programme enables modelling the angles of suspension of the wing itself, the inclination of individual parts of the wing, and various types of angle changes (Fig. 49). The mixing of aerofoils, which had to be determined geometrically during the analytical calculations, is also modelled. The programme automatically generates mixed parameters. It is important to precisely determine the distance from the axis of symmetry in which the aerofoil occurs and to remember to leave space for mixing aerofoils.
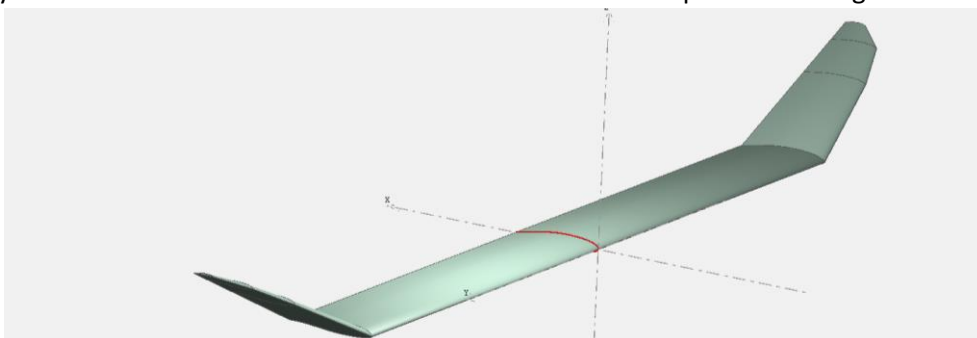
Figure 49 Wing modelled in XFLR5

The tail part was made on the basis of one horizontal stabiliser panel whose surface was tilted according to the design assumptions. Thanks to this, it was possible to reproduce the exact shape of the designed structure (Fig. 50). This model does not allow to determine the controllability of the analysed aircraft, but it allows to determine the stability during flight. Modelling independently placed

wings not joined by a fuselage is acceptable in XFLR5. The programme sees the modelled surfaces as bodies connected by distance and angle constraints.

Figure 50 Tail unit modelled in XFLR5

The XFLR5 programme allows us to model intricate fuselage shapes. There is the possibility of experimental modelling based on moving the surface with a preview of the modelled shape and on the basis of points that can be moved relative to the adopted coordinate system (Fig. 51).
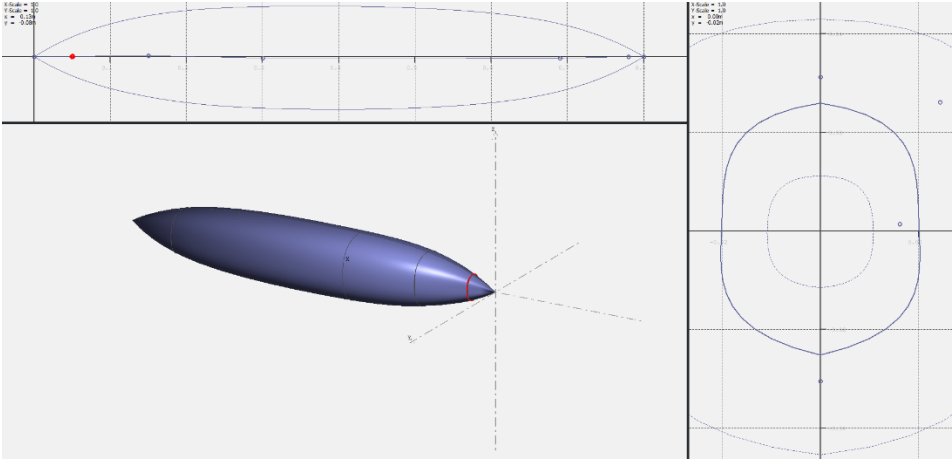
Figure 51 Measuring nacelle model for the designed Twin Stratos 17 UAV

Due to the method of modelling the structure in parts, the programme allows for further modifications of the location and angles of placing all previously prepared components when assembling them to one coherent part of the designed UAV (Fig. 52).
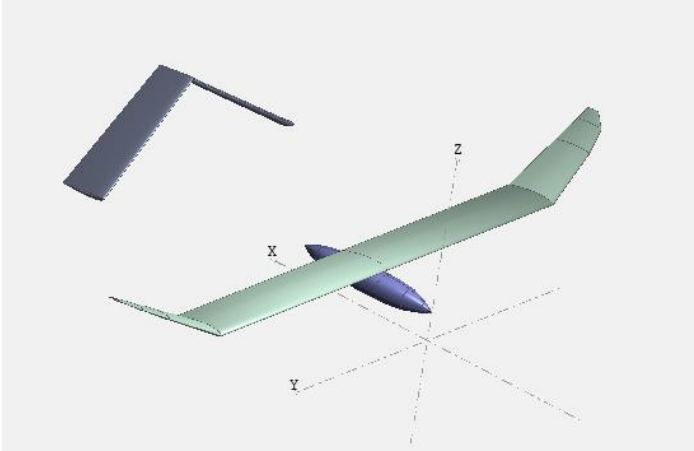
Figure 52 Assembly of modelled components into an aerodynamically analysed whole

Due to the lack of a material base in the software and the degree of simplification of the analysis, it is not possible to assign the analysed structure the thickness of the skin, elastic properties, and stiffness parameters. However, the mass parameters are necessary for the programme to determine

the stability of the system in flight. It is possible to impose additional structural masses on the analysed object. However, they should be discretised to the form of the mass itself and its location. Permanent load modelling is not possible (Fig. 53).

Figure 53 Model TS17 including masses

The mass model of the analysed structure was based on previous analytical calculations and the prepared distribution of elements inside the UAV. In addition, elements such as the main wing, tail, and fuselages themselves were defined as discrete mass models containing information in the form of position relative to the coordinate system. The results of the analysis presented not only the aerodynamic parameters, but also the distribution of loads along the wing span and along the chord (Fig. 54).

Figure 54 Results of the aerodynamic analysis in XFLR5 for TS17

The analysis in the XFLR5 programme was completed by entering the values of the inertia coefficients determined analytically in the previous stages of optimisation. The software allowed for the development of an accurate aerodynamic model and confirmed the results previously obtained. Due to the multitude of analyses carried out, a decision was also made to change the angle of inclination of the tips of the main wing. This allowed for a significant improvement in in-flight stability. The result of optimisation at this stage of the work turned out to be a change in the geometry of the main wing.

5.4. The results obtained in the fourth analysis stage

The last stage of the design developed in the above work assumes the highest precision in mapping the designed structure. It is necessary to take into account the fluid parameters in which the designed

UAV was to move, the material parameters used in the construction of the structure, the stiffness parameters of the structure and the skin, and aerodynamic parameters of the whole. The only solution to develop such an accurate digital twin of the designed UAV was to use Ansys software.

This software allows for modelling structures, determining material parameters, determining the distribution of fibres in composite structures, as well as modelling and analysing their properties [91].

The software itself also allows for the automation of analyses. Thanks to the block model of the programme, individual modules can be selected and combined with each other. In this way, it can automate the parameters adopted by the programme using the module of combining parameters with an EXCEL sheet containing the necessary information, and obtain results by sending the value data directly to the previously prepared sheet. This software made it possible to map the previously adopted optimisation plan presented in the diagram in the following figure (Fig. 55).
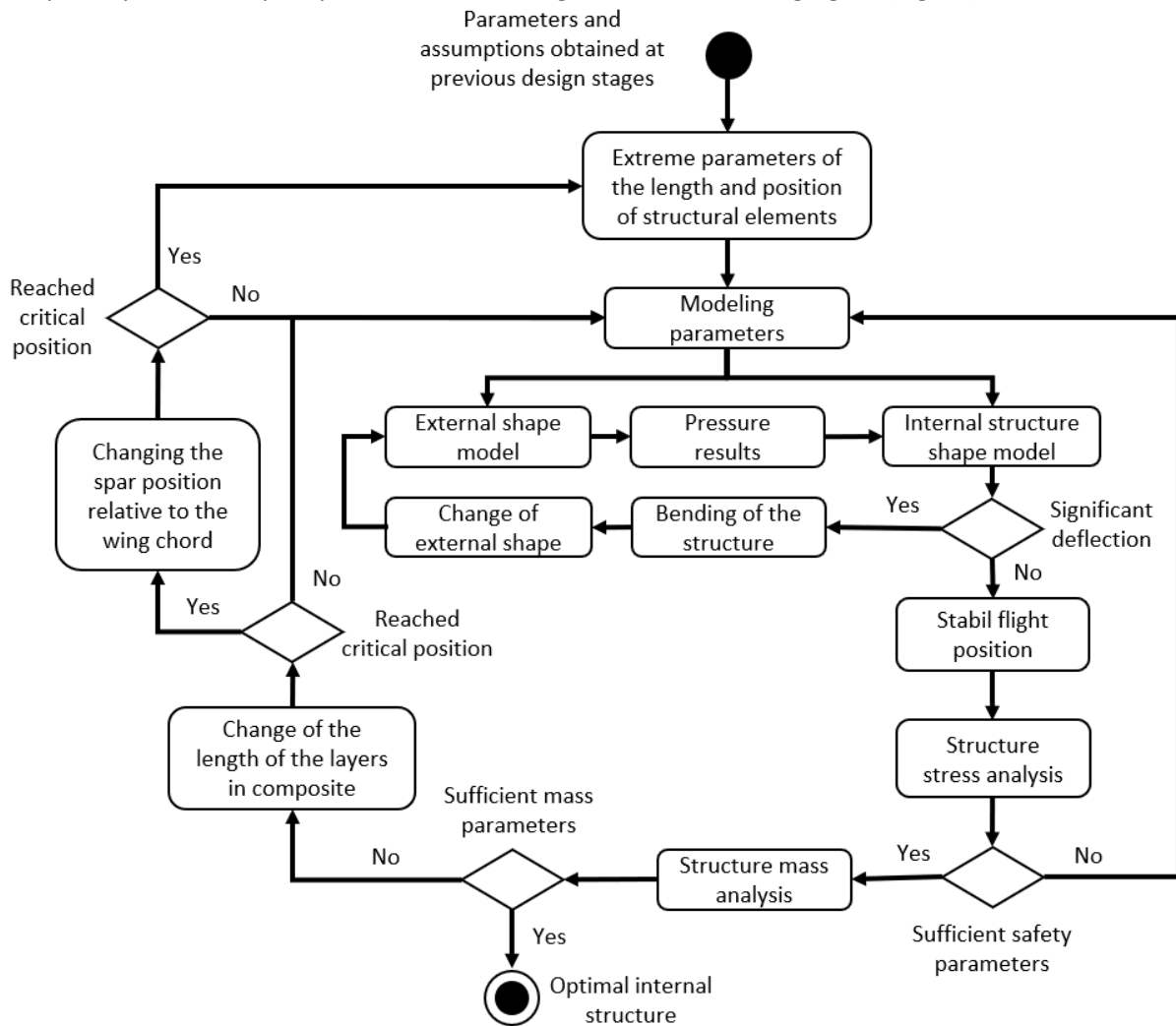
Figure 55 Methodology of the optimisation developed in the last stage of work

5.4.1. Numerical aerodynamic analysis

However, the analysis of the designed UAV required simplifications in order to shorten the time needed to perform the calculations themselves. Therefore, several models of the designed UAV were created, reflecting its external shape, construction, and construction, and the final model containing the parameters of the two previous ones and the parameters of the materials used in the individual parts of the aircraft. The complexity of the models was varied, and they were used alternately for individual optimisation tasks.

5.4.1.1. Determination of the analysis methodology

The analysis methodology was performed as shown in the graph (Fig. 56). It was used during all the analyses presented in the above work. The use of a given analysis methodology unifies the acquisition of results and enables easy comparison of given values.

```
┌─────────────────────────────────────────────────────────┐
│          Critical flight parameters determination        │
└─────────────────────────────────────────────────────────┘
        │                      │                      │
        ▼                      ▼                      ▼
┌───────────────┐     ┌───────────────┐     ┌───────────────┐
│ Critical State I│     │Critical State II│     │Critical State III│
│Aerodynamic Analysis│  │Aerodynamic Analysis│  │Aerodynamic Analysis│
└───────────────┘     └───────────────┘     └───────────────┘
        │                      │                      │
        ▼                      ▼                      ▼
┌───────────────┐     ┌───────────────┐     ┌───────────────┐
│ Determination of│    │ Determination of│    │ Determination of│
│aerodynamic loads acting│ │aerodynamic loads acting│ │aerodynamic loads acting│
│on the tested object in│ │on the tested object in│ │on the tested object in│
│the first critical state│ │the second critical state│ │the third critical state│
└───────────────┘     └───────────────┘     └───────────────┘
```

Figure 56 Methodology of aerodynamic analysis

Analyses conducted in this way allowed to determine the forces acting on the tested object for each of the critical states independently. The loads generated in this way were then used during structural analysis. Each of the analysed structures was analysed for one of the critical states. The others have been disabled for the duration of the tests using the functions "Supress".

5.4.1.2. Development of a model for analysis

A good example of the use of simplification in calculations is the adoption of a full solid model of the designed UAV for numerical aerodynamic calculations. This made it possible to omit the influence of individual material layers on the aerodynamics of the structure and to reduce the analysis time. This simplification has been presented in the visualisation (Fig. 57).
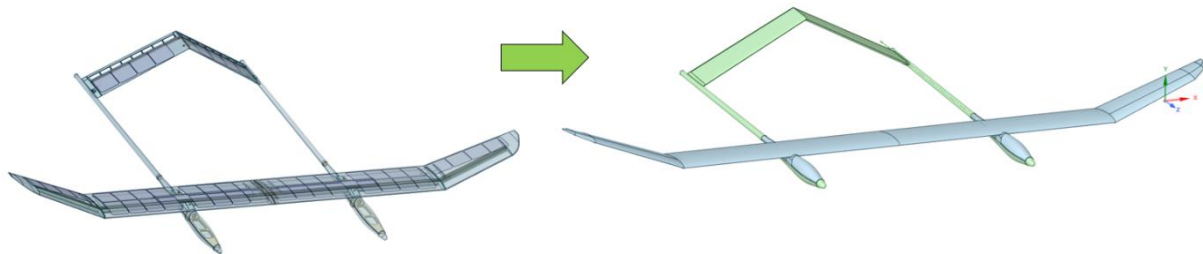
Figure 57 Simplification of the contour for aerodynamic analysis

Further shortening of the analysis time was made by reducing the model itself by intersecting it along the axis of symmetry (Fig. 58). This type of analysis allows testing the UAV in level flight and cannot be used for analyses during manoeuvring of the consider structure. Due to the stage of work related to structural optimisation, this simplification is acceptable.

Figure 58 Simplify the model for aerodynamic analysis

The developed model was also simplified in terms of geometry. Further calculations related to covering the analysed shape with a mesh required significant computational resources. As part of the analysis carried out with the wing tip surfaces in the XFLR5 programme, a simplification was adopted to eliminate the rounding of the wing tip and replace it with a double refraction (Fig. 59). The size of the element in relation to the entire main wing is marginal and allowed for a significant reduction in the number of elements generated on a given part. This, in turn, had a significant impact on the mesh generation time.
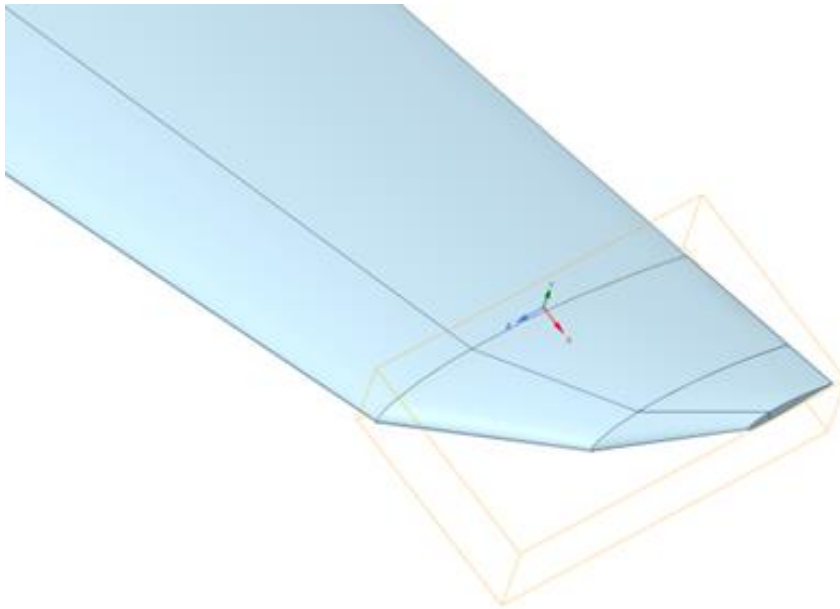
Figure 59 Simplification of the wing tip

The prepared model, representing half of the tested object, was duplicated using the "reflect on the plane" option. The option was applied to the plane of symmetry. The model of external surfaces can be considered ready for analysis. In order to perform accurate analyses, it is possible to use the fluent module. Allows for very accurate flow results in turbulent and laminar flows. To perform a large amount of analysis, the solver based on CFX module is usually used. The computational model has a user-imposed solver to perform the calculations. As a result of the use of a multitude of calculations, a solution based on the CFX module was adopted.

5.4.1.3. Determination of analysis parameters

The development of structural strength analysis in aviation requires the determination of critical flight parameters. They are usually determined from the flight envelope. It is usually carried out according to the rules for a given class of aircraft. The regulations for unmanned aerial vehicles are not as those detailed as for airplanes, so restrictions were adopted based on the EASA regulations (CS22.333) [92] and assumptions described by Chachurski and Choszczewski [88]. The analysis related to the flight envelope was carried out analytically and the methodology on the basis of which the results were developed was mentioned in the chapter 5.3.1. "Development of the flight envelope". Three points of the flight envelope diagram developed for UAV Twin Stratos 1:7 were selected to perform the structural strength analysis (Fig. 60).
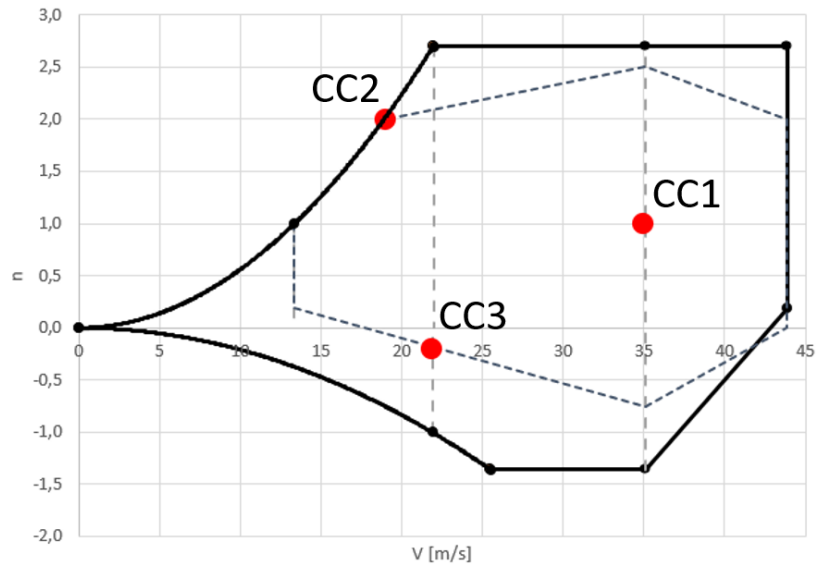
Figure 60 Flight envelope diagram with marked critical points accepted for analysis
where: CC - Critical flight condition, n - overload

The values of speed and angle of attack were read from the graph. In addition, due to the design of the aircraft structure, it was necessary to determine the safety factors. For UAVs, these coefficients have not been legally defined. This required the determination of safety factors by the structural designers themselves. Due to the conditions in which the designed aircraft was to perform the mission, the safety coefficients adopted for structural strength optimisation are at least equal to 1,5. This means that the values of the forces that the structure must withstand are one and a half times higher than the critical values adopted for the analysis. The critical flight parameters adopted during the analyses are presented in the table (Tab. 15).

Tab 15 Critical parameters adopted for structural strength analyses

Flight parameter	Critical flight condition I	Critical flight condition II	Critical flight condition III
View			
Angle of Attack [°]	0	14,25	-5
Flight speed $\left[\frac{m}{s}\right]$	35	19	22

Determining these points was necessary at a given stage because the values of forces acting at later stages of structural tests are determined on the basis of numerical aerodynamic analyses. The next important step was to determine the position of the analysed drone relative to the numerical wind tunnel coordinate system according to the adopted critical positions. For this purpose, the previously prepared model was duplicated and saved in different locations.

5.4.1.4. Preparation of the analysis environment

The next stage related to the numerical aerodynamic analysis was to determine the shape of the numerical wind tunnel. The size of the wind tunnel itself was determined on the basis of multiple mesh analysis and its effect on the results of the analysis itself.

According to research in the literature, calculations are performed using a solver K-ε. Numerical tests are carried out using the pressure method. There are several specific criteria that govern the

65

accuracy of ANSYS Fluent CFX results. The first is to determine the size of the boundary area where the flow analysis is planned. In this study, the boundary size was determined to be 30 times the maximum wing thickness and the length of the wing chord, as shown in the figure (Fig. 61) [93]. Since the control volumes are three-dimensional, volume adaptation of inflation layers and prismatic cells was used. Dimensionless distance from the wall (y^+) shall be assumed as 1 [94]. Thus, the height of the first layer is calculated as 0,1 mm for the selected y+. The growth rate and the number of inflation layers were defined as 1,2 and 30. These selections create a mesh with 2569785 elements and a maximum draught value of 1°. Approximately 100 iterations are performed to ensure convergence. The methodology to determine the mesh parameters of the analysed object has been mentioned in Subsection 4.3.1. "Development of the external structure of the analysed aircraft and numerical aerodynamic analysis".

Prepared in accordance with the critical assumptions, the aircraft model can be cut out of the shape of the modelled wind tunnel. The prepared external geometry model will no longer be needed in the analysis and has been disabled. The most important component of the analysis itself is the prepared wind tunnel with the shape of the analysed aircraft cut out in its volume. A visualization of a generated tunnel is shown in the Figure (Fig. 61).
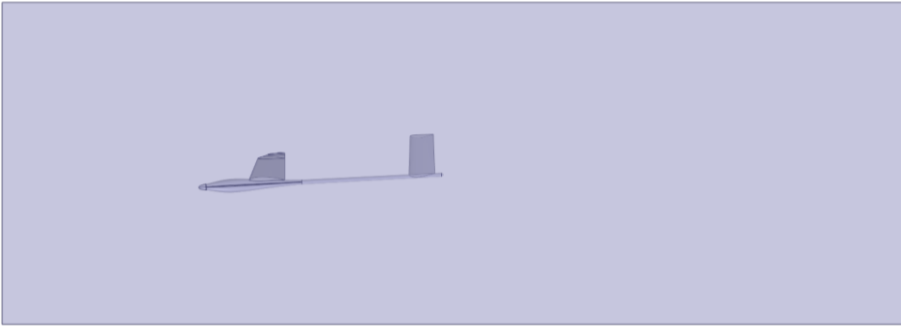
Figure 61 The shape of a numerical wind tunnel developed in the ANSYS environment

Determining the parameters of the analysis for the horizontal flight was simple, the problem was to carry out the analysis for the other two critical flight conditions. There are two methods for specifying the parameters. The method of changing the angle of attack of the aircraft and the method of changing the angle of the airflow. The comparison is shown in the figure (Fig. 62).
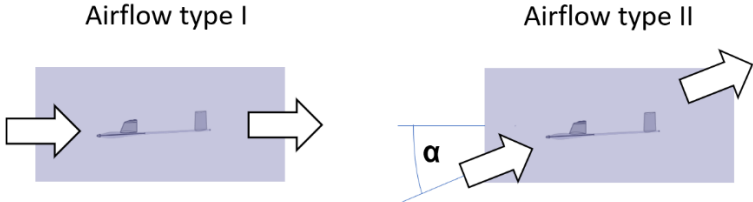
Figure 62 Presentation of flow types in a modelled wind tunnel

Analysis based on changing the direction of air flow is effective and useful in situations of analysis with variable flight speed. Mesh generation is not duplicated in this way, which significantly reduces the analysis time. In the case described in the above work, the flight speeds are constant and there are three variable states of flight. In addition, each of the states is later used in structural analyses. This requires three separate, non-interfering aerodynamic analyses and selective selection of loads during further structural strength analyses.

Due to the previously adopted analysis plan and the need to perform three strength analyses, a decision was made to choose the method of constant airflow and variable angle of attack. The analysis also requires determining the type of surface of the analysed area. Due to the type of analysis, they were adopted according to the assumptions presented in the table (Tab. 16).

Tab 16 Boundary conditions of numerical aerodynamic analysis

Boundary type	The parameters used and their sizes	Places of application
Inlet	Flow Regime: Subsonic Mass And Momentum: Option: Normal Speed,	Front face of the solid
Outlet	Flow Regime: Subsonic Mass And Momentum: Option: Static Pressure Relative Pressure: 0 [Pa]	Back wall of generated wind tunnel
Opening	Flow Regime: Subsonic Mass And Momentum: Option: Opening Pressure Relative Pressure: 0 [atm] Turbulence: Low	The sidewall of a generated wind tunnel
Wall	Mass And Momentum: Option: No Slip Wall Wall Roughness: Smooth Wall	The analysed wing

On this basis, a decision was made to determine the flow parameters as shown in the picture below (Fig. 63).
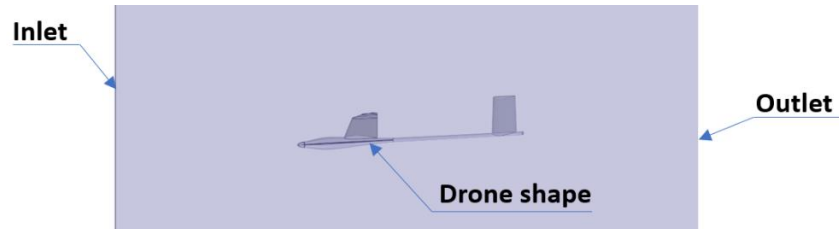
Figure 63 Determination of external elements of the prepared wind tunnel

5.4.1.5. Development of the mesh used during the analysis

Analysis with appropriate accuracy requires determining the parameters of the size of the analysed elements. This problem is even more apparent and convoluted in fluid flow analysis. Inaccuracies in the mapping of curvature, slight simplifications or excessive size of elements bordering the edges have a significant impact on the results of the analysis itself. The Ansys programme automatically determines the parameters that can be adopted to generate the mesh of elements. Unfortunately, these quantities are usually not suitable for carrying out analyses and the accuracy of the results obtained in this way is negligible. A visualisation showing the predefined discretization of the analysed solid is shown in the visualization (Fig. 64).
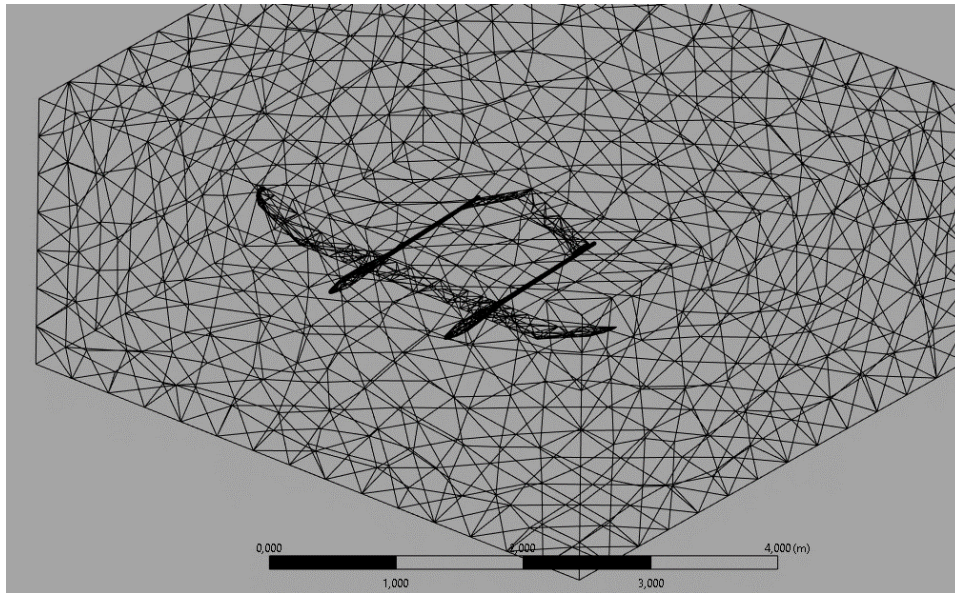
Figure 64 Pre-generated meshing model

Meshing is started by double clicking on the "Mesh" tab in the CFX workspace. In Meshing, each control volume surface must be individually selected and named. This nomenclature is used in later settings to identify the purpose of each surface [91].

A good quality mesh can be defined as one that has appropriate refinements around the main areas of interest. The edges and shape of the geometry should also remain well defined and should not be altered by the mesh in any way. For a better definition of the boundary layer, a suitable layer of inflation growing out of the body is also necessary. An "all quad" mesh is preferred for computational purposes, and an attempt was made to sweep the computational domain with quad elements, but it was rejected by the mesh generator.

As can be seen in the figure (Fig. 65), element sizes are different for ich of part of the analysed drone. This is due to the size of the analysed elements themselves and, above all, their rounding and thickness. Too small elements of the generated mesh caused inaccuracies in the discretization of elements.
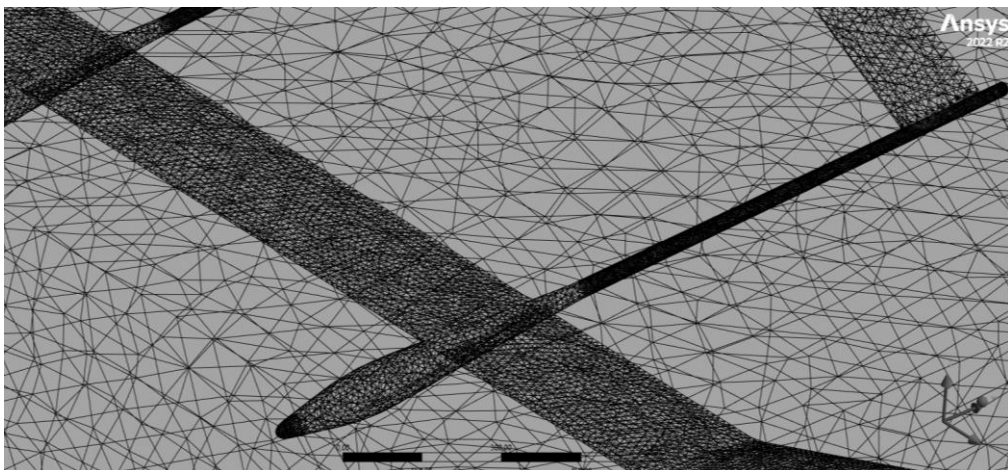
Figure 65 Mesh compaction for key elements of aerodynamic analysis

The surfaces or geometries of the aircraft being analysed can also be selectively named to further refine these geometries. In this analysis, the leading and trailing edges and surfaces of the components that cover the part were selected for further refinement. The refinement settings used are summarised in the table (Tab. 17).

68

Tab 17 Elements with specific mesh sizes

Nr	Element	Element size
1	Box	100 [mm]
2	Main wing	8 [mm]
3	Tail wing	12 [mm]
4	Tail Beams	5 [mm]
5	Fuselages	8 [mm]
6	Fuselages Noses	5 [mm]

In addition, an operation was performed to increase the accuracy around the entire aircraft model. For this purpose, the option of mesh inflation around the tested object was used. The inflation parameters are presented in the table below (Tab. 18).

Tab 18 Inflation parameters

Inflation Option	First Layer Thickness
Thickness of First Layer	0,1
Maximum Layers	30
Growth Rate	1,2
Inflation algorithm	Pre

Increasing the accuracy of the mesh in the vicinity of the analysed aircraft has a positive effect on the accuracy of the analyses themselves. As demonstrated during the analyses described in point 6.5. "Determination of the extreme values of the position parameters of the structure elements", Accuracy when preparing the structures mapping of the analysed is of key importance for the correctness of the results obtained. The model obtained on the basis of the parameters specified above is presented in the visualization (Fig. 66).
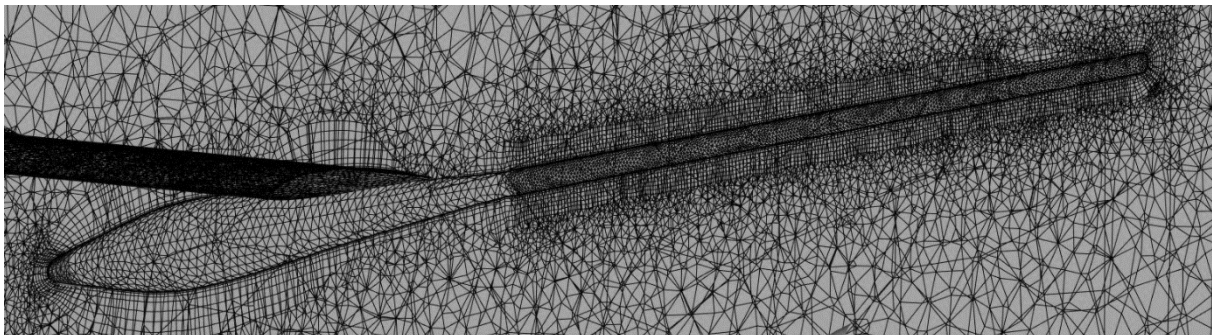
Figure 66 Generated mesh inflation at the contour of the aircraft

The methodology of preparing a mesh of elements model for aerodynamic analysis of aircrafts, presented by Wee [91], turned out to be optimal for the analysis of the designed UAV. The accuracy of the mesh was checked by performing a large number of analyses. The general principle of validation is to gradually increase the number of elements for which flow analysis is performed. Having previously developed information on determining the size of the numerical wind tunnel area itself and the speed and angle of attack of the drone itself, only the number of mesh elements was increased. After several attempts, the plot of the average results of the analyses performed, depending on the number of elements, should assume one value. This is the (exact) limit value. Increasing the number of elements in this case does not affect the results obtained.

Further stages of work related to improving the quality of the mesh focus on point densities or reducing the number of less significant elements during the analysis. This procedure is the reason for the different sizes of the mesh elements for the individual parts of the UAV tested. The accuracy of the tail section does not have to be as high as that of the main wing, as shown in the photo below (Fig. 67).
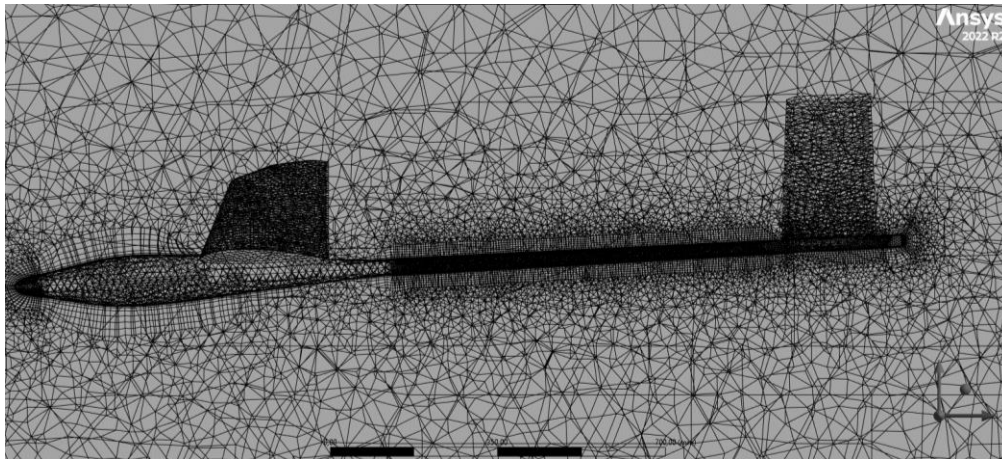
Figure 67 Difference in the size of the mesh elements between the tail part and the main wing

On the basis of the guidelines and analyses described above, the final type of mesh describing the analysed model was generated. The parameters of the generated mesh are presented in the table (Tab. 19). The summary shows meshes generated for three critical flight states. Despite the use of identical parameters, the number of elements for each case is as follows.

Tab 19 Mesh parameters for the considered flight cases – All elements analysis

Parameter	Case I	Case II	Case III
Angle of Attack	0 [°]	14,25 [°]	-5 [°]
Velocity	35 [m/s]	19[m/s]	22[m/s]
Physics Preference	CFD	CFD	CFD
Solver Preference	CFX	CFX	CFX
Element Order	Linear	Linear	Linear
Transition	Slow	Slow	Slow
Span Angle Centre	Fine	Fine	Fine
Minimum Edge Length	1,017 [mm]	1,017 [mm]	1,017 [mm]
Smoothing	Medium	Medium	Medium
Transition Ratio	0,77	0,77	0,77
Maximum Layers	5	5	5
Growth Rate	1,2	1,2	1,2
Nodes	996529	1074072	1089116
Elements	5433916	5161563	5227953

The prepared mesh describing the tested object is presented in the visualisation (Fig. 68). The purpose of the developed mesh was to determine the mapping of the shape of the analysed object and the state of detail that should be adopted.

70
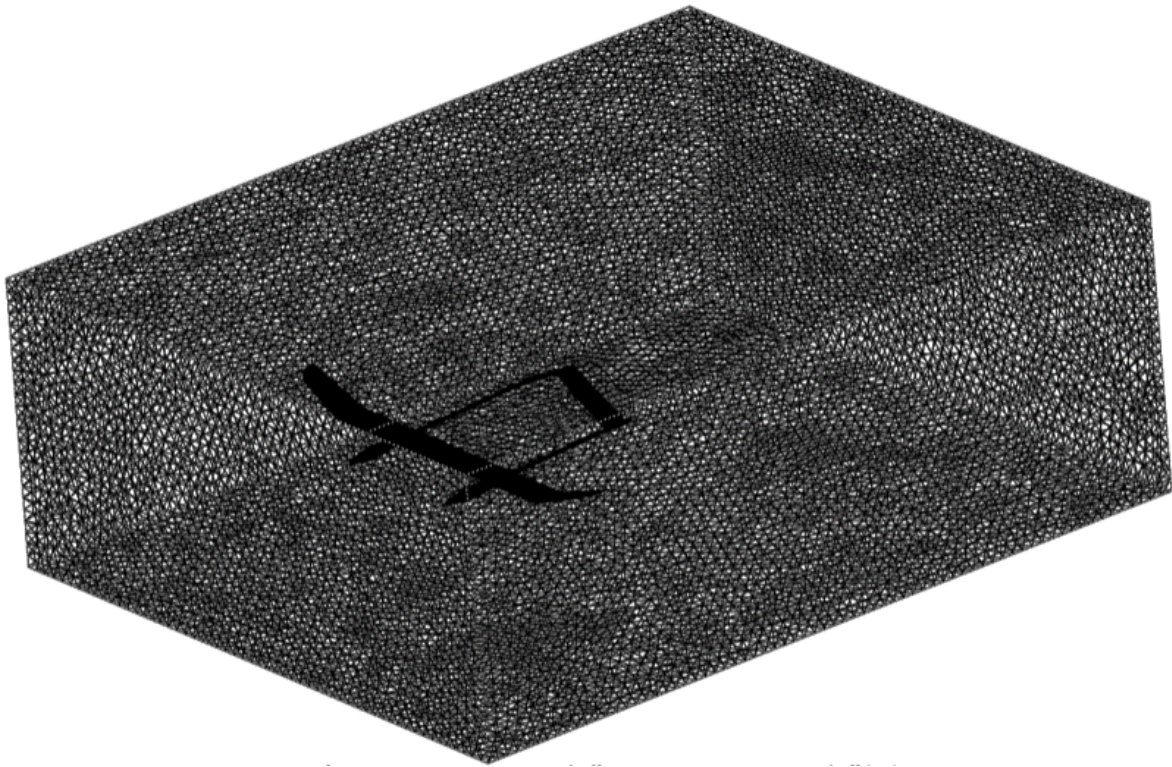
Figure 68 Mesh generated for test TS17 in horizontal flight at a speed of 35 [m/s]

5.4.1.6. Determination of boundary conditions for a solid and presentation of results

The analysis requires the parameters introduction of the previously described, such as the fluid flow velocity and determining which of the given surfaces is the inlet and which is the outlet in the prepared numerical wind tunnel. This is also the stage in which the solver is determined that will analyse the previously prepared model. At this stage of the work, the parameters of the fluid filling the block were also determined. Thanks to such a set of data, it was possible to carry out the first aerodynamic analyses in the Ansys environment.

The parameters selected to determine the boundaries of the working area are shown in the table (Tab. 20). Determining the boundaries of the designed wind tunnel is a key moment in the preparation of analyses. The shape of the surface, determination of the parameters of the medium in which the analysis is performed, and the removal of errors during the preparation of the external shape of the analysed object affect the quality of the results obtained. The procedures to determine the parameters were carried out based on the tests presented in the 4.3.1 "Development of the external structure of the analysed aircraft and numerical aerodynamic analysis". The table below shows the parameters defined for the first critical case. The differences specified for each case are only related to the determination of the air inlet velocity for the "Inlet" wall. Other parameters of the analysis remain unchanged due to the earlier preparation of models for the analyses. Due to this procedure, the results obtained during the analyses can be comparable and, in further stages, applied interchangeably to the model representing the structure of the analysed UAV, taking into account the material parameters adopted for each of the elements. The described analysis are presented in further chapters of the presented work. This analysis is the main goal of optimisation. Thanks to this procedure, a matrix of results was determined, which determines the optimal structure for the object tested.

Tab 20 Elements of the prepared area analysis with parameters

Element	Task	Selected parameters
Domain	Analysis area. It is an element that determines the parameters of the medium that fills the interior of the previously prepared solid. This element also defines the solver used during the flow analysis. The methodology for determining the solver is presented in Subsection 7.1.6. Due to the simplifications of the analyses adopted and described in the previous chapters, the parameters adopted during the analysis were defined as presented.	1) Domain Type: Fluid Domain 2) Material: Air at 25 [°] 3) Morphology: Continuous fluid 4) Reference pressure: 1 [atm] 5) Buoyancy Model: Non Buoyant 6) Domain Motion: Stationary 7) Mesh Deformation: None 8) Heat Transfer: None 9) Turbulence: k-Epsilon 10) Wall Function: Scalable 11) Combustion: None 12) Thermal Radiation: None
Inlet	It defines the place of air inlet to the analysed space. The modelled shape "let in" the air stream over the entire surface. The air flow is always perpendicular to the inlet wall and directed into the analysed solid.	1) Boundary Type: Inlet 2) Flow Regime: Subsonic 3) Mass And Momentum: a) Option: Normal Speed b) Normal Speed: 35 [m/s] 4) Turbulence: Medium (Intensity=5%)
Opening	The side walls of the designed wind tunnel define the area of analysis. The assumed parameters allow for air flow. The flow at the wall elements is influenced by the inlet and outlet parameters of the designed wind tunnel. At increased flight speeds, the flow directed inside the analysed area can be seen. This is due to the curvature of the inlet and reduces the losses of the analysed flows. The reduced pressure caused by the flow from the inlet wall to the outlet wall causes additional streams to be drawn into the system.	1) Boundary Type: Opening 2) Flow Regime: Subsonic 3) Mass And Momentum: a) Option: Opening Pres. And Dirn b) Relative Pressure: 0 [Pa] 4) Flow Direction: Normal to Boundary Condition 5) Turbulence: Medium (Intensity=5%)
Outlet	The outlet part of the designed wind tunnel. A wall specified as penetrable. The parameters adopted for the selected element cause the flow only to flow in the direction of this wall. The static pressure was assumed to be 0 [Pa], which causes a constant flow toward a given wall. The velocity of the flow itself is determined by the wall defined as the inlet.	1) Boundary Type: Outlet 2) Flow Regime: Subsonic 3) Mass And Momentum: a) Option: Average Static Pressure b) Relative Pressure: 0 [Pa] c) Pres. Profile Blend: 0.05 4) Pressure Averaging: Average Over Whole Outlet
UAV	A part cut from the area of the designed wind tunnel. It maps the external shape of the analysed UAV. Inside this structure there is no medium assigned to the whole, in this case in the form of air.	1) Boundary Type: Wall 2) Mass And Momentum: No Slip Wall 3) Wall Roughness: Smooth Wall

Parameters concerning solver, air, boundaries, and everything that turned out to be necessary to carry out the analysis are presented in the table (Tab. 21).

Tab 21 Solver parameters specified in ANSYS

Parameter	Response	Choosen parameter
Solution Units	Parameters defining the unit data adopted during the analysis. Also specify the units in which the results of the analysis are obtained.	1) Mass Units: [kg] 2) Length Units: [m] 3) Time Units: [s] 4) Temperature Units: [K] 5) Angle Units: [Rad] 6) Solid Angle Units: [sr]

Solver Control	The parameters defined at this point describe the values related to the calculation itself. They affect the minimum and maximum number of calculated iterations. Small amount of iterations will not allow to obtain a stable value of the results and will reduce the accuracy of the analyses performed.	1) Advection Scheme: High Resolution
		2) Turbulence Numerics: First Order
		3) Convergence Control:
		  a) Min. Iterations: 100
		  b) Max. Iterations: 1000
		4) Fluid Timescale Control:
		  a) Timescale Control: Auto Timescale
		  b) Length Scale Option: Conservative
		  c) Timescale Factor: 1.0
		5) Convergance Criteria:
		  a) Residual Type: RMS
		  b) Residual Target: 1.E-4
		6) Interrupt Control
		  a) Option: Any Interrupt
		  b) Convergence Conditions: Default Conditions
		7) Equation Class: Continuity
		8) Dynamic Model Control: Global Dynamic Model Control

Output Control	Parameters defining the type of saving of the results and the format of the files. Ansys allows to save in formats that are acceptable to other programmes. The determined values also affect the area of greatest interest. In the case of the presented analysis, this area is the outer contour of the analysed drone.	1) Option: Standard
		2) File Compresion: Default
		3) Monitor Objects: Monitor Points and Expressions:
		  a) Monitor point: Expression
		    i) Expression Value: force ()@REGION:TS17

The finally prepared aerodynamic analysis environment is presented in the visualisation (Fig. 69). To facilitate the determination of the correctness of the constraints imposed on the measurement system, the Ansys programme presents the boundary conditions in the form of visualisation. The arrows applied to each of the edges of the solid defining the shape of the numerical wind tunnel show the possible or forced flow direction of the medium inside. As can be seen, the constraints were imposed correctly because the arrows indicate the direction of flow according to the previously adopted assumptions.
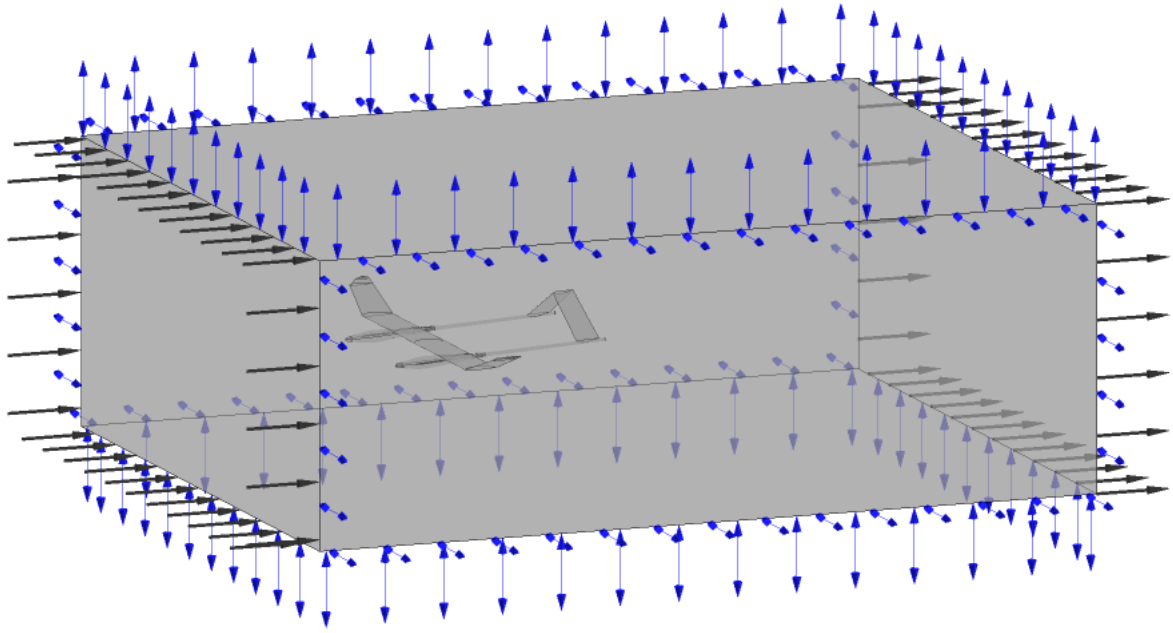
Figure 69 Development of preliminary parameters for aerodynamic analysis

5.4.1.7. Aerodynamic analysis results for three assumed critical states

The analysis scheme was identical for each of the flight states. The visualisation (Fig. 70) shows the first of them defining the level flight.

The results obtained for the conducted analyses were determined on the flow models specified in the previous sections. The correctness of the preparation of the external model was confirmed by the compliant flow presented in the visualisation (Fig. 70). As can be seen from the colour of the observed streams, the pressure value is stable in all volume of the numerical wind tunnel.
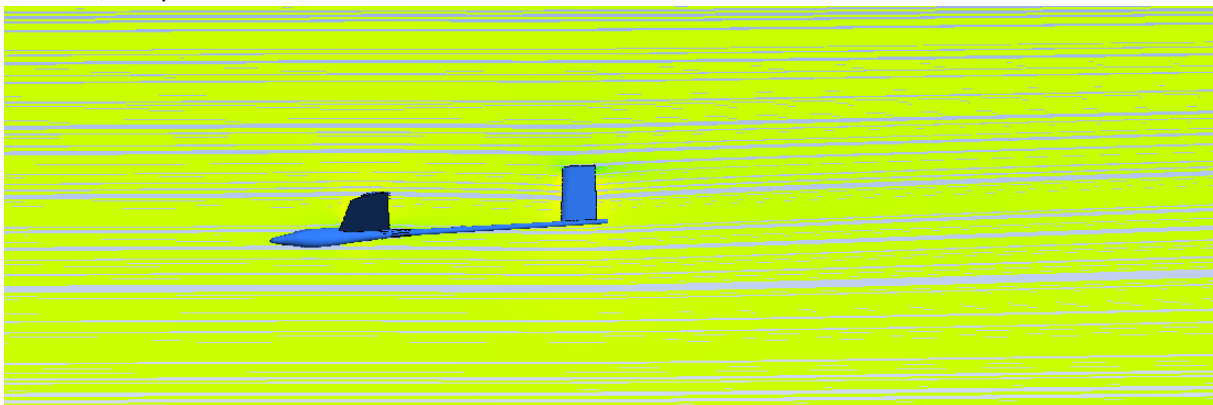
Figure 70 The flow of air streams in the modelled environment

Stream compaction was defined as a one-dimensional procedure. Lateral curvature modelling could have caused disturbances in the flow velocity in the vicinity of the wingtips of the tested object. This could cause incorrect results to be read during the analysis. Increasing the size of the analysed area would have a negative impact on the calculation time. Due to the test area affected only the distribution of flows along the "Z" axis, the height of the tested object (Fig. 71).
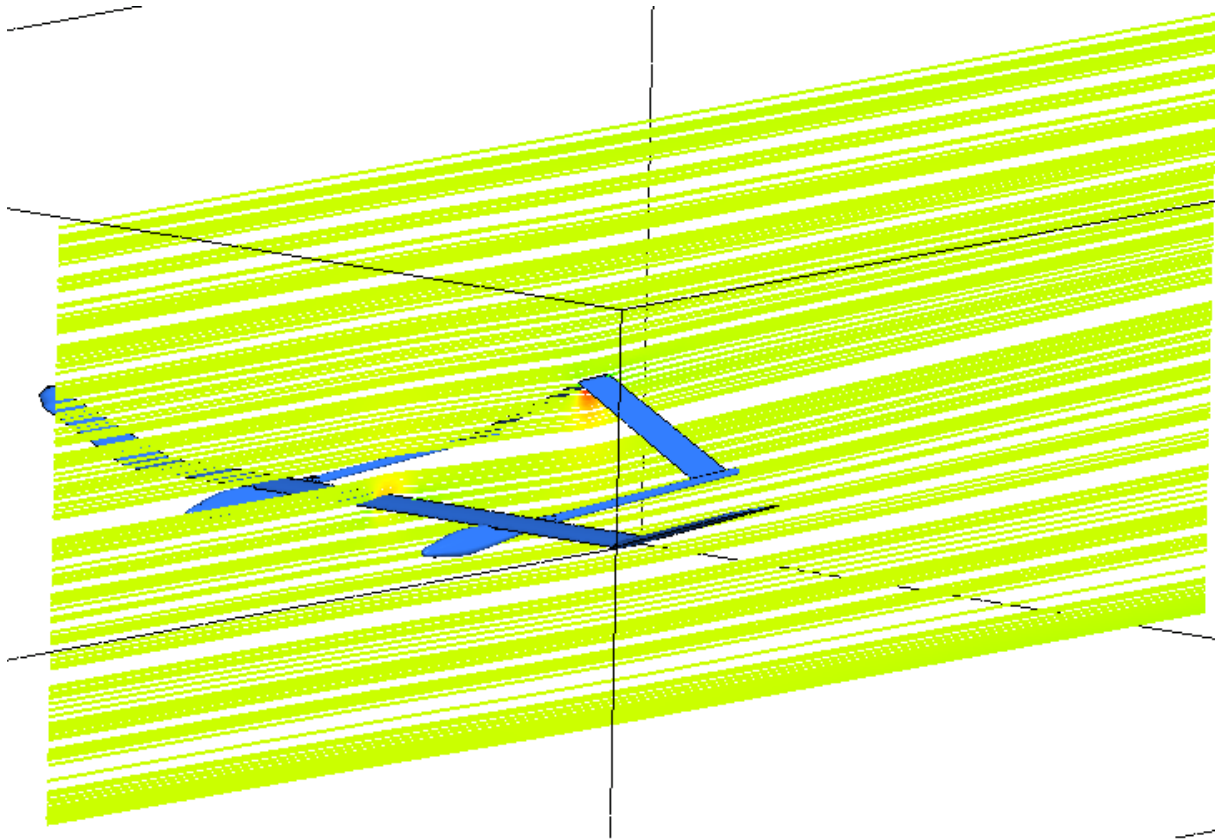
Figure 71 Air flows in the plane of symmetry of the test object

The results obtained during the analyses are presented in the table, and the methodology for determining critical parameters on this basis was used in the structural analysis of the optimised airplane. As can be seen from the example of the visualisation presented in the second considered critical flight case, the occurrence of turbulent flow is one of the problems that causes a reduction of the flight parameters of the designed UAV.

The main parameters determined for each of the critical states during the analysis are presented in the table (Tab. 22). They refer to the values that were used to confirm the correctness compared to previously determined coefficients. The meshing parameters have been the same for each of the critical states, this allows to compare the values while maintaining the confidence in the correctness of the analyses carried out. All analyses were performed on the same computer.

The use of a variable angle of attack of the tested object instead of a variable angle of flow also had a positive effect on the simplicity of determining the parameters of the lift force and drag force generated by the tested object. These parameters were determined in the "Expression" function. Determining the resultant force of the entire object along the selected axis was made by creating a new function. The use of a constant coordinate system of the environment tested and variable inclination of the tested object allowed the determination of the resultant forces along the axis of the coordinate system of the tested area. There was no need to recalculate the force values as components. Due to this, these values could be read directly and then transferred as parametric values.

Tab 22 Comparison of parameters obtained during the analysis of each of the critical flight states for all airplane

Name	I critical flight condition	II critical flight condition	III critical flight condition
Results view			
AoA	0 [°]	14,25 [°]	-5 [°]
Horizontal speed	35 [m/s]	19[m/s]	22[m/s]
Air pressure [atm]	1	1	1
Air temperature [°C]	25	25	25
Lift Force	245,8 [N]	272,01 [N]	-42,44 [N]
Drag Force	22,4 [N]	46,83 [N]	10,16 [N]
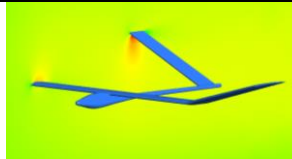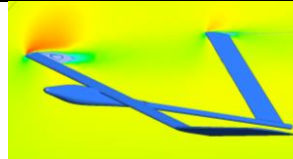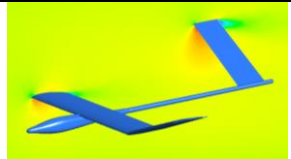
5.4.2. Numerical structure strength analysis

Due to complex issues and software requirements, it was necessary to perform numerical aerodynamic analyses. They were carried out for specific flight parameters such as speed, angle of attack, air density, and temperature. The analysis was carried out based on the extreme flight parameters specified in the table (Tab. 22). Temperature and static pressure was the same for all of testing critical conditions.

There are many practical engineering problems for which an exact solution can be obtained. The inability to obtain an exact solution can be attributed to the complex nature of differential equations or to the difficulty of dealing with boundary and initial conditions. To deal with such problems, a numerical approximation can be used. There are three common classes of numerical methods:

- Finite Difference Method.
- Finite Element Method.
- Boundary Element Method.

Engineers routinely use the finite element method (FEM) to solve everyday problems of stress, deformation, heat transfer, fluid flow, electromagnetism, etc. using commercial and speciality computer codes; ANSYS is one of the most comprehensive and widely used commercial finite element software.

5.4.2.1. Development of a model of the drone's internal structure based on the external shape

Aircraft structure elements are highly redundant and require simplification or idealisation before they can be analysed. A high degree of accuracy can only be achieved using computer techniques, such as the finite element method. Finite element analysis will be used to derive displacement, stress, eigenfrequency, and dynamic response, as these are considered the main design parameters.

The finite element method has developed in parallel with the increasing use of high-speed electronic digital computers and the growing emphasis on numerical methods in engineering analysis. Although this method was originally developed for structural analysis, the general nature of the theory on which it is based has also enabled it to be effectively applied to problem solving in other domains of structures by means of a set of subdivisions called finite elements. These elements are considered interconnected in connections that are called nodes or nodal points [95].

For the analysis, SHELL181 was selected to mesh the entire wing structure where appropriate for the analysis of thin and thick shell structures. It has translations in the x, y, and z directions and rotations around the x, y, and z axes, giving six degrees of freedom at each node, and consists of four nodal elements. SHELL181 is suitable for non-linear, high rotation, linear and large deformation applications. Changes in coating thickness are taken into account in non-linear analyses [96]. SHELL181

is used for sandwich applications to model sandwich structures or composite shells. First-order shear deformation theory (usually called Mindlineissner shell theory) is used to model composite shells to improve modelling accuracy. The element formula is based on logarithmic measures of actual stress and strain.

The analysis based on the surface model requires determining the offset in the case of performing strength analyses. It is also necessary to assign connections between modelled elements. Parametric modelling requires a very precise determination of these values in order to keep the elements moved parametrically within the previously used limits and to change the position of only planned elements parametrically. Incorrect constraint assumptions can distort the model when parametrically repositioning assumed components. The initial model has been presented in the visualisation (Fig. 72). All elements of the structure were based on a given geometry.
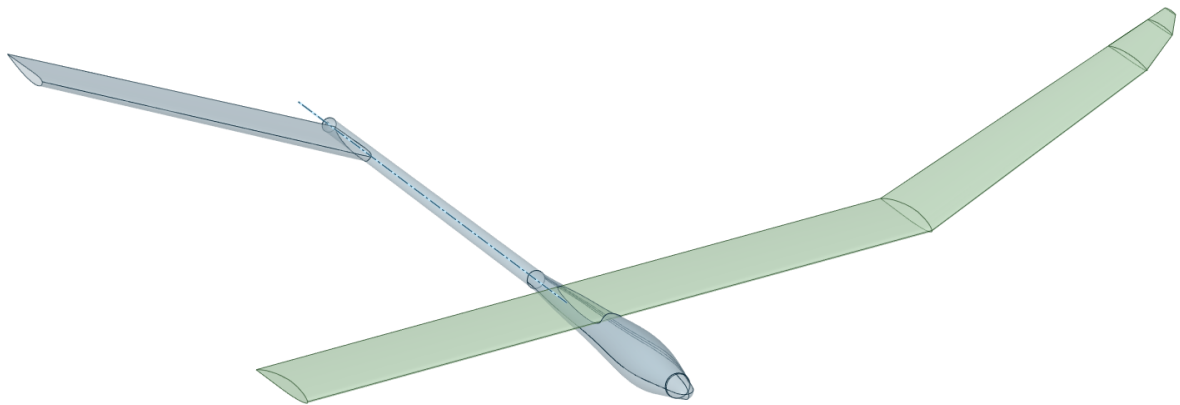
Figure 72 Preliminary surface model determining the analysed object

Modelling of elements was based on surfaces. Because of the use of a generative model, it is the only possibility to recreate the structure, material and automatically generate the mesh. The modelled and analysed elements of the wing are presented in the table (Table 23). The assumed methodology of placing composites by appropriate modelling of the direction and number of layers in composite materials was also taken into account. Due to the complexity of the work and the need to analyse the wing of the tested object at a given stage, the parameters of the fuselage structure, tail beams and the empennage itself were defined as substitutes. This procedure is aimed at reducing the complexity of calculations and improving the accuracy of the results obtained for the analysed wing structure.

Tab 23 Specification of elements of the modelled wing

Nr	Part name	Assumed materials for the part	Thickness / Number of layers
1	Main wing – top skin	Carbon fabric 80 [g/m^2] + Sandwich foam PVC 60 [kg/m^3] + Carbon fabric 80 [g/m^2]	1x: 45° -45° + 2 [mm] + 1x: 45° -45°
2	Main wing – bottom skin	Carbon fabric 80 [g/m^2] + Sandwich foam PVC 60 [kg/m^3] + Carbon fabric 80 [g/m^2]	1x: 45° -45° + 2 [mm] + 1x: 45° -45°
3	Wing tip – top skin	Carbon fabric 80 [g/m^2] + Sandwich foam PVC 60 [kg/m^3] + Carbon fabric 80 [g/m^2]	1x: 45° -45° + 2 [mm] + 1x: 45° -45°

		Carbon fabric 80 [g/m^2] + Sandwich foam PVC 60 [kg/m^3] + Carbon fabric 80 [g/m^2]	1x: 45° -45° + 2 [mm] + 1x: 45° -45°
4	Wing tip – bottom skin		
5	Main wing – wing spar	Carbon fabric 80 [g/m^2]	2x: 45° -45°
6	Wing tip – wing spar	Carbon fabric 80 [g/m^2]	2x: 45° -45°
7	Spar grid –sandwitch foam	Sandwich foam PVC 60 [kg/m^3]	3 [mm]

Each material is described in terms of thickness. This procedure is necessary to determine the required offset between the modelled surfaces. The automatic generation model, together with the material parameters described in this way, allows for automatic shifting of the spar along the chord by the assumed pitch and covering the appropriate surfaces with the given material. The determination of the mass parameters is the result of the shape function defining each element and the parameters of the material in the form of density. Based on the model developed in this way and the analyses carried out in this way, it was possible to prepare the graph of results presented in the next part of the work. The arrangement of the initially assumed sash materials adopted in the project is shown in the visualisation (Fig. 73).
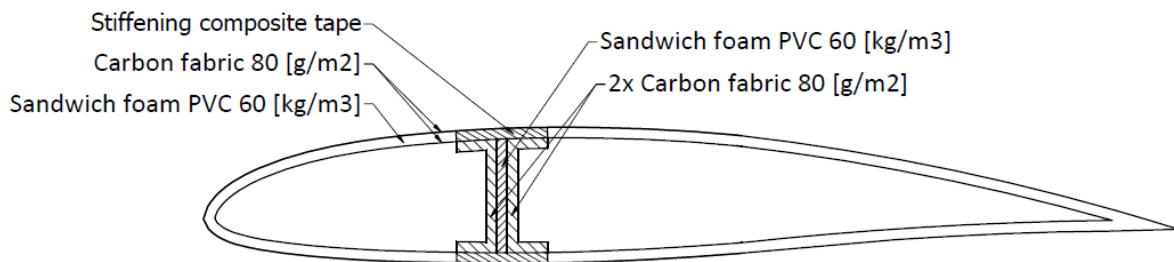
Figure 73 Arrangement of layers assumed in the project

6. Optimisation of the structure of the main wing of the analysed UAV

The methodology developed for the analysis assumes the introduction of structural changes. The problem with the analysis is to combine all the changes in one test environment. Assuming that only the main wing should be optimised, and more precisely the position of the main spar part and the number of layers of stiffening material in a given cross-section, it is necessary to determine the response matrix for each of the assumed states. The analysis began with determining the values of the extreme positions of the supporting spar, the thickness of the materials themselves, the length of these materials, and the masses that are an integral part of the optimisation of aircraft.

Optimisation of the analysed object can be carried out on several basic methodologies; they were presented and described by Wróbel and Stanicki [97]. Czop, Sławik, and Wszołek presented a comparison of the methodology based on the experimental tests of the optimised parts and the numerical optimisation based on mathematical models [98]. Due to the simplification of the analysis and optimisation based on the assumed stiffener distributions, the analysis was carried out as a set of numerical experiments for all assumed states, not taking into account intermediate states due to production constraints. Due to the type of optimised object and the way it is used, the optimisation parameters were defined in the form of a three-dimensional chart consisting of the following values:
- Location of the main spar wall about the length of the wing chord;
- Type of stiffening layers applied;
- Values of the safety factor based on Tsai-Wu destruction criteria of an optimised wing;

Changing step with which the values of the location relative to the chord, the minimum and maximum number of stiffening layers, and the extreme lengths of the stiffening values were assumed. The assumptions established a map of possible changes and the number of calculations that should be carried out was predetermined. It should be remembered that the determined safety factor for each of the main wing spar positions must be analysed for three cases of critical flight parameters.

Due to the multitude of calculations planned to be carried out, it was necessary to develop a method to systematise the calculations. Due to such a need, an attempt was made to automate the calculations based on the parameterisation of the model. The main requirement for automation was to define the path of changes of parameters placed in the model, to determine the constants, and in what order the analyses should be performed. The developed calculation plan is presented as a diagram shown in the figure (Fig. 74). The assumptions of the calculation method were based on the time required to change a given value. During the analyses, the load parameters were changed once for all parameters. Then the values of the position of the main spar along the reference chord of the wing were changed, taking into account the change in the height of the spar. Finally, the lengths of the layers of material used for the stiffening of the spar cap were changed. Due to the type of calculations defined in this way, it was possible to automate the analyses based on the MS Excel spreadsheet combined with the proceeds generated in the Ansys software.
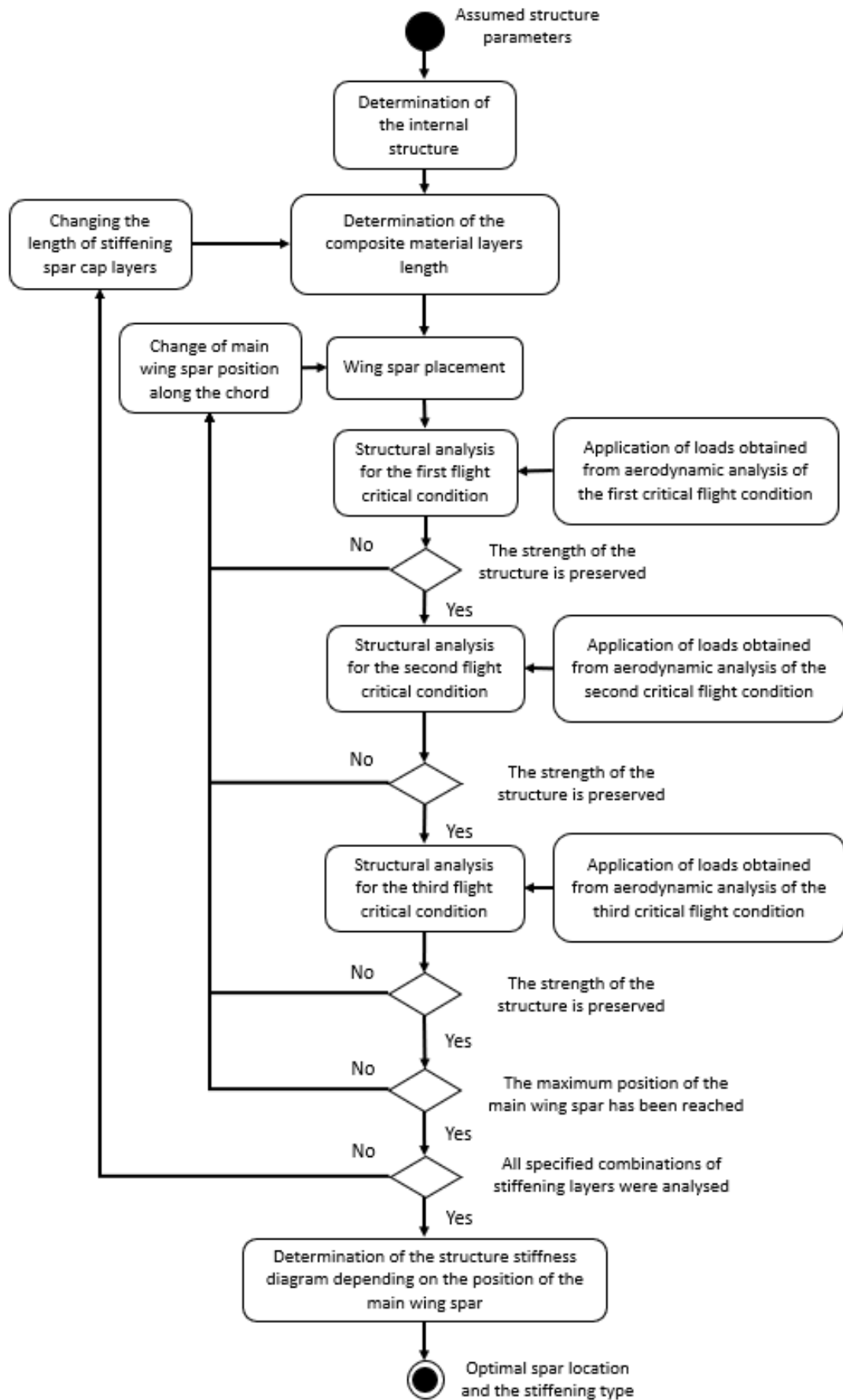
Figure 74 Diagram of the procedure for analysing the spar influence of the position on the parameters of the structure

The developed work plan was transferred to the Ansys Workbench environment, where an attempt was made to combine the analysis path itself and the parameters used during modelling and analysis with the prepared path (Fig. 75). The main assumption of using the calculation sheet was the ability to generate a large number of result matrices presenting the safety factor of the optimised wing for the assumed parameters.
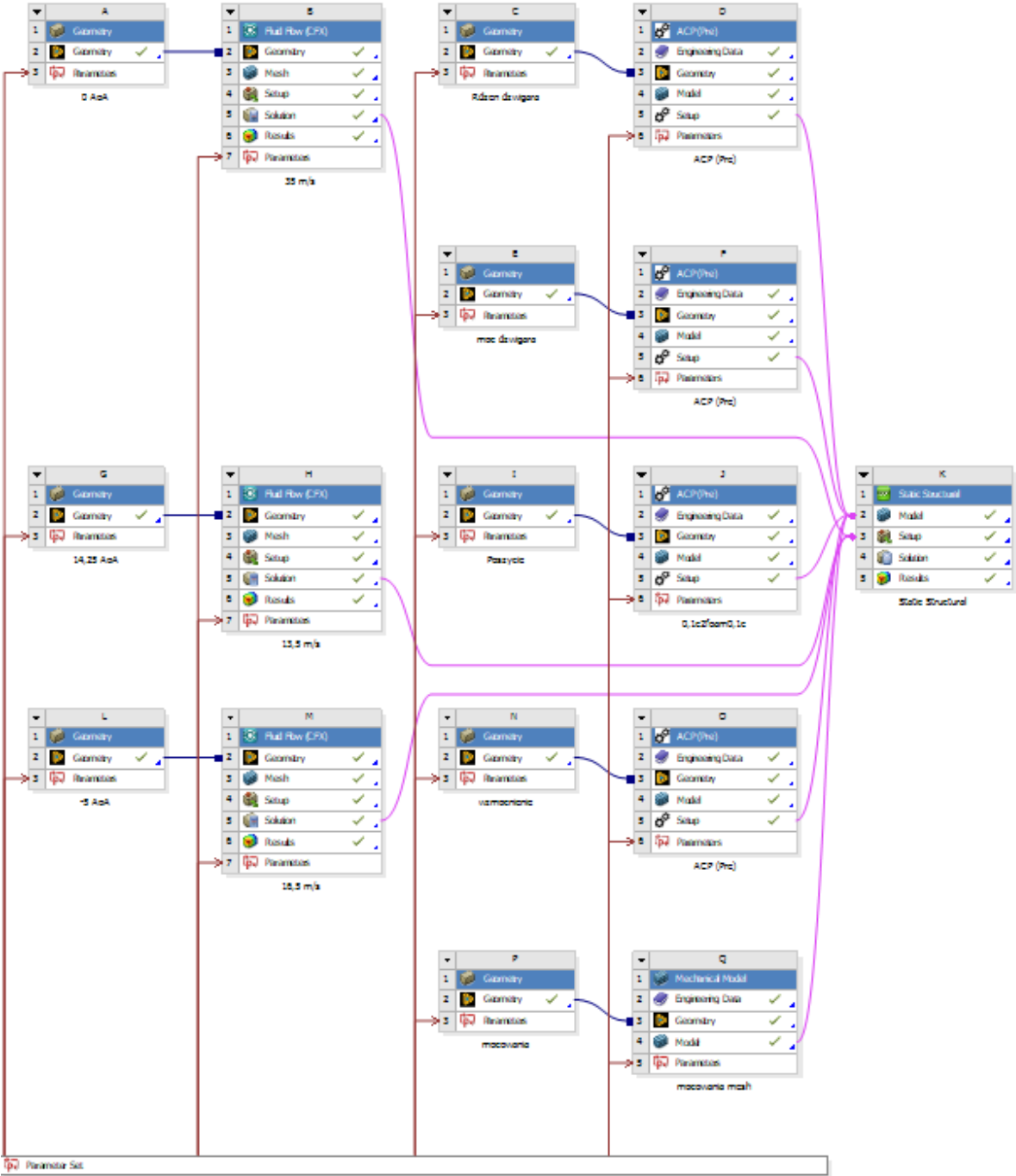
Figure 75 Diagram of analyses performed in Ansys

Due to the assumptions regarding the tested object and the analytically determined loads acting on the wing of the aircraft, they were developed based on the information contained in point 5.2.2 "Determination of the exact external shape of the analysed UAV and the distribution of aerodynamic loads". Load analysis in the form of pressures acting on the wing in the assumed critical states was performed for the wing of the analysed structure.

The loads acting on a given element determined during analytical tests and preliminary numerical calculations resulted in the development of the designed object and the abandonment of the use of thickened composite layers over the entire surface of the analysed wing (Fig. 31). The design has been developed with laminated stiffeners only at the connection point of the main spar to the wing. In order to stiffen, unidirectional carbon roving tapes were used.

The decision was made to lay the main wing spar cap stiffening straps as follows (Fig. 76). The layers specified in the visualisation below are intended to increase the load capacity of the wing. Due to this, the installation of an additional load in the form of measuring equipment in the central part of the analysed aircraft will be safe for the structure.
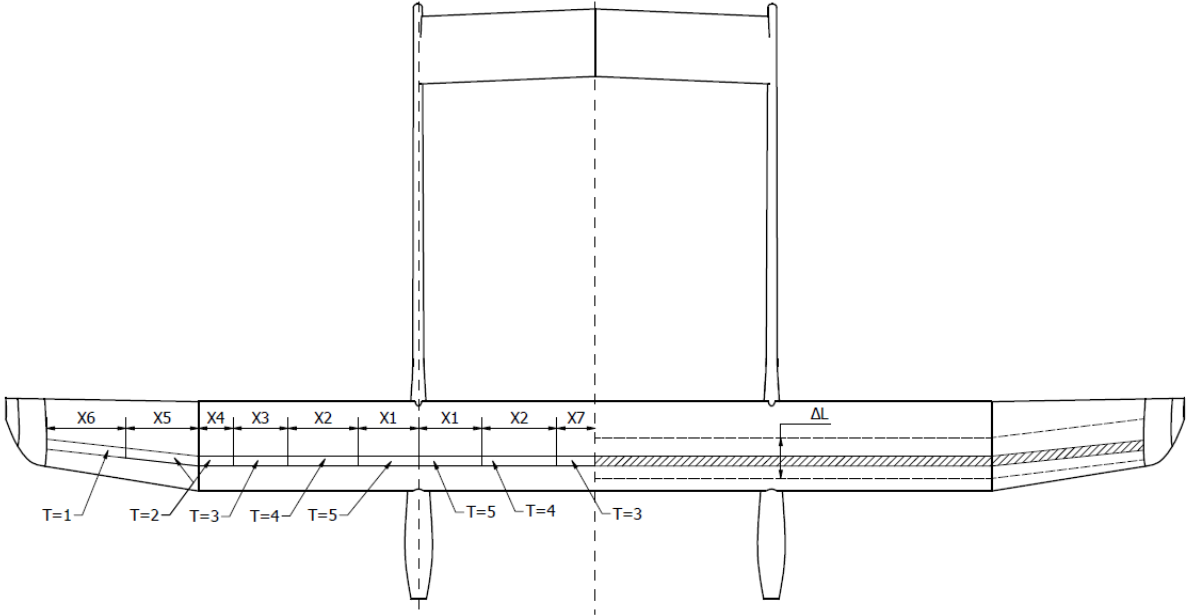
Figure 76 Presentation of assumptions regarding the parameterization of the model

As can be seen, the distances of the optimised stiffening strip with five and four layers (T=5 and T=4) are symmetric to the fuselage. This assumption aims to eliminate too low a stiffness in the fuselage axis. If the analyses show that there is no need to use five-layer stiffeners along the length of the wing from the fuselage axis to the aircraft axis, the thinnest stiffening material on the aircraft axis is the material with three additional layers of composite.

The location of the main wing spar of the designed aircraft was also optimised. The ΔL parameter shown in the figure is responsible for change of position (Fig. 76). This parameter assumes the limit possibility of displacement of the wing spar. The parametric change of position is done by dividing a given distance into a number of steps and then performing analyses for each of the assumed positions.

Data on the optimised parameters are presented in the table (Tab. 24). The parameters are also presented as functions of length. This procedure allowed to reduce the number of variables used in the analyses.

Tab. 24 Variable parameters adopted during modelling

Nr	Name of parameter	Symbol	Max value	Min value
1	Distance from the axis of symmetry of the fuselage to the end of the layer T=5	X1	550 [mm]	0 [mm]
2	The length of the layer T=4 from the end of the layer T=5	X2	X2=550-X1 [mm]	0 [mm]
3	The length of the layer T=3 from the end of the layer T=4	X3	X3=550-(X2+X1) [mm]	0[mm]
4	The length of the layer T=2 from the end of the layer T=3 to the end of the wing tip	X4	100 [mm]	100 [mm]
5	Layer length T=2 from the end of the wing tip	X5	350 [mm]	0 [mm]
6	Layer length T=1 from end of layer T=2	X6	X3=500-X5 [mm]	0 [mm]
7	Possibility to move the main spar along the wing chord	ΔL	130 [mm]	50 [mm]

The results of the analyses and the duration of the calculations are closely related to the care with which the model is prepared and the mesh describing its shape has been defined. Any deviation from the actual model may result in incorrect results.

When optimising the wing of the analysed object, it was necessary to carry out a large number of calculations coupled with the use of many geometrical variables of the structure. A decision was made to separate the optimisation analyses into two parts.

The first part is related to the change in the position of the spar along the chord of the tested object. For this analysis, a five stiffening layers number was assumed throughout the entire width of the analysed panel. The impact of changing the position of the spar and spar cap with stiffening layers was determined on the basis of the Equivalent (von Mises) Stress results and Composite Failure based on the Tsai-W criterion.

The second part of the conducted analysis is related to determining the appropriate distribution of individual layers that stiffen the structure of the analysed object. The analysis was carried out for the spar positions determined as the most favourable on the analyses performed in the first part and based on the developed distribution of the stiffening layers.

6.1. Mesh parameters for aerodynamic analyses

The parameters affecting the size of the elements and those used to determine the mesh developed for the analysis are presented in Table (Tab. 25). The given parameters were used for all aerodynamic analyses of the tested wing.

Tab 25 Options used during generating the mesh used for aerodynamic analysis

Option	Parameters used and their multiplicities	Places of application
Mesh	Element size = 500 [mm]	The shape of a numerical wind tunnel
Inflation	First Layer Thickness = 0,10 [mm], Maximum Layers = 30, Growth Rate = 1,2	The entire main wing skin
Edge Sizing	Number of Divisions = 300	The leading and trailing edges of the analysed wing
Face Meshing	Element Size = 4 [mm] Curvature Normal Angle = 1°	The entire main wing skin

The correctness of the density of the elements was confirmed by performing aerodynamic analyses for a different number of elements and comparing their values. In the case of a properly developed mesh density, the size of the forces obtained during the analyses does not increase in the required accuracy range in the case of further increasing the number of elements.

On the basis of a given analysis, the parameters generated by the wing during tests performed for a given critical state were determined. The results for the critical states are presented in the table (Tab. 26).

Tab 26 Results of aerodynamic wing analysis of critical states

Parameter	Case I	Case II	Case III
AoA	0 [°]	14,25 [°]	-5 [°]
Horizontal speed	35 [m/s]	19[m/s]	22[m/s]
Elements in mesh	12 626 397	9 452 386	14 464 121
Nodes in mesh	5 069 389	4 405 073	6 784 243
Lift Force	162,33 [N]	226,00 [N]	-49,70 [N]
Drag Force	10,40 [N]	22,85 [N]	5,87 [N]
Comparative analytical results			
Lift Force	200,15 [N]	228,12 [N]	-44,28 [N]
Drag Force	4,25 [N]	8,69 [N]	2,56 [N]

The cross section of the modelled object in the form of its mapping using a mesh filling the aerodynamically analysed body is shown in the visualisation (Fig. 77).
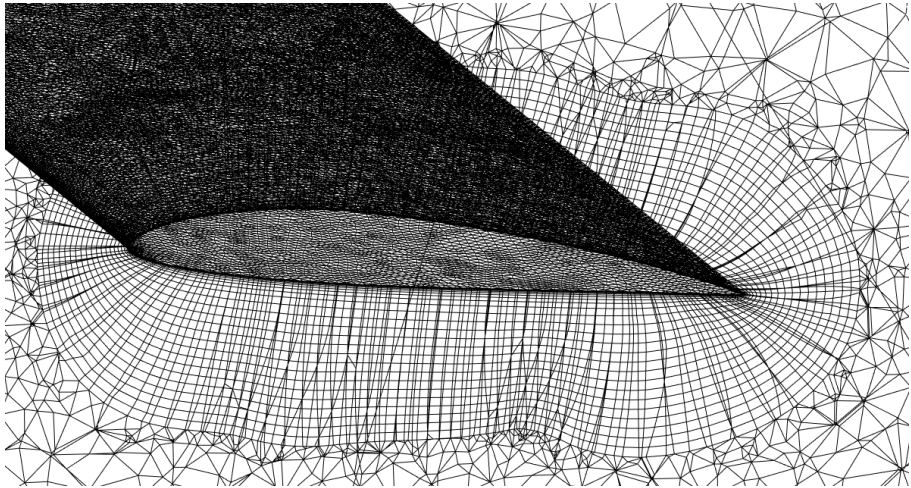
Figure 77 Cross-section of the modelled object with the generated mesh based on specific parameters

6.2. Development of a parametric model of the internal structure

In accordance with the parameters adopted at the previous stages of the analysis, a model of the internal structure of the analysed wing was developed. Structural elements defined as "movable" were designed based on the "Blocks" function that is available in the Space Claim Modeller extension of the Ansys software (Fig. 78). Without activating a given option during model preparation, it is not possible to determine the parameters of modelled elements.

Figure 78 Blocks icon to start model change history

When this option is activated, all options and dimensions defined during modelling are saved on an ongoing basis. An additional advantage is the launch of a window that presents the parameters used in the model being executed. The window presenting the parameters is a facilitation on the basis of which it is possible to determine the correctness of the assigned parameters (Fig. 79).

Figure 79 Space Claim Modeller view with Blox enabled

The correctness of the generated model for extreme positions was tested by entering the extreme distances and starting the automatic generation of the model to obtain information about errors. Extreme positions are shown in the form of the distance between the front wall of the spar grid and the wing leading edge. On the visualisation (Fig. 80) shows the extreme frontal position considered, where the distance from the shear web to the wing leading edge is 60 [mm]. On the visualisation (Fig. 81) shows the extreme rear position considered, where the distance from the spar wall to the leading edge is 110 [mm]. The properties of the material adopted and types of fastenings between individual elements of the structure moved according to changes in the position of the main spar. The generative modelling stage was performed correctly and in accordance with the assumptions set out in the earlier stages of the work.
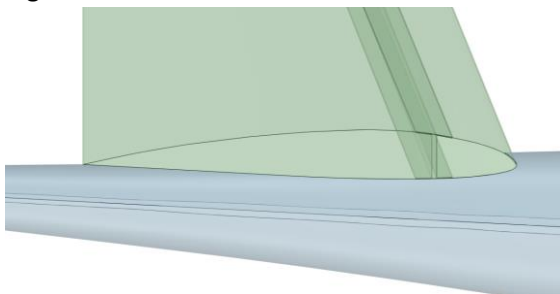
Figure 80 Extreme front position of the main wing spar
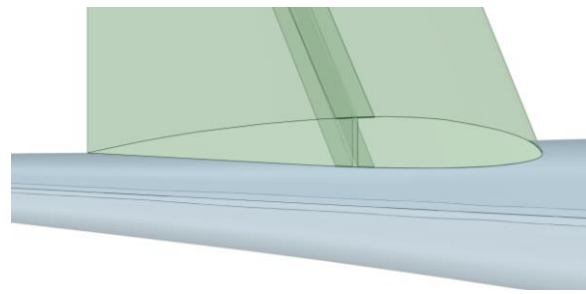
Figure 81 Extreme rear position of main wing spar

Confirmation of the automatic generation of the model based on the prepared parameters made it possible to proceed to further stages of analysis, which are the development of the mesh of the tested object based on the assumed structure elements.

The stiffening layers were placed on the planes that represent the spar cap. The mapping allowed for the most accurate possible modelling of the tested composite in a given place. The loads obtained during the aerodynamic analyses are assigned directly to the surfaces that represent the outer skin of the wing. The modelling method is presented in a simplified way in the graphic (Fig. 82).
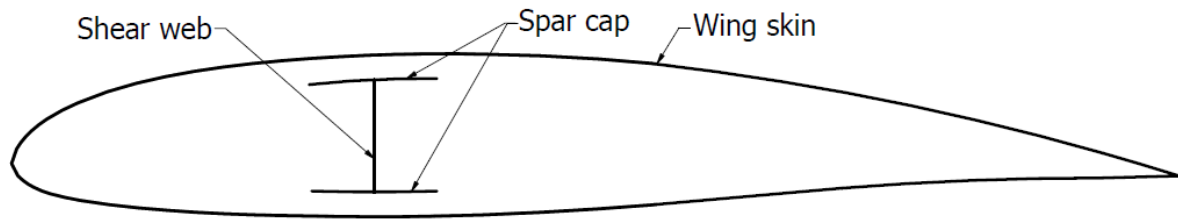
Figure 82 Presentation of the modelling method of the tested structure surface.

Finally, the object structural model of the analysed is presented in the visualization (Fig. 83). The developed model retains the parameterisation and the spar change of position along the chord do not affect the distance offset of the plane representing the wing skin and the spar parts parallel to them.
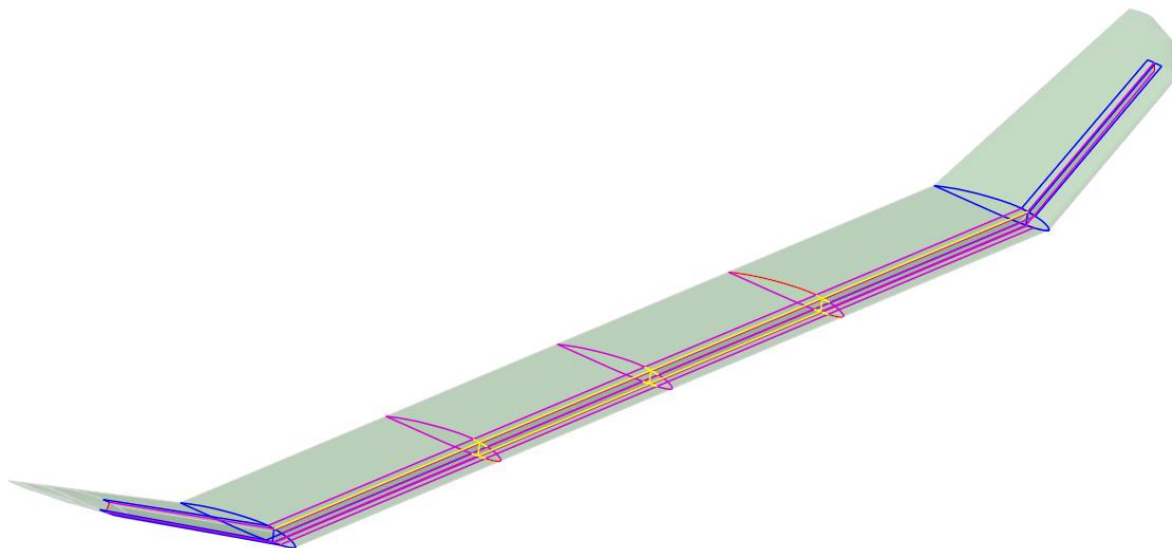
Figure 83 Parametric surface model of the examined structure developed for analysis

6.3. Determination of material parameters of the analysed structure

The properties of the materials used in the analysed structure are difficult to assess. The most accurate method to determine the given parameters is to perform bench tests performed on real samples. Due to the conduct of the analysis in a numerical environment, the possibilities related to the determination of parameters are very narrow and are based mainly on ready-made material databases and data provided by other scientists working on the tested materials.

The types of materials from which the leaf was planned to be made are presented in the table (Tab. 23). It was decided not to optimise the structure elements consisting of hybrid composites (sandwich materials), but to reproduce them using the APC module of the Ansys software.

The distribution of stiffening composites and the relationships between the layers are specified in the table (Tab. 24). The problem lies in mapping a given structure. For this reason, a decision was made to further discretise the materials used on the given components.

Knowing the density of the assumed material and having the data provided by the manufacturers of materials with similar parameters, the most appropriate materials were selected [99]. The materials used in the modelling of the analysed structure were taken from the Ansys software library. The materials used are shown in the table (Tab. 27).

Tab 27 Mechanical properties of selected materials.

Material	Density $\left[\frac{kg}{m^3}\right]$	Young's Modulus			Shear Modulus		
		Ex [Gpa]	Ey [Gpa]	Ez [Gpa]	XY [MPa]	YZ [MPa]	XZ [MPa]
Epoxy Carbon UD (230 GPa) Wet	1518	123,34	7,78	7,78	5000	3080	5000
PVC Foam	60	0,07	0,07	0,07	27	27	27

The distribution of individual layers of the material was determined in accordance with those adopted in the chapter 6 "Optimisation of the structure of the main wing of the analysed UAV". The exact arrangement of the layers, the type of material used, and the directions of the fibres are shown in the table (Tab. 28).

Tab 28 Arrangement of layers of materials on the tested components.

Materiał	Layer thickness	The number of layers	Direction relative to the span
Wing skin			
Epoxy Carbon UD (230 GPa) Wet	0,05 [mm]	1	45°
Epoxy Carbon UD (230 GPa) Wet	0,05 [mm]	1	-45°
PVC Foam	2 [mm]	1	0°
Epoxy Carbon UD (230 GPa) Wet	0,05 [mm]	1	45°
Epoxy Carbon UD (230 GPa) Wet	0,05 [mm]	1	-45°
Wing spar			
Epoxy Carbon UD (230 GPa) Wet	0,1 [mm]	1	45°
Epoxy Carbon UD (230 GPa) Wet	0,1 [mm]	1	-45°
PVC Foam	3 [mm]	1	0°
Epoxy Carbon UD (230 GPa) Wet	0,1 [mm]	1	45°
Epoxy Carbon UD (230 GPa) Wet	0,1 [mm]	1	-45°
Spar cap base components			
Epoxy Carbon UD (230 GPa) Wet	0,1 [mm]	1	45°
Epoxy Carbon UD (230 GPa) Wet	0,1 [mm]	1	-45°
Additional stiffening layers			
P1 - Epoxy Carbon UD (230 GPa) Wet	0,1 [mm]	1	0°
P2 - Epoxy Carbon UD (230 GPa) Wet	0,1 [mm]	2	0°
P3 - Epoxy Carbon UD (230 GPa) Wet	0,1 [mm]	3	0°
P4 - Epoxy Carbon UD (230 GPa) Wet	0,1 [mm]	4	0°
P5 - Epoxy Carbon UD (230 GPa) Wet	0,1 [mm]	5	0°

The mapping, however, consists in arranging the directions of the individual layers of the composite material according to the actual layout. Due to the possibility of using unidirectional fibres or woollen material, a decision was made to simulate the arrangement of a fabric composite by applying two layers of unidirectional composite at an angle of 90 ° to each other. Using such a simplification, it was possible to reproduce the carbon composite fabric, and the fibre arrangement of the outer skin layer was developed as in the picture (Fig. 84).
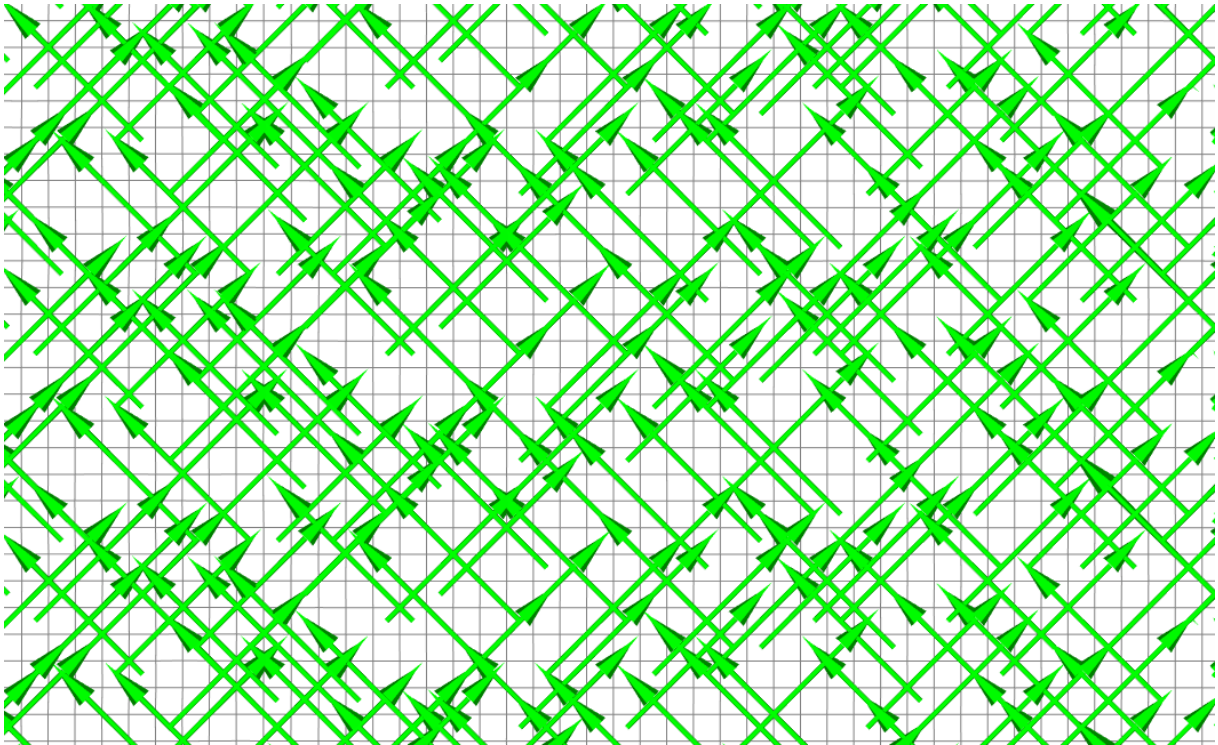
Figure 84 Fibre arrangement of the composite of the outer layers of the skin

The optimised main panel was divided into components whose layering was reproduced in accordance with the initial design. On the visualisation (Fig. 85) the arrangement of the fibres of the main spar reinforcing layers is shown.
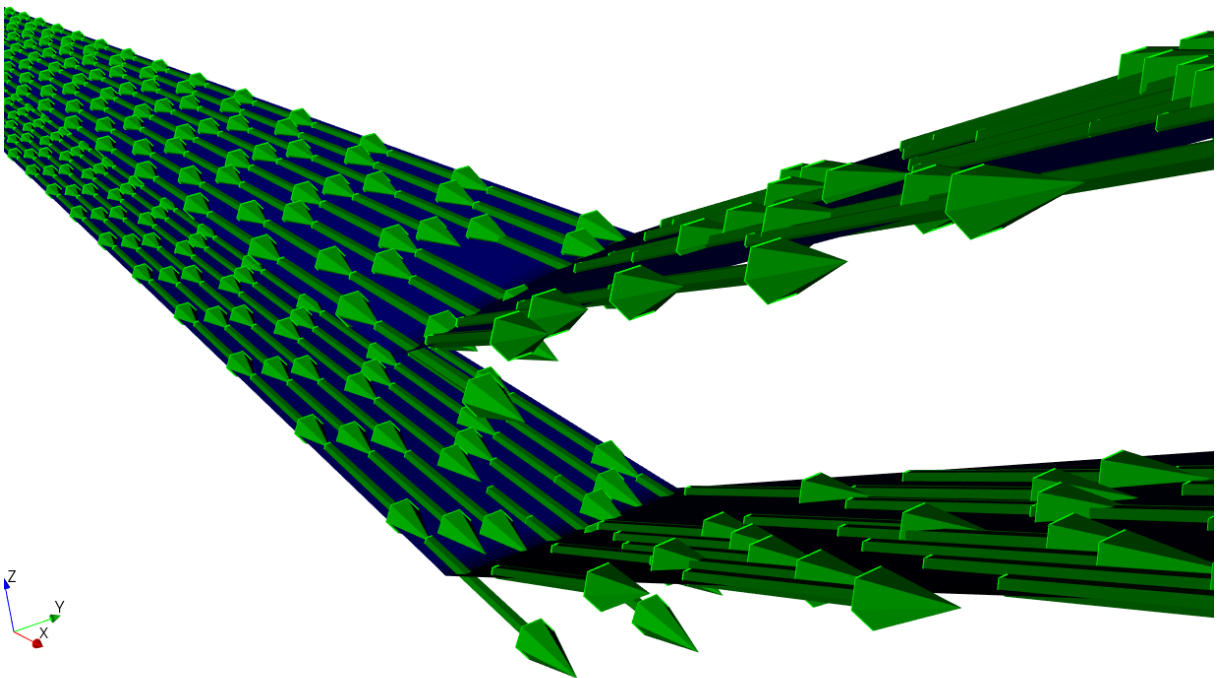
Figure 85 Laying of the fibres of reinforcing layers of the spar cap

6.4. Developing a mesh for the structure model

The model of the object analysed was developed as a combination of individual layered components. Due to the use of the APC (PRE) module, which allows to generate the directional arrangement of

individual composite layers, it was necessary to develop independent meshes representing each of the components.

Components mapped with a mesh and covered with properly arranged composite layers specified in Subchapter 6.3 "Determination of material parameters of the analysed structure", were sent to the Static Structural Mechanical module. To improve the quality and reproduce the structure as accurately as possible, the parameters of the size of external elements were determined according to the aerodynamic analyses carried out. Determining meshes with possibly similar density in the most vulnerable places allows for maintaining the correctness of results and reduces the problem of stress concentration in places of mesh thinning.

The options used to describe the component data and parameter sizes are shown in the table (Tab. 29).

Tab 29 Mesh parameters of the structure of the analysed wing

Option	Parameters used and their multiplicity	Mesh generation result
Wing Skin		
Face Sizing	Element size = 4 [mm]	Elements: 131000 Nodes: 132301
Edge Sizing	Element Size = 2 [mm]	
Ceep radius		
Spar components		
Face Sizing	Element size = 4 [mm]	Elements: 21731 Nodes: 20870
Ribs with fuselage connections and in the symmetry plane of airplane		
Edge Sizing	Element Size = 8 [mm]	Elements: 1229 Nodes: 1044

Bindings of individual components of the analysed structure were developed inside the Static Structural - Mechanical module, in which the assumed structural analyses will be performed. To avoid possible stress concentrations occurring during the analysis of layered models, the MPC option was used, allowing smooth transitions between components. Taking into account the lamination method of real composite structures, a decision was made to use a transition between elements with a radius equal to the thickness of the thinnest joined element.

The created mesh that describes the object analysed consists of 153960 elements and 154215 nodes. In the visualisation (Fig. 86) a close-up of a section of the analysed wing showing the mapping of the analysed structure is shown.
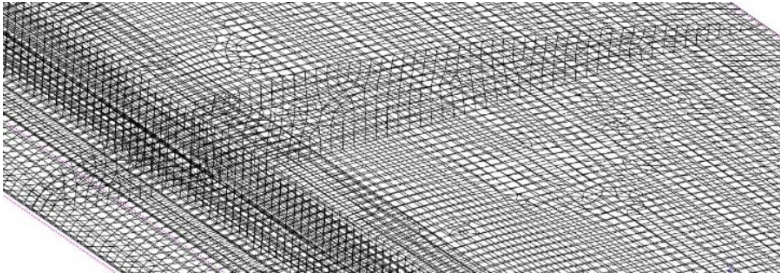
Figure 86 View of the mesh representing the analysed object

6.5. Determination of the extreme values of the position parameters of the structure elements

As part of the optimisation, analytical and mass tests, restrictions on the movement of individual components of the optimised wing were introduced. One of the limitations is the location of the main spar along the chord of the analysed wing. It was planned to limit this position in the range of 60 - 110 mm from the leading edge. To increase the accuracy of the analyses, a decision was made to increase

the number of analysed positions, and the boundary was defined in the range of 50 - 140 mm from the leading edge, maintaining a constant displacement step of 10 mm.

The assumptions regarding the change in the length of individual stiffening layers were determined according to the equations described in the table (Tab. 24). Based on the assumptions, five types of adopted stiffeners were developed, which were analysed for selected spar positions. The boundaries developed in this way made it possible to optimise the structure of the main wing of the object tested.

To increase the accuracy of the results and a more accurate representation of the analysed airplane wing, a decision was made to determine the bonds as shown in the visualisation (Fig. 87). The applied bindings were used in each of the analyses performed. Bindings were applied to the edges of the surfaces, reproducing the shape of the ribs that allow the fuselages to attach.
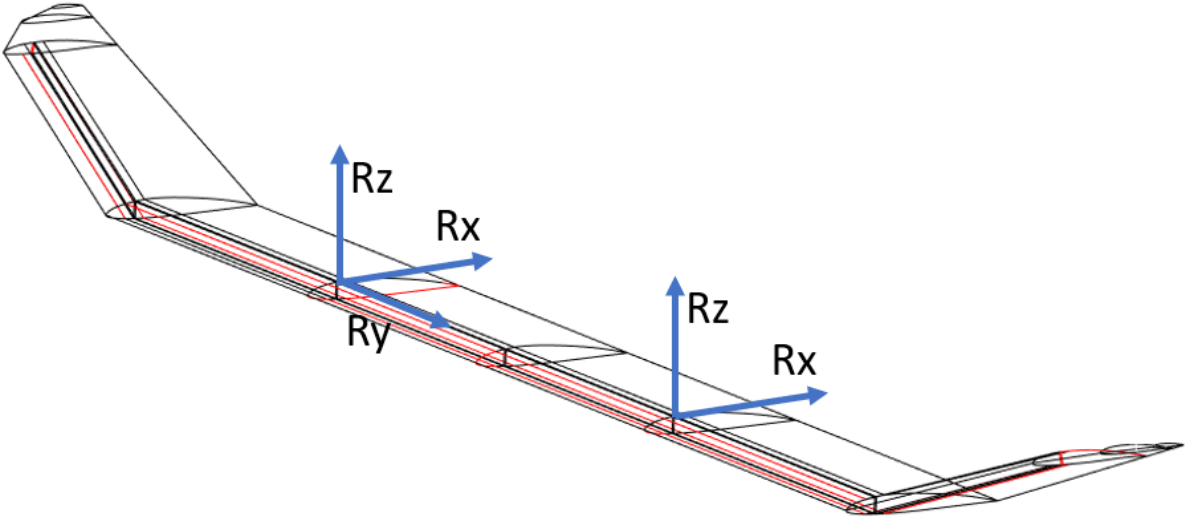
Figure 87 Mounting of the test system during analysis
Where: Rx – Reaction along the "X" axis [N], Ry – Reaction along the "Y" axis [N], Rz – Reaction along the "Z" axis [N]

The use of this solution was to reproduce the layout of the tested object, using two fuselages, which, despite the stiffening of the analysed wing, can work independently in relation to each other in given axes. Determining the fasteners in the following way allowed for analysis of the system in a way that allowed deformation of the wing and displacement of the supports relative to each other. Due to the fuselages connected by the tail part, which were designed in a form similar to a closed round aerofoil, it was considered that the wing mounting in the symmetry plane of the analysed wing would be incorrect due to restrictions on the movement of the fuselages relative to each other caused by the wing and the tail part.

6.6. Influence of spar location on structure properties

The test results described in the following were carried out in order to confirm the correct operation of the generative model, to determine the quality of the mesh developed for the analysed model and to approximate the area where the location of the main wing spar will be most advantageous. The position of the spar relative to the length of the wing chord is evaluated because of the stresses occurring inside the structure and the Tsai-Wu safety factor. The results were developed based on the assumptions presented in point 6.4 "Laying of the fibres of reinforcing layers of the spar cap

Developing a mesh for the structure model". The material parameters of the tested object are specified in the chapter 6.3 "Determination of material parameters of the analysed structure". To simplify the analysis, during the described test, the spar cap stiffening layers obtained a uniform thickness of 0.5 mm throughout the wing span.

The results of the analysis were presented in the form of the location of the main wing spar in a given percentage of the reference chord and the values of the evaluation criteria. The results of the

system analysed for three critical states are described in the table (Tab. 30). Based on the results, the positions of the main wing spar used during a further optimisation analysis of the tested wing were determined.

The table shows the maximum values to which the other results relate in percentage terms. The use of a given treatment allowed to generate graphs in one percent scale, which facilitated further analysis of the results. Appropriate development of the analysis results requires presentation as a percentage in relation to the maximum deformation values, maximum stress, and the Tsai-Wu failure criterion. The Tsai-Wu failure criterion allows for nine failure stresses and three additional coupling factors. It is the general standard and preferred over Tsai Hill, as it distinguishes between tensile and compressive strength.

Tab 30 Main wing spar position change along symmetrical plain analysis results

Nr	Spar position [mm]	Spar position in % MAC	I critical flight parameter			II critical flight parameter			III critical flight parameter		
			Total Deformation [mm]	Inverse Reserve Factor (Tsai-Wu)	Equivalent (Von-Mises) stress [Mpa]	Total Deformation [mm]	Inverse Reserve Factor (Tsai-Wu)	Equivalent (Von-Mises) stress [Mpa]	Total Deformation [mm]	Inverse Reserve Factor (Tsai-Wu)	Equivalent (Von-Mises) stress [Mpa]
1	50	18,3	8,48	0,614	122,65	4,26	0,310	61,14	0,61	0,031	8,91
2	60	22,0	8,69	0,539	121,07	4,37	0,271	60,49	0,62	0,030	8,91
3	70	25,6	7,90	0,629	123,06	3,96	0,317	61,54	0,56	0,030	9,06
4	80	29,3	8,22	0,569	119,43	4,12	0,287	59,87	0,58	0,026	8,98
5	90	33,0	8,20	0,576	117,59	4,09	0,290	58,87	0,58	0,029	8,87
6	100	36,6	8,19	0,576	119,38	4,05	0,289	59,66	0,58	0,027	8,90
7	110	40,3	7,89	0,597	120,80	3,89	0,299	60,17	0,57	0,028	8,81
8	120	44,0	8,29	0,609	124,93	4,02	0,302	62,19	0,64	0,030	9,07
9	130	47,6	8,72	0,632	126,14	4,21	0,313	62,74	0,69	0,032	9,25
10	140	51,3	8,66	0,647	128,26	4,33	0,374	63,94	0,58	0,037	8,30

In order to accurately determine the appropriate location of the wing main spar, power-law trendlines versus chord position were generated for the data. Visualizations of the results developed in the form of a percentage to the maximum value obtained were presented on the graphs (Fig. 88 – 90).
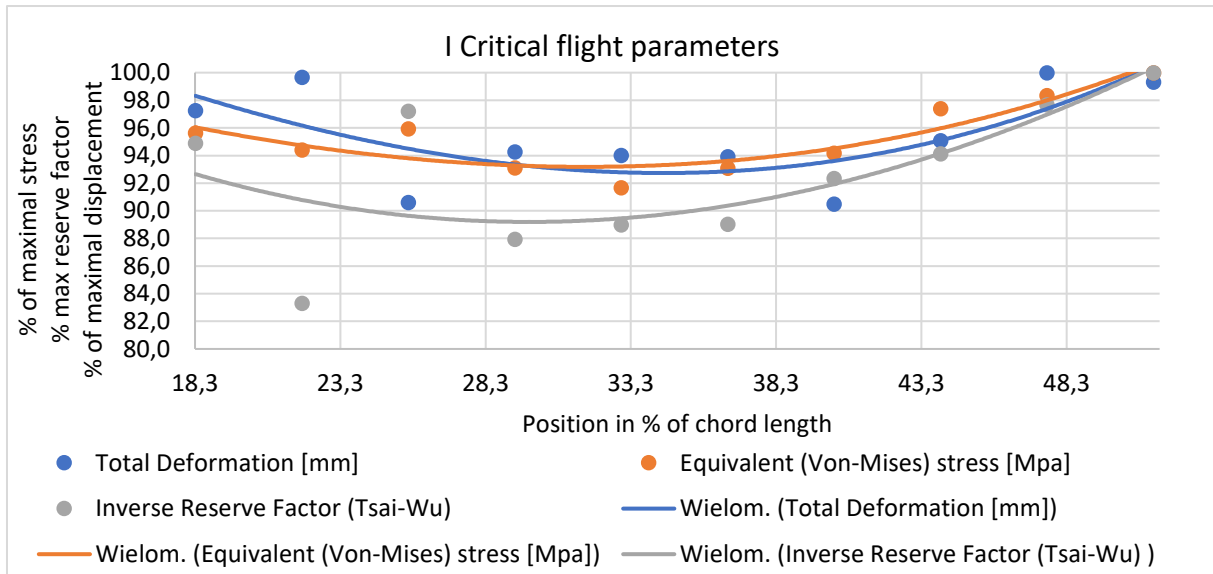
Figure 88 Results of the first analysis of the first critical state
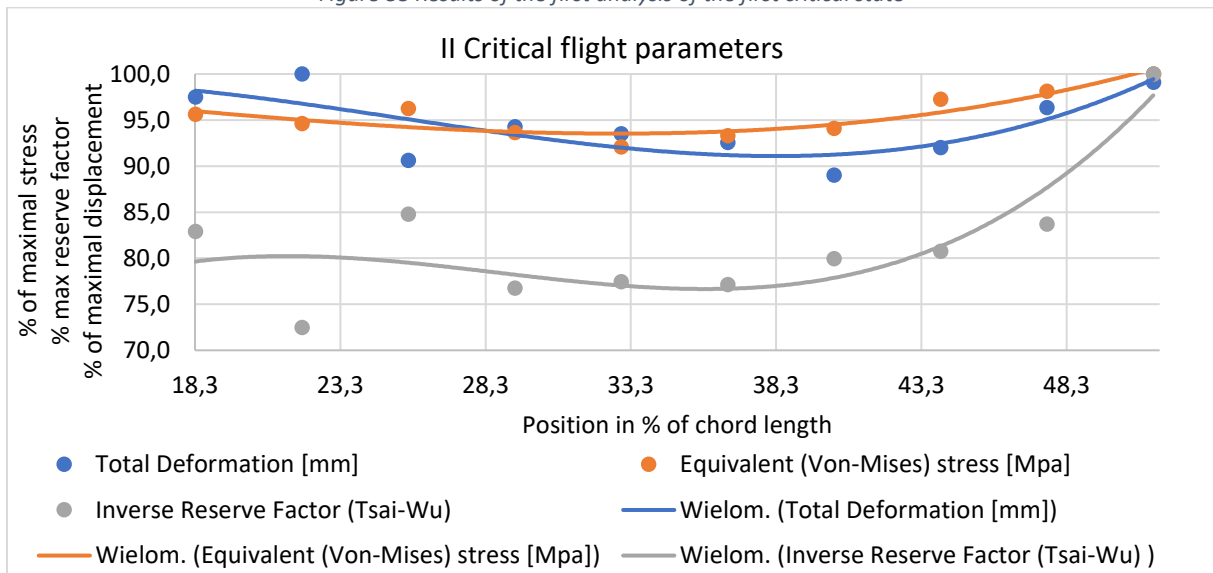
Figure 89 Results of the first analysis of the second critical state
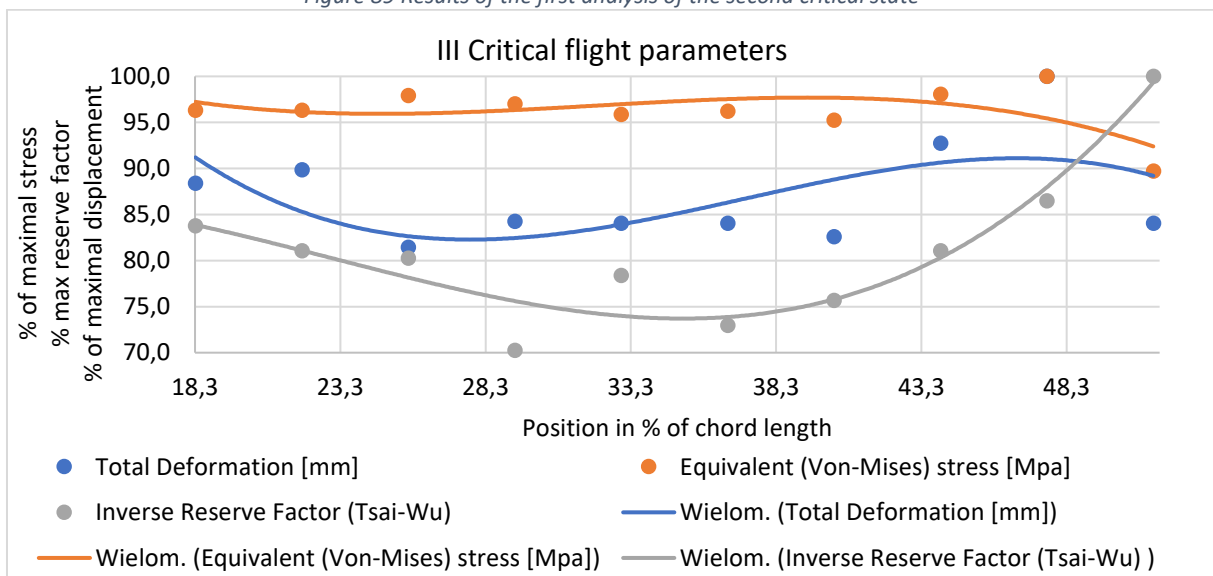
Figure 90 Results of the first analysis of the third critical state

It was noted that the maximum deformations occur in different places depending on the position of the main wing spar along the chord. The first condition is the deformation that occurred at the main wing spar position "X" less than 25% of the MAC and at the main wing tips when the spar position "X" is greater than or equal to 25% of the MAC (Fig. 91). The maximum deformations occurring at the wing tips are consistent with the deformations occurring in the airframes.
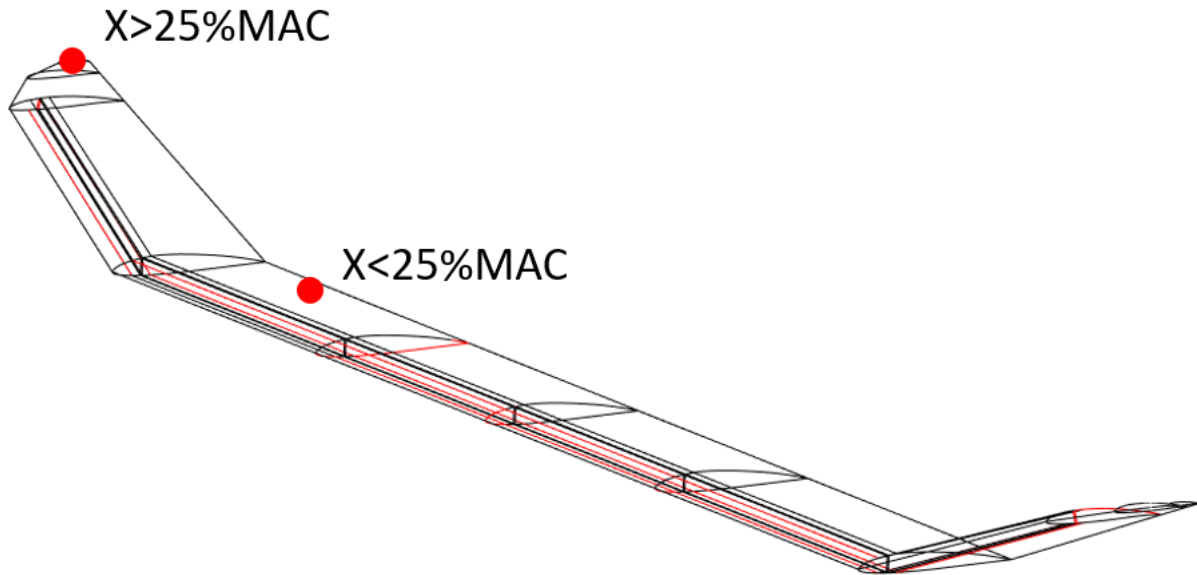
Figure 91 Occurrence of maximum deformation

The results of the analysis developed for the spar position in the position more than 25%MAC are presented in the visualisation (Fig. 92).
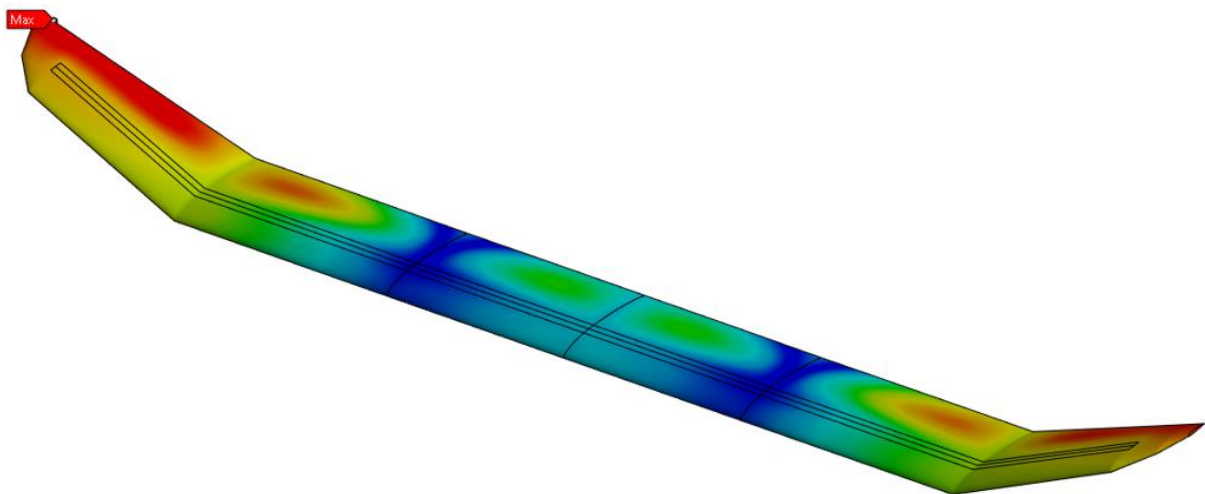
Figure 92 Maximum deformation when X<MAC

The highest stresses and the highest risk of delamination of the composite occur in many places, depending on the analysis (Fig. 93). Normally, extreme values occur in the same place. Each time, the extreme values obtained occur at the places where the main wing spar connects with the ribs used to fasten the fuselages (positions 1 and 3), the central rib allowing the wing to unfold (position 2) or at the connection of the main wing with the wing tip (position 4). The extreme values were reached at the presented points, regardless of the critical state.
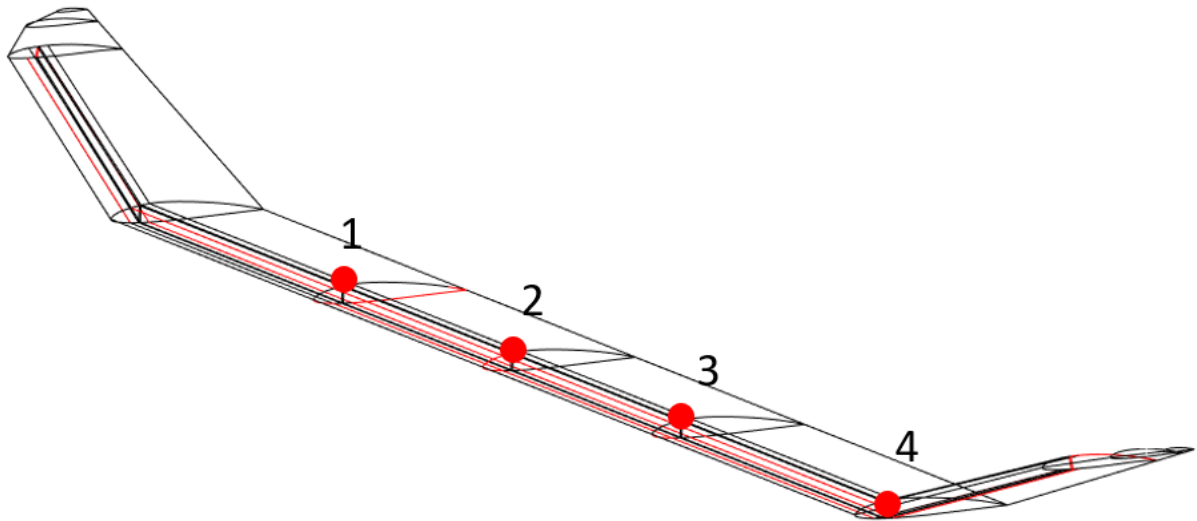
Figure 93 Occurrence of maximum stress and risk of delamination

The location of the maximum stresses in the vicinity of the third position occurred most frequently. The view of the possibility of composite failure according to the Tsai-Wu criterion is shown in the picture (Fig. 94).
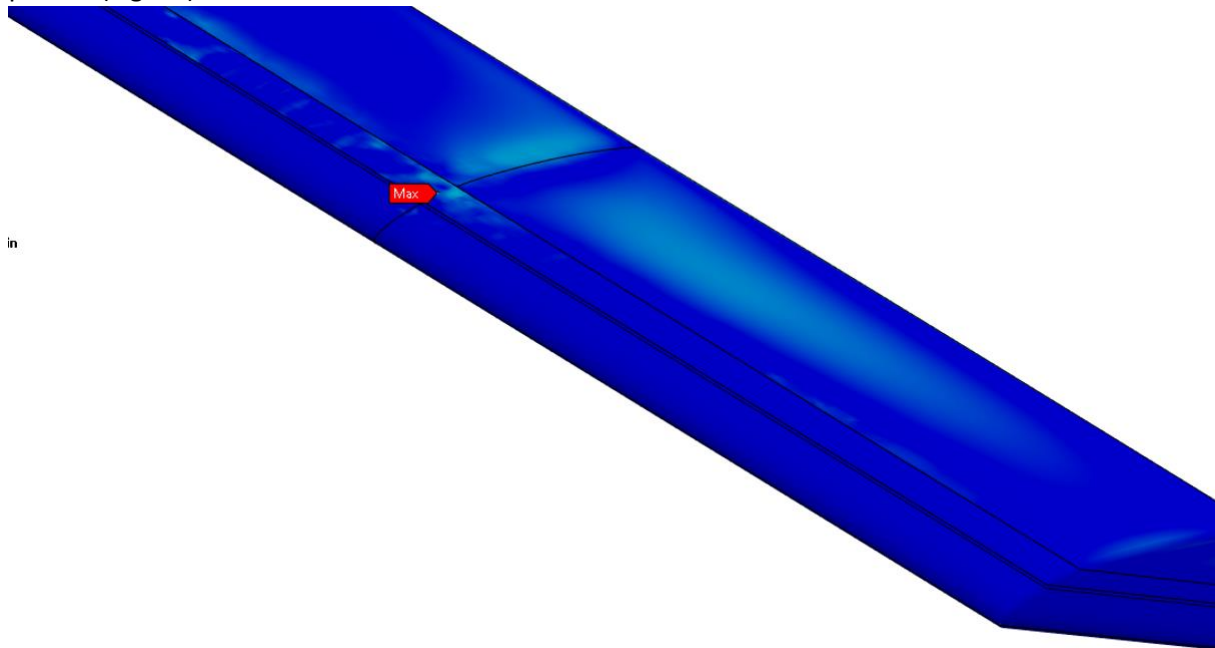
Figure 94 The location of the greatest risk of destruction according to the Tsai-Wu criterion

Conclusions

The graphs developed on the basis of the analyses are drawn in accordance with the assumptions regarding the design of aircraft. As can be seen, the parameters trend lines of the analysed in each of the critical states are slightly different. In first critical flight conditions line decrease along with the displacement of the main wing spar until it reaches the value of about 30% of the chord length, and then they increase again. The dependence is clear, and thus the mesh parameters of the developed for the presented analysis are sufficient to optimise the location of the spars and the length of the individual spar reinforcement layers.

The Tsai-Wu failure criterion shows the same dependence, while the trend line reaches the lowest values of a given parameter in different places depending on the critical state of the analysed structure. The coefficient determines the possibility of damage to the composite, where a value of 1 means the

occurrence of damage, while values between "1" and "0" can be treated as a percentage of the possible occurrence. Due to this fact, it was assumed that the next analysis will be carried out for the main wing spar position of the analysed wing in the range from 25% MAC to 37% MAC, with a step of 3%.

6.7. Presentation of the results of the optimisation analysis

The analyses described in the section 6.6. "Influence of spar location on structure properties" allowed to determine the positions along the chord with which the main wing should be optimised. According to the equations developed in the previous stages of the work, the dependencies of the lengths of individual stiffening layers of the main wing spar were determined.

Due to the simplification of the analysis, a plan of action was developed, presented in the graphic (Fig. 95). The research plan, despite its simplification, is closely related to the research path presented in the visualisation (Fig. 54). Taking into account the results obtained during the previous analyses presented in Section 6.6. "Influence of spar location on structure properties", it was decided to conduct analysis based on one critical condition of the flight at this stage of the research. The first critical state, i.e. horizontal flight with maximum speed, was adopted for the analysis.
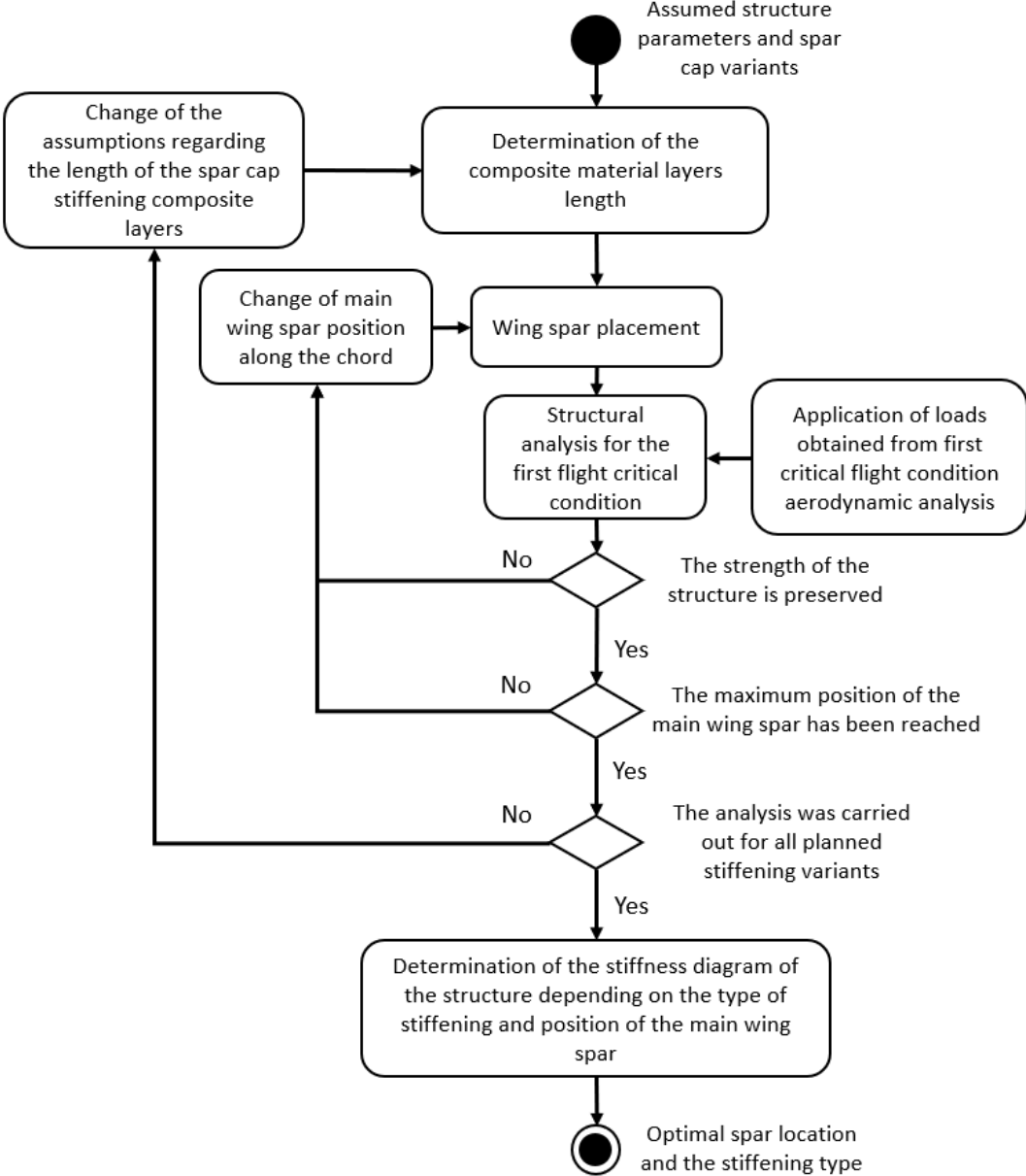
Figure 95 Conducting analyses scheme

95

To map the analysis path, the diagram of the Ansys software presented in the picture (Fig. 75) was developed. The main reinforcement belt was divided into smaller elements that represent individual layers of the material analysed. Each of the materials used in the spar elements was developed in one APC module. Steady elements such as wing skin and ribs were designed end covered by designed materials in separate APC modules The diagram is shown in the figure (Fig. 96).
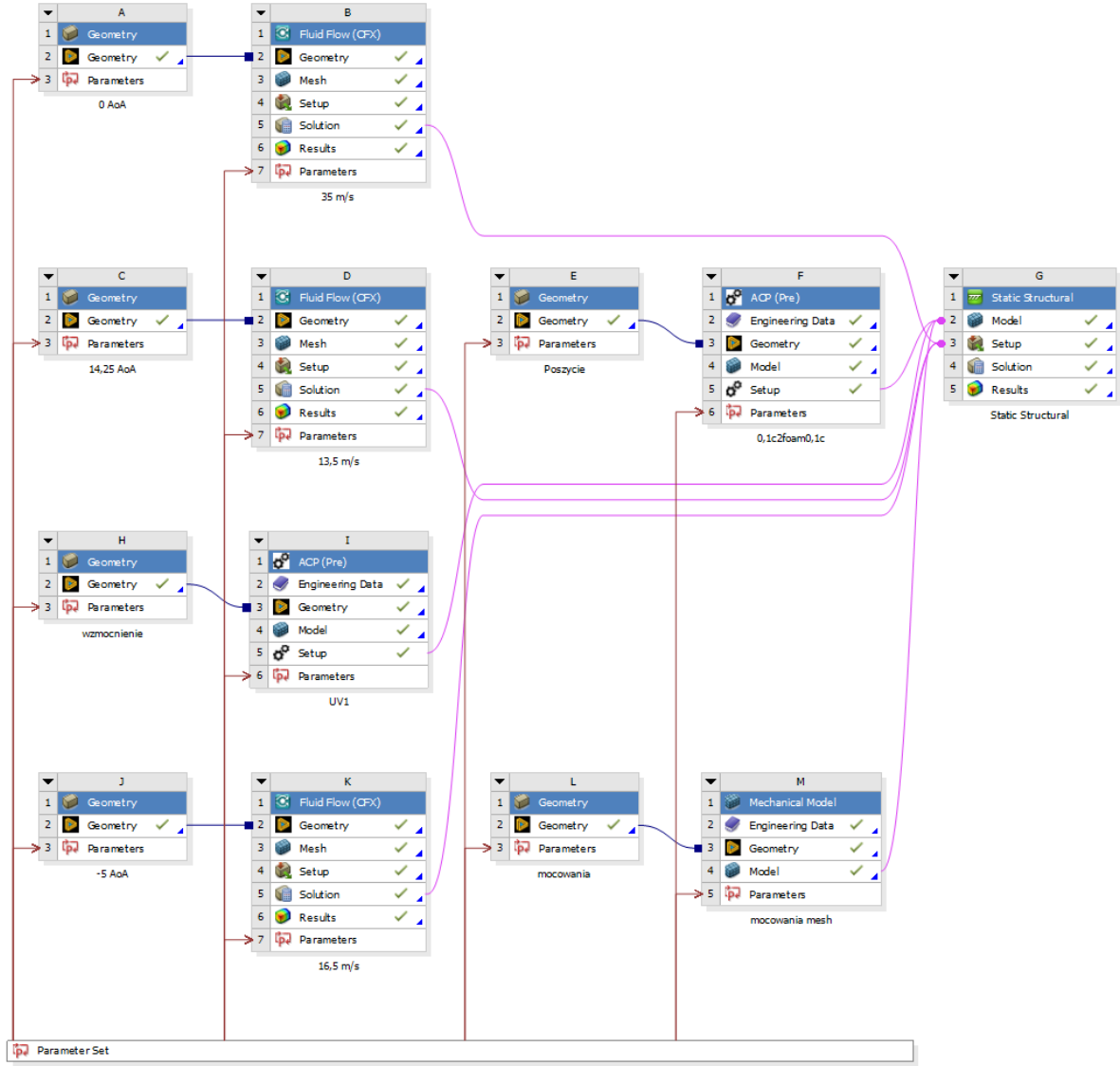
Figure 96 Diagram developed in Ansys for the second stage of analysis

6.7.1. Development of an extensive optimisation model

In the model used to carry out a given stage of optimisation of the analysed wing compared to the previous version, the surfaces reflecting the exact thickness of the stiffening layer were developed (Fig. 97). This is a direct extension of the developed generative model. The use of additional geometric parameters allowed for the automation of the length of individual stiffening layers and obtaining results for five assumed spar cap.
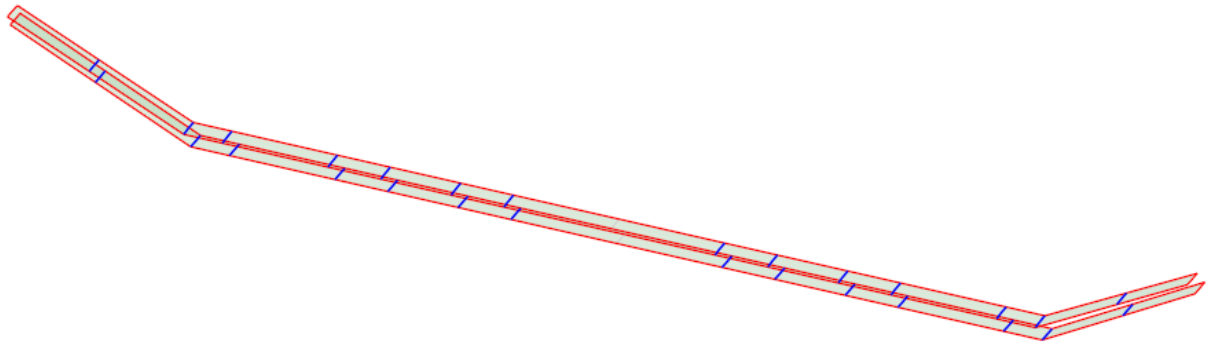
Figure 97 View of a divided surface representing the spar cap

6.7.2. The results of the described analysis

Due to the dependencies between the lengths of the layers, the analyses were carried out for the critical state, which, in the previous analyses, showed the highest structural stresses and deformations of the analysed object. Recognising the correctness of the results determined on the basis of previous analyses, the area of change in the position of the main supporting spar was limited between 25% and 37% of the chord length of the analysed wing, maintaining the position change step every 3%. Five spar stiffening arrangements are specified, from lightest to heaviest. The systems for which the analysis was performed consisted of assumed layers of a specific length. According to the description of individual stiffening layers set out in point 6. "Optimisation of the structure of the main wing of the analysed UAV", the arrangements of the analysed stiffener arrangement, developed for the purposes of optimisation studies, are presented in the table (Tab. 31).

Tab 31 Assumed distribution of stiffening layers

Spar cap stiffening type	Visualization of the system adopted for analysis	Length of stiffening layers
I		T=1: 1000 [mm] T=2: 200 [mm] T=3: 2200 [mm] T=4: 0 [mm] T=5: 0 [mm]
II		T=1: 800 [mm] T=2: 400 [mm] T=3: 2000 [mm] T=4: 200 [mm] T=5: 0 [mm]
III		T=1: 600 [mm] T=2: 600 [mm] T=3: 1600 [mm] T=4: 400 [mm] T=5: 200 [mm]
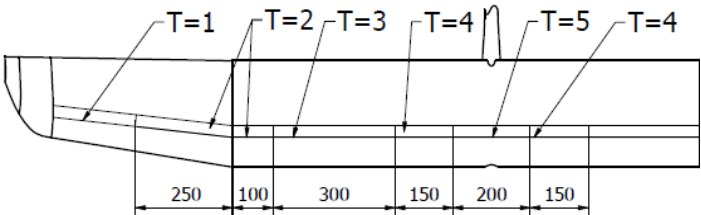
IV	T=1 ⌐T=2 ⌐T=3 ⌐T=4 ⌐T=5 ⌐T=4 250 ⏐100⏐ 300 ⏐150⏐ 200 ⏐150	T=1: 500 [mm] T=2: 700 [mm] T=3: 1200 [mm] T=4: 600 [mm] T=5: 400 [mm]
V	T=1 ⌐T=2 ⌐T=3 ⌐T=4 ⌐T=5 ⌐T=4 300 ⏐100⏐ 200 ⏐ 200 ⏐ 300 ⏐ 200	T=1: 400 [mm] T=2: 800 [mm] T=3: 800 [mm] T=4: 800 [mm] T=5: 600 [mm]
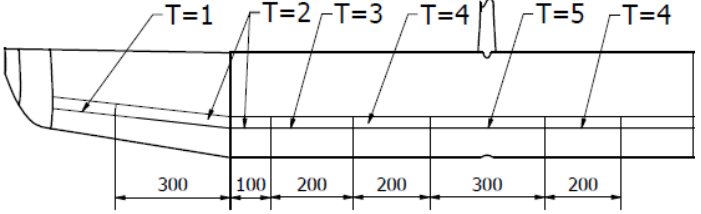
The analyses carried out allowed for the generation of maps of critical stresses and the Tsai-Wu coefficient in the functions of the spar position as well as the location variants of individual stiffening layers. As part of the investigation, it was necessary to determine the load correctness of the transfer between the components of the structure. As part of confirming the correct binding, an analysis was performed in accordance with the assumptions, and then the wing skin model was turned off and the stress distribution view was turned on for the remaining elements. Figure (Fig. 98) represents the given test. In this way, the connections of individual components and the smooth transfer of stresses between the skin, assembly ribs, spars, and reinforcing layers were confirmed.
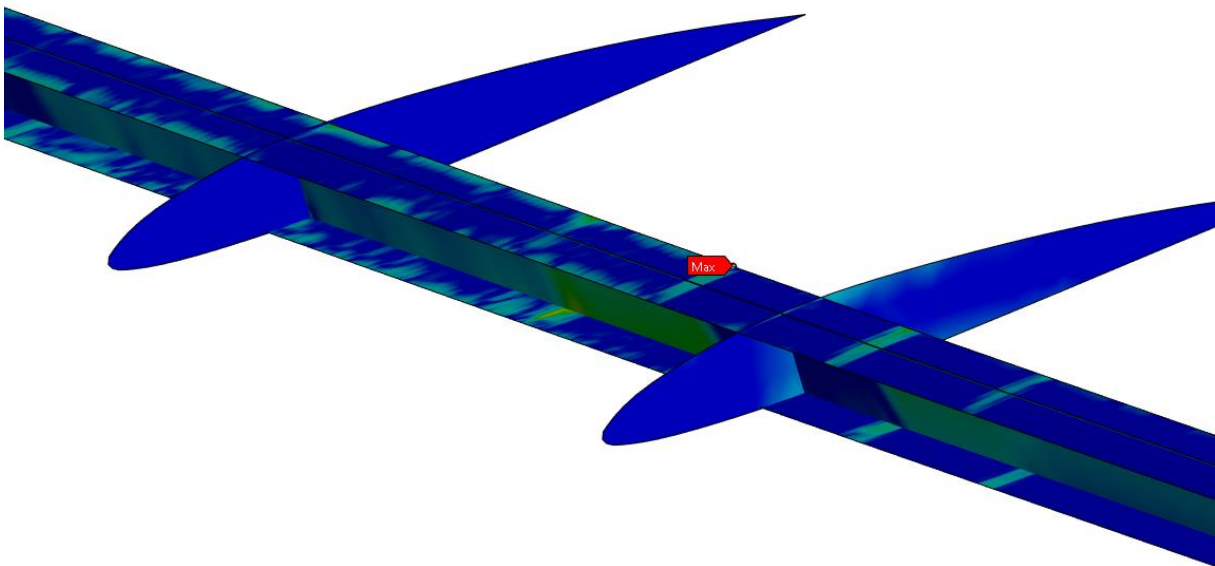
Figure 98 Stress distribution inside the structure of the tested object

Structural stresses are transferred directly from the skin to the internal structure, regardless of the type of stiffener used or the position of the spar along the chord (Fig. 99). Therefore, it is possible to determine the correct selection of bonds between the individual components of the structure.
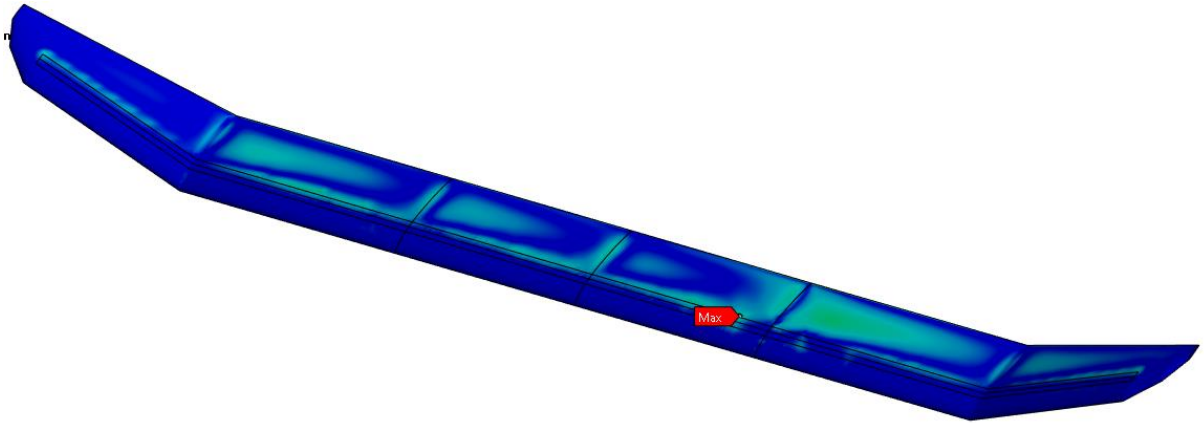
Figure 99 Stress distribution on the wing

Optimisation was based on the size of the failure criterion. Taking into account whose adopted safety factor, the value is equal to 1.5, a decision was made to limit the acceptable threshold of the failure criterion value to 0.75. During the analysis, the maximum structural stress and maximum displacement parameters were determined. These parameters were considered useful when it was impossible to determine the optimal system using the failure criterion. The results determined during the optimisation analysis are presented in the tables (Tab. 32 - 34). The tables also contain the occurrence of given extreme values. The positions are numbered and refer to the visualisation showing the analysed wing with markers defining the places where the maximum value occurs (Fig. 100).

Tab 32 Optimisation analysis of Inverse Reserve Factor (Tsai-Wu) results

Wing spar position		Inverse Reserve Factor (Tsai-Wu)									
		Result value					Max value occurrence (Fig. 100)				
[mm]	[%] MAC	I	II	III	IV	V	I	II	III	IV	V
68,25	25	1,03	0,91	0,80	0,75	0,73	2	2	2	4	4
73,71	28	1,07	0,91	0,68	0,71	0,66	4	4	4	2	4
79,17	31	0,97	0,91	0,71	0,68	0,72	4	4	4	4	4
84,63	34	0,85	0,88	0,80	0,69	0,73	4	4	4	4	4
90,09	37	0,99	0,97	0,83	0,74	0,77	4	4	4	4	4

Tab 33 Optimisation analysis of Maximum stress results

Wing spar position		Maximum stresses									
		Result value [MPa]					Max value occurrence (Fig. 100)				
[mm]	[%] MAC	I	II	III	IV	V	I	II	III	IV	V
68,25	25	217,02	207,46	191,42	172,26	150,33	2	2	2	4	4
73,71	28	208,69	200,41	167,75	166,19	156,67	2	2	4	2	4
79,17	31	184,75	183,03	170,76	155,99	162,97	2	2	4	4	4
84,63	34	201,74	191,57	164,23	158,81	163,63	4	2	2	4	4
90,09	37	206,36	197,52	172,10	153,18	158,45	4	2	2	4	4

Tab 34 Optimisation analysis of Maximum deformation results

Wing spar position		Maximum deformation									
		Result value [mm]					Max value occurrence (Fig. 100)				
[mm]	[%] MAC	I	II	III	IV	V	I	II	III	IV	V
68,25	25	28,00	27,20	25,80	25,07	24,34	1	1	5	5	5
73,71	28	27,77	26,98	25,60	24,86	24,50	5	5	5	5	5
79,17	31	28,16	27,22	26,58	25,11	24,79	5	1	5	5	5
84,63	34	28,45	27,70	28,53	26,15	25,23	5	1	1	1	1
90,09	37	28,97	28,33	26,98	26,11	25,45	1	1	1	1	1
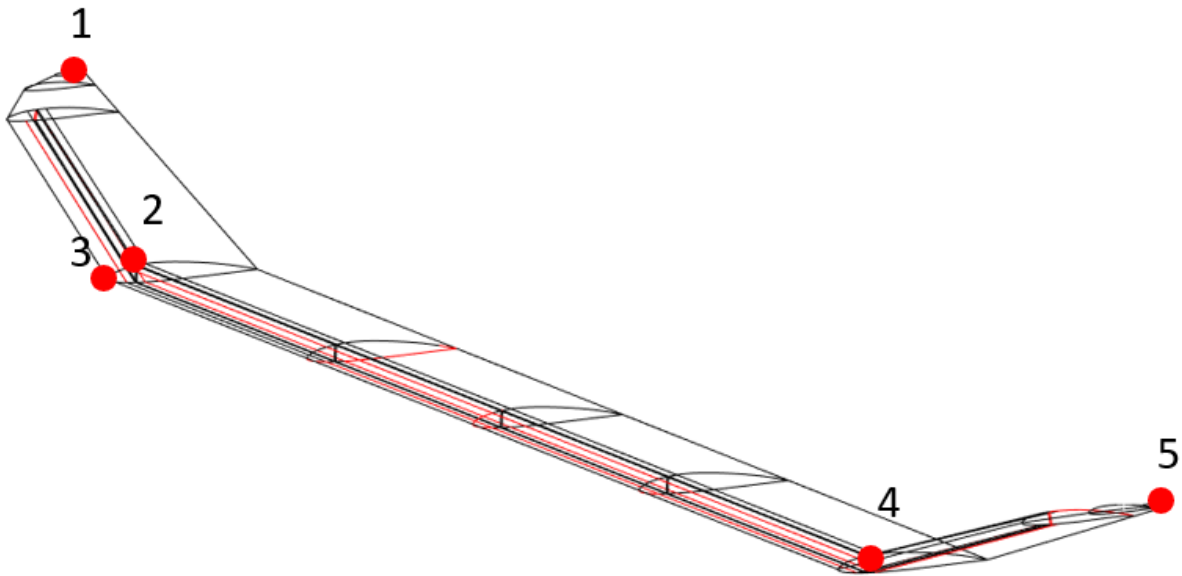
Figure 100 Map of the occurrence of extreme values in the wing

Based on the results obtained, a map of the Inverse Reserve Factor (Tsai-Wu) values was also developed depending on the location of the spar and the type of stiffener tested (Fig. 101). Results with values greater than 0,75 were considered unsafe options and rejected. Values are marked in yellow in each table. The selection criterion was also the weight of the stiffener type analysed, because of that, next assumed first type of stiffening composite layers was the acquisition of the Tsai-Wu criterion. The column with data specified for a given stiffener type is marked on blue in each of the diagrams. The results obtained for the third planned method of laying the stiffening layers presented enough properties for two spar positions. The optimal position of the main wing spar for the assumed stiffening type was determined with the lowest structural stress and deformation. The values determined for the optimal arrangement of the stiffening composite and the position along the chord are marked in green in each of the tables.
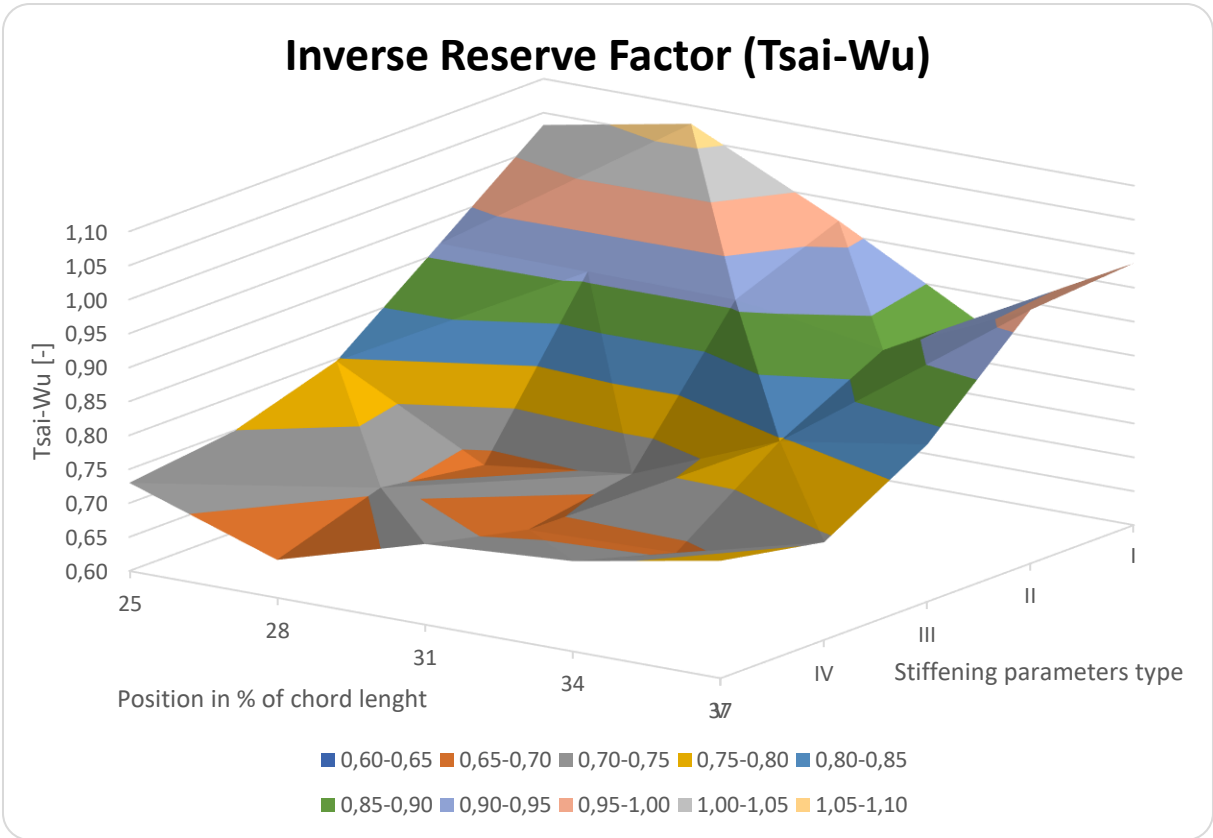
Figure 101 Inverse Reserve Factor (Tsai-Wu) depending on the location of the main wing spar along the chord and the type of stiffener used

Based on the analysis carried out, it is possible to conclude that the third proposed main wing spar stiffening system and its location in 28% of the MAC are the optimal location for the test object. Taking into account the results obtained, the position of the main wing spar will be moved to a distance of 76 [mm] from the leading edge during the construction of the optimised Twin Stratos 1:7 UAV structure.

7. Summary

The thesis concerns the methodology for the research and optimisation of unmanned aerial vehicles with extended or unlimited flight endurance. The research was carried out as part of the LEADER project, and the subject of the research is the Twin Stratos aircraft. The HALE UAV Twin Stratos is designed for high altitudes.

Due to the specific flight conditions and assumptions regarding the project, the UAV limits the availability of energy are battery packs and photovoltaic cells, as well as the specific, flexible design of the aircraft. Taking into account the large weight reductions, it was necessary to optimise the main wing so that it was optimally durable and the possibility of mounting the measuring equipment was retained.

The construction and analysis of unmanned aircraft is problematic due to the small number of structures of this type, the parameters and capabilities of which are generally available. Typically, developed structures of this type are protected property of the manufacturer. This results in an incomplete state of art database, allowing the adoption of initial parameters for the designed facility.

HALE UAV constructions are rare in air traffic. This is due to the lack of rules on the flights of the aircraft concerned. European regulations, and thus aviation regulations in Poland do not cover Twin Stratos aircraft to the extent that allows them to develop their full flight capabilities.

The research methodology proposed for standard aircraft allows estimating the parameters achieved at sea level but does not take into account the parameters at altitudes reached by HALE UAV structures. Changes in air parameters and conditions at high altitudes have a significant impact on the structural properties of materials, which become less plastic under the influence of temperature.

The purpose of this doctoral dissertation was to develop a UAV HALE optimisation methodology. The research began with state-of-the-art analysis focused on analytical and numerical computational methods. This led to a multi-stage optimisation.

First, a review of the analytical methods was performed. On the basis of this step, it was concluded that the analysis methodology does not differ from the methodology used for small aircraft or glider.

In the next step, the numerical methods were reviewed and those that allowed one to obtain the most accurate results were selected. The methodology of wing analysis and optimisation for long endurance UAV was presented.

7.1. Conclusions

The research carried out during the thesis has led to the following conclusions:
- The doctoral dissertation resulted in the development of an optimal in terms of the requirements posed by the use of the wing of the analysed object. To obtain the result, the methodology for conducting the analysis and optimisation itself was defined. Analytical tests of the optimised object were performed, legal requirements were analysed, critical flight parameters were determined, composite materials were proposed, and the parameters of materials accepted for numerical analyses were determined. The optimisation was based on the generative model and the coupling of numerical aerodynamic analyses with structural strength analyses. The issue required the formulation of assumptions regarding the analysed object and the determination of initial parameters on the basis of which the design stages were made.
- The assumed methodology for analysis and optimisation of the considered structure was divided into four main stages:
    - The first stage of optimisation assumes initial geometrical assumptions, the size of the control surfaces related to them, and the assumption of mass parameters, determination of the type of propulsion and initial flight parameters.

- o The second stage of design concerned aerodynamic and geometrical parameters, mass distribution, determination of moments, and forces.
  - o The third stage concerned the development of internal structures, numerical analyses, and determination of optimisation parameters for the analysed structure.
  - o The fourth stage was related to design optimisation. Static analyses of the structure were performed for selected critical parameters and the structure was optimised to reduce its mass.
- Analyses based on analytical calculations, presented in subchapter 4.2 "The second designing stage" showed the flight parameters of the designed object. A dependence was observed between the aspect ratio and the high flexibility of UAVs. Due to the need to perform many calculations, a spreadsheet was prepared that allows to determine the main parameters automatically after changing the geometry of the optimised wing. The analytical methods for testing unmanned aerial vehicles coincide with the methodology for analysing airplanes and gliders. Divergences in requirements that are not yet so extensive result in overly high safety parameters when complying with the rules for aeroplanes and gliders.
- After analysing the regulations regarding UAVs, it can be concluded that they primarily concern flight safety. Drone regulations are constantly evolving due to evolving technologies and the potentially growing use of UAVs. To a large extent, the literature on drone design and safety regulations is based on books on aircraft and glider construction.
- The lack of regulations specifying the safety factors of unmanned aerial vehicle structures requires the designer to specify the given parameters. This causes a significant impact of the design assumptions on the performance of the designed UAV. The load envelope generated to determine critical flight conditions is fully dependent on the parameters adopted by the designer.
- The generative model, presented in subchapter 6.2 "Development of a parametric model of the internal structure", of the optimised wing allowed for partial automation of the analysis. The use of model parameterisation allows for a significant shortening of optimisation studies.
- Separation into bindings on individual axes allowed for partial mapping of the structure of the analysed object and simulating the possibility of displacement of the fuselage mounting points relative to each other. The proposed system takes into account the given relationship without the need to model the entire structure of the tested object.
- The analytical determination of the mass forces and moments of the tested object was carried out on the basis of the literature. This analysis is intended to determine the stability and controllability of the aircraft.
- As a result of the developed methodology and the analysis stages, the optimal location of the main support spar of the optimised wing was indicated.
- Due to the type of structure and the small forces acting on the analysed object, the high flexibility of the tested wing was numerically confirmed by the maximum displacement results presented in subchapter 6.7.2 "The results of the described analysis".
- Due to the very complex and unique nature of the structure, it is expected in the next steps to impose on a specific methodology a proposal of further criteria resulting from the properties of the installed panels and their distribution, the temperatures prevailing at given altitudes and the influence of side winds occurring at the considered flight altitudes. In the current state of knowledge, it is not possible to address a given issue in a quantifiable manner, but in subsequent studies attempts will be made to pursue this goal, therefore, the presented optimisation methodology is trade-offs and identification of phenomena rather than finite objective functions.

- Due to the possible wide use of HALE UAV, the structure used in the LEADER project was selected as a research facility. It is an unusual construction, which can be an alternative to satellites. The UAV has two fuselages and is powered by electricity generated by photovoltaic panels. The drone has a large wingspan and is very flexible, which defined the main research problem, i.e. the analysis of the wing and the need to optimise such structures.

7.2. Future works

- In the future, it is planned to create a more automated construction optimisation methodology using the ANSYS programme. The use of a direct connection of the parameters responsible for the location of the main elements of the structure with the functions defined in the Ansys environment will allow for full automation, which will result in optimal values for the given goals and parameters.

- Due to the complexity of the tested object and the numerical models generated at the present stage of research, it will be possible to carry out numerical, dynamic aeroelastic analyses of the optimised wing. The assumptions regarding static analyses must be extended to include the remaining parts of the research problem, which is TS17.

- Attempts were made to develop an analysis of the plating of the stability of the tested object based on the increase in flight speed. To improve the accuracy of the object under consideration, it is planned to extend the composite covering the tested object with surfaces that mimic photovoltaic panels.

- To determine the optimal shape of the tested wing, tests are planned to determine the impact of using a wing with a constant cross section over the entire span as a function of the energy generated by additional photovoltaic panels and the additional aerodynamic drag generated by the wing tips.

- It is planned to carry out bench tests of the impact of conditions at specific altitudes. For this purpose, the wing is planned to be placed in a climatic chamber and loaded according to the forces occurring during the flight in critical conditions at a given altitude.

- The designed and optimised aircraft is the first built demonstrator, the purpose of which is to experimentally confirm the endurance of the flight, determined on the basis of analytical and numerical analyses. Further work will be related to the confrontation of the results obtained during numerical analyses with the results obtained during bench analyses for the TS17 UAV, and then the implementation of fine-tuned numerical models for Twin Stratos 1:2 analyses, which is a direct development of the TS17 project.

Bibliography

[1]   K. Nonami, „Prospect and Recent Research & Development for Civil Use Autonomus Unmanned Aircraft as UAV and MAV," *Journal of System Design and Dynamics, Vol. 1, No. 2,* pp. 120-128, 24 January 2007.

[2]   N. H. Motlagh, M. Bagaa i T. Taleb, „UAV-Based IoT Platform: A Crowd Surveillance Use Case," *IEEE Communications Magazine,* pp. 128-134, February 2017.

[3]   EASA, „Access Rules for Unmanned Aircraft Systems 2019/947," European Union,, 2022.

[4]   EASA, „Access Rules for Unmanned Aircraft Systems - Regulations (EU) 2019/945," European Union, 2022.

[5]   D. B. S. Powietrznych, „Wdrożenie przepisów unijnych dla Bezzałogowych Statków Powietrznych," Urząd Lotnictwa Cywilnego, 2020.

[6]   S. Agostino, M. Mammone, M. Nelson i T. Zhou, „CLASSIFICATION OF UNMANNED AERIAL VEHICLES," The University of Adelaide, 2006.

[7]   P. Posea, „Dronesgator," 2021. [Online]. Available: https://dronesgator.com/best-high-altitude-drones/. [Data uzyskania dostępu: 25 październik 2022].

[8]   Airbus, „Airbus.com," 2018. [Online]. Available: https://www.airbus.com/en/products-services/defence/uas/uas-solutions/zephyr. [Data uzyskania dostępu: 25 październik 2022].

[9]   JOUAV, „jouav.com/," 2022. [Online]. Available: https://www.jouav.com/products/cw-25.html. [Data uzyskania dostępu: 25 październik 2022].

[10]   P. Posea, „Dronesgator," 2022. [Online]. Available: https://dronesgator.com/how-fast-can-drones-fly/. [Data uzyskania dostępu: 25 październik 2022].

[11]   Challenger Aerospace & Defense, „challengeraerospace.com," 2022. [Online]. Available: https://challengeraerospace.com/wp-content/uploads/2019/04/WOLFHOUND.pdf. [Data uzyskania dostępu: 2025 Październik 2022].

[12]   Aerospace Technology, „www.aerospace-technology.com," 2022. [Online]. Available: https://www.aerospace-technology.com/projects/pipistrel-heavy-cargo-hybrid-vtol-drone/. [Data uzyskania dostępu: 25 październik 2022].

[13]   G. Mortimer, „sUAS News - the business of drones," 11 april 2014. [Online]. Available: https://www.suasnews.com/2014/04/worlds-largest-multirotor-makes-successful-maiden-flight/. [Data uzyskania dostępu: 25 październik 2022].

[14]   A. Malewar, „InceptiveMind," 24 october 2022. [Online]. Available: https://www.inceptivemind.com/skyfront-perimeter-8-drone-sets-new-world-record-drone-flight-time/18180/. [Data uzyskania dostępu: 25 październik 2022].

[15]   DroneTech, „www.dronetechuav.com," 2021. [Online]. Available: https://www.dronetechuav.com/av2-pelican. [Data uzyskania dostępu: 25 październik 2022].

[16] P. Berry, „The Sunriser - A Design Study in Solar Powered Flight," *AIAA Paper 2000-01-5507,* 2000.

[17] M. D. Bailey i M. V. Bower, „High Altitude Solar Power Platform," *NASA TM-103578,* 1992.

[18] S. A. Brandt i F. T. Gilliam, „Design Analysis Methodology for Solar-Powered Aircraft," *JOURNAL OF AIRCRAFT, Vol. 32, No. 4,* pp. 703-709, 1995.

[19] G. Romeo, G. Frulla, E. Cestino i G. Corsino, „HELIPLAT: Design, Aerodynamic, Structural Analysis of Long-Endurance Solar-Powered Stratospheric Platform," *JOURNAL OF AIRCRAFT, Vol. 40, No. 6,* pp. 1505-1520, 2004.

[20] G. Romeo, G. Frulla i E. Cestino, „Design of a High-Altitude Long-Endurance Solar-Powered Unmanned Air Vehicle for Multi-Payload and Operations," *Journal of Aerospace Engineering, Vol. 221, No. 119,* pp. 199-216, 2007.

[21] A. Noth, „Design of Solar Powered Airplanes for Continuous Flight," *Ph.D. Dissertation, Ecole Polytechnique Fédérale de Lausanne, ETH ZÜRICH, Switzerland,,* 2008.

[22] FAI - Fédération Aéronautique Internationale, „www.FAI.org," Maison du Sport International, [Online]. Available: https://www.fai.org/record/18683. [Data uzyskania dostępu: 18 March 2023].

[23] T. E. Noll, J. M. Brown, M. E. Perez-Davis, S. D. Ishmael, G. C. Tiffany i M. Gaier, „Investigation of the Helios Prototype Aircraft Mishap," *NASA Report,* Jan 2004.

[24] J. A. Duffie i W. A. Bechman, „Solar Engineering of Thermal Processes," *3rd ed., JOHN WILEY & SONS, New Jersey,,* 2006.

[25] M. Chang, Z. Zhou i Y. Li, „An Effective Theoretical Analysis of Persistent Flight Altitudes of Solar-Powered Airplanes," *Journal of Northwestern Polytechnical University, Vol. No,* 2012.

[26] M. Chang, Z. Zhou, R. Wang i X. Xu, „A General Design Methodology for Year-Round Solar-Powered Stratospheric UAVs from Low to Middle Latitudes," *29th Confress of the International Concil of the Aeronautical Science,* September 2014.

[27] P. Schor, „AERODYNAMIC LOAD OF AN AIRCRAFT WITH A HIGHLY ELASTIC WING," *Acta Polytechnica 57(4),* p. 272–281, 2017.

[28] T. Noll, J. Brown i J. Perez-davis, „Investigation of the Helios Prototype Aircraft Mishap - Volume I Mishap Report," *National Aeronautics and Space Administration,* 2012.

[29] C. E. Cesnik i W. Su, „49th AIAA Aerospace Sciences Meeting including the New Horizons Forum and Aerospace Exposition," w *Nonlinear Aeroelastic Simulation of X-HALE: a Very Flexible UAV*, Orlando, Florida, 4 - 7 January 2011.

[30] G. Romeo, G. Frulla i E. Cestino, „HELIPLAT®: a high altitude very-long endurance solar powered platform for border patrol and forest fire detection," *WIT Transactions on The Built Environment, Vol 82,* pp. 459-469, 2005.

[31] A. Noth, R. Siegwart i W. Engel, „Design of Solar Powered Airplanes for Continuous Flight," w *ETHZ - Advances in Unmanned Aerial Vehicles, State of the art and the road to autonomy*, Zurich, Springer, 2006.

[32] X. Zhu, Z. Guo i Z. Hou, „Solar-powered airplanes: A historical perspective and future challenges," *Progress in Aerospace Sciences 71,* pp. 36-53, 2014.

[33] Y. Gibbs, „www.nasa.gov," NASA, 7 August 2017. [Online]. Available: https://www.nasa.gov/centers/armstrong/news/FactSheets/FS-068-DFRC.html. [Data uzyskania dostępu: 6 March 2023].

[34] H. Runge, „A SOLAR POWERED HALE-UAV FOR ARCTIC RESEARCH," w *1st CEAS European Air and Space Conference,*, Berlin, 2007.

[35] G. Frulla i E. Cestino, „Zaprojektowanie, wykonanie i przetestowanie demonstratora strukturalnego UAV firmy HALE," *Composite Structures,* pp. 143-153, April 2008.

[36] K. Mateja, W. Skarka, M. Peciak, R. Niestrój i M. Gude, „Energy Autonomy Simulation Model of Solar Powered UAV," *MDPI - Energies,* 1 January 2023.

[37] Polnor Leader, „Polnor Leader - About Us," 2019. [Online]. Available: https://polnor-leader.eu. [Data uzyskania dostępu: 21 January 2023].

[38] M. Mozaffari, W. Saad, M. Bennis, Y.-H. Nam i M. Debbah, „A Tutorial on UAVs for Wireless Networks: Applications, Challenges, and Open Problems," *IEEE - Communications Surveys & Tutorials,* 2019.

[39] A. Fotouhi, H. Qiang, M. Ding, M. Hassan, L. G. Giordano, A. Garcia-Rodriguez i J. Yuan, „Survey on UAV Cellular Communications: Practical Aspects, Standardization Advancements, Regulation, and Security Challenges," *IEEE COMMUNICATIONS SURVEYS & TUTORIALS, VOL. 21,,* pp. 3417-3442, 4 November 2019.

[40] F. Heintz, P. Rudol i P. Doherty, „From Images to Traffic Behavior - A UAV Tracking and Monitoring Application," w *10th International Conference on Information Fusion*, Quebec, QC, Canada, 2007, pp. 1-8, doi: 10.1109/ICIF.2007.4408103, 2007.

[41] J. Zheng, H. Fu, W. Li, W. Wu, L. Yu, S. Yuan, W. Y. Tao, T. K. Pang i K. D. Kanniah, „Growing status observation for oil palm trees using Unmanned Aerial Vehicle (UAV) images," *ISPRS Journal of Photogrammetry and Remote Sensing, Volume 173,* pp. 95-121, March 2021.

[42] A. Shakirova, L. Nichman, N. Belacel, C. Nguyen, N. Bliankinshtein, M. Wolde, S. DiVito, B. Bernstein i Y. Huang, „Multivariable Characterization of Atmospheric Environment with Data Collected in Flight," *MDPI "atmosphere",* 19 October 2022.

[43] E. Klejnowska i U. Kossowska-Cezak, „Encyklopedia PWN," [Online]. Available: https://encyklopedia.pwn.pl/haslo/meteorologiczne-pomiary-i-obserwacje;3940082.html. [Data uzyskania dostępu: 09 03 2023].

[44] komes.pl, „komes.pl," [Online]. Available: https://komes.pl/czym-sa-symulacje-cfd/. [Data uzyskania dostępu: 09.03.2023].

[45]   O. Dababneh i T. Kipouros , „A review of aircraft wing mass estimation methods," *Aerospace Science and Technology, Volume 72,* pp. 256-266, January 2018.

[46]   xflr5.tech, „About stability analysis using XFLR5," [Online]. Available: http://www.xflr5.tech/docs/XFLR5_and_Stability_analysis.pdf. [Data uzyskania dostępu: 09 03 2023].

[47]   G. Binodolino, G. Ghiringhelli, S. Ricci i M. Terraneo, „Multilevel Structural Optimization for Preliminary Wing-Box Weight Estimation," *Journal of Aircraft, Vol. 47, No. 2,* 22 May 2012.

[48]   X. Zhang, H. Yu, W. Tang i J. Wang, „General Mass Property Measurement Equipment for Large-Sized Aircraft," *MDPI - SENSORS,* 21 May 2022.

[49]   S. L. Chernyshev, . S. V. Lyapunov i . A. V. Wolkov, „Modern problems of aircraft aerodynamics," *Chernyshev et al. Advances in Aerodynamics,* 7 January 2019.

[50]   A. Jameson, „Computational Aerodynamics for Aircraft Design," *Science, Vol. 245,* pp. 361-371, 28 July 1989.

[51]   A. R. Soemaryanto i N. H. Rosid, „VERIFICATION OF SCHRENK METHOD FOR WING LOADING ANALYSIS OF SMALL UNMANNED AIRCRAFT USING NAVIER," *Jurnal Teknologi Dirgantara Vol. 15 No.2,* pp. 161-166, December 2017.

[52]   J. Gołdasz i B. Sapiński, „Application Of CFD To Modeling Of Squeeze Mode Magnetorheological Dampers," *acta mechanica et automatica,* pp. 129-134, 7 November 2015.

[53]   W. Regulski, „Modelowanie Komputerowe Przepływów Turbulentnych Lab 6 i 7," Wydział Mechaniczny Energetyki i Lotnictwa, Politechnika Warszawska, Warszawa.

[54]   P. S. Sharkey i F. R. Menter, „A Numerical Investigation of the Turbulent Flow around a Scale Model JBC Hull using the Generalized k- OMEGA (GEKO) Turbulence Model," *11th International Workshop on Ship and Marine Hydrodynamics,* 22-25 September 2019.

[55]   B. Górecki, „Modelowanie Komputerowe Przepływów Turbulentnych Lab 8," Wydział Mechaniczny Energetyki i Lotnictwa, Politechnika Warszawska,, Warszawa.

[56]   F. R. Menter, A. V. Garbaruk i Y. Egorov, „Explicit algebraic reynolds stress models for anisotropic wall-bounded flows," *Progress in Flight Physics, Volume 3,* pp. 89-104, 29 January 2013.

[57]   R. M. Masood, C. Rauh i A. Delgado, „CFD simulation of bubble column flows: An explicit algebraic Reynolds stress model approach," *International Journal of Multiphase Flow, Volume 66,* pp. 11-25, November 2014.

[58]   S. WALLIN i A. V. JOHANSSON, „An explicit algebraic Reynolds stress model for incompressible and compressible turbulent flows," *Journal of Fluid Mechanics , Volume 403,* pp. 89-132, 25 January 2000.

[59] M. Palermo i R. Vos, „Experimental Aerodynamic Analysis of a 4.6%-Scale Flying-V Subsonic Transport," *AIAA SciTech Forum,* 6-10 January 2020.

[60] O. Gur i A. Rosen, „Comparison between blade-element models of propellers," *THE AERONAUTICAL JOURNAL, VOL. 112 NO. 1138,* pp. 689-704, December 2008.

[61] P. Burgers, „A thrust equation treats propellers and rotors as aerodynamic cycles and calculates their thrust without resorting to the blade element method," *International Journal of Aviation, Aeronautics, and Aerospace, Vol. 6,* 2019.

[62] C. Mingtai, „Static Thrust Measurement for Propeller-driven Light Aircraft," *The 2nd International Conference on Computer Application and System Modeling,* pp. 650-652, 2012.

[63] M. OL i C. Zeune, „Analytical – Experimental Comparison for Small Electric Unmanned Air Vehicle Propellers," *26th AIAA Applied Aerodynamics Conference,* 18-21 August 2008.

[64] H. A. Kutty i P. Rajendran, „3D CFD Simulation and Experimental Validation of Small APC Slow Flyer Propeller Blade," *MDPI Aerospace, Vol 4,* 25 February 2017.

[65] Z. Dąbrowski, J. Dziurdź i P. Deuszkiewicz, „Modelling of Composite Elements of Power Transmission Systems Considering Nonlinear Material Characteristics," *Journal of Machine Construction and Maintenance,* pp. 87-94, March 2018.

[66] T. H. Megson, An Introduction to Aircraft Structural Analysis, Oxford: Elsevier Ltd, 2010.

[67] W. Durisch, J. Urban i G. Smestad, „Characterisation of Solar Cells and Modules Under Actual Operating Conditions," *Renewable Energy, Vol. 8, No. 1-4,* pp. 359-366, 1996.

[68] D. A. Scheiman, P. P. Jenkins, D. J. Brinker i J. Appelbaum, „Low Intensity Low Temperature (LILT) Measurements and Coefficients on New Photovoltaic Structures," *Progress in Photovoltaics: Research and Applications, Vol.4: John Wiley and Sons, Inc,* 1996.

[69] N. Hall, „www.grc.nasa.gov/," National Aeronautics and Space Administration, 13 May 2021. [Online]. Available: https://www.grc.nasa.gov/www/k-12/airplane/atmosmet.html. [Data uzyskania dostępu: 13 March 2023].

[70] W. Stafiej, Obliczenia stosowane przy projektowaniu szybowców, Warszawa: Politechnika Warszawska, 2000.

[71] T. Benson, „grc.nasa.gov," Glenn Research Center - NASA, [Online]. Available: https://www.grc.nasa.gov/www/k-12/VirtualAero/BottleRocket/airplane/presar.html. [Data uzyskania dostępu: 19 March 2023].

[72] P. Szeptyński, „Podstawy wytrzymałości materiałów i mechaniki układów prętowych "14 – Ugięcia"," Creative Commons CC BY-NC-SA 3.0 PL.

[73] F. L. Ribeiro, P. Paglione, R. G. Silva i M. S. Sousa, „AEROFLEX: A TOOLBOX FOR STUDYING THE FLIGHT DYNAMICS OF HIGHLY FLEXIBLE AIRPLANES," *CONEM 2012 «Engenharia em destaque» VII Congresso Nacional de Engenharia Mecânica,* August 2012.

[74] techWinder, „xflr5.tech," Xfoil, 14 January 2021. [Online]. Available: http://www.xflr5.tech/. [Data uzyskania dostępu: 23 January 2023].

[75] R. B. Langtry i F. R. Menter, „Correlation-Based Transition Modeling for Unstructured Parallelized Computational Fluid Dynamics Codes," *AIAA JOURNAL, Vol. 47, No.12,* pp. 2894-2906, December 2009.

[76] S. M. Aftab, A. S. Mohd Rafie, N. A. Razak i K. A. Ahmad, „Turbulence Model Selection for Low Reynolds Number Flows," *PloS one, vol. 11, no. 4, article e0153755,* 2016.

[77] R. Lanzafame, S. Mauro i M. Messina, „Wind turbine CFD modeling using a correlation-based transitional model," *Renewable Energy, vol. 52,* pp. 31-39, 2013.

[78] A. a. h. Ali i M. W. Saeed, „Stability Improvement of an Unmanned Aerial Vehicle's Wing using Active Vibration Control," *International Journal of Computer Applications, Volume 157– No10,* pp. 30-36, January 2017.

[79] „Airfoil Tools," AirfoilTools.com, [Online]. Available: http://airfoiltools.com/. [Data uzyskania dostępu: Feb 2023].

[80] O. Schrenk, „A simple approximation method for obtaining the spanwise lift distribution," Work of the US Gov. Public Use Permitted., 1940.

[81] Dassault Systèmes SolidWorks Corporation, „discover.solidworks," [Online]. Available: https://discover.solidworks.com/. [Data uzyskania dostępu: 23 January 2023].

[82] K. Zenowicz i W. Skarka, „Analysis and Optimization of the Propeller Shape for a Stratospheric Drone Research Platform.," *TRANSDISCIPLINARY ENGINEERING FOR RESILIENCE: RESPONDING TO SYSTEM DISRUPTIONS,* pp. 465-473, 2021.

[83] K. Zenowicz i W. Skarka, „Verification of flutter method for the purposes of building a very flexible wing generative model.," w *Advances in Transdisciplinary Engineering Vol.12*, Delft, 2020.

[84] K. Zenowicz, P. Zenowicz, W. Skarka i W. Moczulski, „Analiza podłużnej stateczności statycznej statku powietrznego w zależności od położenia środka ciężkości," w *Metody komputerowe - 2022. Studencka konferencja naukowa, Gliwice, czerwiec 2022*, Gliwice, Politechnika Śląska (PolSL), 2022, pp. 185-188.

[85] P. Zenowicz, K. Zenowicz, W. Moczulski i W. Skarka, „Wstępna analiza stateczności statycznej lotu bezzałogowego statku powietrznego o nietypowej konfiguracji," w *Metody komputerowe - 2022. Studencka konferencja naukowa, Gliwice, czerwiec 2022*, Gliwice, Politechnika Śląska (PolSL), 2022, pp. 189-192.

[86] S. Danielecki, Konstruowanie samolotów : wyznaczanie obciążeń, Wrocław: Oficyna Wydawnicza Politechniki Wrocławskiej, 2004.

[87] C. Galiński, Wybrane Zagadnienia Projektowania Samolotów, Warszawa: Wydawnictwa Naukowe Instytutu Lotnictwa, 2016.

[88] R. ChachurskI i M. Choszczewski, „Obciążenia będące wynikiem pracy zespołu napędowego bezzałogowego statku powietrznego klasy mini," w *Prace Instytutu Lotnictwa*, Warszawa, Instytut Lotnictwa, 2011, pp. 39-48.

[89] K. K. Versteeg i W. Malalasekera, An introduction to Computational Fluid Dynamics, London: Person Education Limited, 2007.

[90] D. S. Körpe i Ö. Ö. Kanat, „Aerodynamic Optimization of a UAV Wing subject to Weight, Geometric, Root Bending Moment, and Performance Constraints," *Hindawi - International Journal of Aerospace Engineering,* Volume 2019, Article ID 3050824, 14 pages.

[91] H. C. Wee, AERODYNAMIC ANALYSIS OF A CANARD MISSILE CONFIGURATION USING ANSYS-CFX, Monterey, CA 93943-5000: Naval Postgraduate School, 2011.

[92] EASA, „Certification Specifications for Sailplanes and Powered Sailplanes CS-22," *European Aviation Safety Agency,* 2008.

[93] ANSYS, „Fluent Theory Guide,," p. 2013.

[94] F. R. Menter, R. B. Langtry, S. R. Likki, Y. B. Suzen, P. G. Huang i s. Volker, „A Correlation-Based Transition Model Using Local Variables-Part I: Model Formulation," *Journal of Turbomachinery,* pp. 413-422, 1 march 2004.

[95] G. Harily, „Fundamentals of the finite element method," *Mac Millan pubishing Co,* 1989.

[96] A. Abdul-Razzakand i J. H. Haido, „Free Vibration Analysis of Rectangular Plates Using Higher Order Finite Layer Method," *al-Rafidain Engineering Vol.15, No.3,* 2007.

[97] I. Wróbel i J. Stadnicki, „Nonlinear FEM models optimization on example of a stamping die," *Mechanik Vol. 91 No. 7,* pp. 484 - 486, 9 July 2018.

[98] P. Czop, D. Sławik i G. Wszołek, „Development of an optimization method for minimizing vibrations of a hydraulic damper," *Simulation: Transactions of the Society for Modeling and Simulation International,* pp. 1073-1086, 29 May 2013.

[99] Technologie kompozytowe P&G, „r-g.com.pl," Shoper.pl, [Online]. Available: https://r-g.com.pl/pl/p/Wegiel-non-crimp-Tkanina-ST-80-gm2-UD-50-cm%2C-rolka-10-m/2142. [Data uzyskania dostępu: 22 March 2023].

[100] Z. Goraj, „High altitude long endurance unmanned aerial vehicle of a new generation – a design challenge for a low cost, reliable and high performance aircraft," *BULLETIN OF THE POLISH ACADEMY OF SCIENCES,* 2004.

[101] D. Hoche, „Novel Magnesium Based Materials: Are They Reliable Drone Construction Materials? A Mini Review," *Frontiers in Materials,* 23 April 2021.

[102] M. Baras, „Aeroelastic evaluation of a flexible high aspect ratio wing UAV: Numerical simulation and experimental flight validation," *Aerospace Science and Technology,* 10 February 2022.

[103] Urząd Lotnictwa Cywilnego, „www.ulc.gov.pl," Urząd Lotnictwa Cywilnego, 2023. [Online]. Available: https://www.ulc.gov.pl/pl/drony/wdrazanie-przepisow-ue/4944-akty-prawne. [Data uzyskania dostępu: 08 02 2023].

[104] M. Chang, Z. Zhou i Y. Li, „An Effective Theoretical Analysis of Persistent Flight Altitudes of Solar-Powered Airplanes," *Journal of Northwestern Polytechnical University, Vol. No.,* 2012.

[105] I. H. Abbott i A. E. Doenhoff, „Theory of Wing Sections, Including a Summary of Airfoil Data," *Dover Publications, New York, USA,,* 1959.

[106] A. Abbas, J. Viente i E. Valero, „Aerodynamic technologies to improve aircraft," *Aerosp. Sci. Technol. 28,* p. 100–132, 2013.

[107] D. H. H. a. E. H. Dowell, NONLINEAR EQUATIONS OF MOTION FOR THE ELASTIC BENDING AND TORSION OF TWISTED NONUNIFORM ROTOR BLADES, Washington, D. C.: NATIONAL AERONAUTICS AND SPACE ADMINISTRATIO, 1974.

[108] D. M. Schuster, D. D. Liy i L. J. Huttsel, „Computational aeroelasticity," *success, progress, challenge, J. Aircr. 40 (5),* p. 843–856, 2003.

[109] J. G. Marshall i M. Imregun, „review of aeroelasticity methods with emphasis on," *J. Fluids Struct. 10 ,* p. 237–267, 1996.

[110] J. H. Ferziger i M. Perić, „Computational Methods for Fluid Dynamics," *3rd edition, Springer, Berlin, Germany,,* 2002.

[111] C. Hirsch, „Numerical Computation of Internal and External Flows," *Vol. I and II, Wiley, New York, USA ,* 1991.

[112] O. O. Bendiksen, „Transonic aeroelasticity: theoretical and computational challenges," *ICNPAA Congress: Mathematical Problems in Engineering, Aerospace and Sciences (ICNPAA 2010), São José dos Campos, São Paulo, Brazil,* 2010.

[113] E. H. Dowell i D. M. Tang, „Nonlinear aeroelasticity and unsteady aerodynamic," *AIAA J. 40 (9),* p. 1697–1707, 2002.

[114] M. Drela, „Low Reynolds Number Aerodynamics," w *XFOIL: An Analysis and Design System for Low Reynolds Number Airfoils*, Berlin, 1989.

[115] M. Drela i M. B. Giles, „Viscous-inviscid analysis of transonic," *AIAA Journal, vol. 25, no. 10,* p. 1347–1355, 1987.

[116] J. Katz i A. Plotkin, Low-speed aerodynamics, from wing theory to panel methodsmcgraw-hill, New York, 1991.

[117] Z. Czyż, I. Ilhan, M. Akcay i J. Czarnigowski, „AIR FLOW ANALYSIS AROUND THE AUTOGYRO FUSELAGE," *Journal of Technology and Exploitation in Mechanical Engineering,* pp. 13-20, 30 June 2017.

[118] R. Bielawski, WYBRANE ZAGADNIENIA Z BUDOWY STATKÓW POWIETRZNYCH, Definicje, pojęcia i klasyfikacje, Warszawa: Wydawnictwo Akademii Obrony Narodowej, 2015.

[119] R. Bielawski, Badanie i modelowanie połączeń nitowych w lotniczych strukturach kompozytowych, Warszawa: POLITECHNIKA WARSZAWSKA, 2016.

Abstract

Unmanned aerial vehicles (UAVs) are an increasing part of air traffic, from military applications, through traffic observation, to telecommunications applications. The capabilities of UAVs are appreciated in many industries and the flight parameters they offer are not limited by crew limitations. The rapid development of the control method, automatic flight control, the development of the materials used, and the introduction of accurate numerical methods of analysis and design, allows to achieve of higher flight speeds, increase the endurance of the flight and leads to reaching stratospheric flight altitudes. The combination of extended flight endurance at high altitudes has created a completely new group of unmanned aerial vehicles HALE UAV (High Altitude Long Endurance - Unmanned Aerial Vehicle).

The purpose of this doctoral dissertation was to determine the research and optimisation methodology of the HALE UAV aircraft and the optimisation of the internal structure of the main wing for the Twin Stratos 1:7 structure based on a parametric model coupled with the results of a numerical aerodynamic analysis. As part of the work, all design stages were presented, such as the applied parameters, the method of optimisation, and the results obtained. Optimisation analysis were developed in the Ansys environment, which allowed for the coupling of numerical aerodynamic, material, structural, and optimisation analyses.

The result of the author's work is the development of the optimal internal structure of the main wing of the TS17 unmanned aerial vehicle (Twin Stratos 1:7) and the development of a four-stage methodology for designing and conducting analyses for HALE UAV aircraft. As part of the work, the author also presented a map of optimisation results obtained for the developed internal structure depending on the location of the main wing spar and the number of layers stiffening the structure.

The optimisation tests carried out were used to determine the location of the main load-bearing spar along the reference chord and to determine the arrangement of the roving layers stiffening the spar along the span of the optimised wing. The results were obtained based on numerical analysis of the model of the analysed object, taking into account the thickness of individual composite layers, the parameters of materials selected based on design assumptions, and the exact direction of the fibres of the composite structures used. The analysis were carried out based on a fixing system of the analysed object reflecting the unusual arrangement of the fuselages. The optimal shape of the tested structure was determined based on the parameters of maximum displacement, maximum stress within the structure, and the Tsai-Wu failure criterion.

Streszczenie

Bezzałogowe statki powietrzne (BSP) stanowią coraz większą część ruchu lotniczego. Od zastosowań militarnych, poprzez obserwacje ruchu drogowego, aż po zastosowania telekomunikacyjne. Możliwości które oferują BSP są doceniane w wielu gałęziach przemysłu a parametry lotu jakie oferują nie są ograniczane przez ograniczenia załogi. Szybki rozwój sposobu sterowania, automatyka kontroli lotu, rozwój stosowanych materiałów, wprowadzenie dokładnych numerycznych sposobów analiz i projektowania, pozwalają na osiąganie większych prędkości lotu, zwiększają długotrwałość lotu oraz prowadzą do osiągania stratosferycznych wysokości lotu. Połączenie możliwości wydłużonej długotrwałości lotu na dużej wysokości spowodowało powstanie całkowicie nowej grupy bezzałogowych statków powietrznych HALE UAV (High Altitude Long Endurance – Unmanned Aerial Vehicle).

Celem niniejszej rozprawy doktorskiej było określenie metodyki badań oraz optymalizacji statku powietrznego typu HALE UAV oraz optymalizacja struktury wewnętrznej głównego płata nośnego dla konstrukcji Twin Stratos 1:7 opartej na parametrycznym modelu sprzężonym z wynikami wirtualnej analizy aerodynamicznej. W ramach prac przedstawiono wszystkie etapy projektowania zastosowane parametry, sposób przeprowadzania optymalizacji oraz uzyskane wyniki. Analizy optymalizacyjne zostały opracowane w środowisku Ansys, co pozwoliło na sprzężenie wirtualnych analiz aerodynamicznych, materiałowych, strukturalnych oraz optymalizacyjnych.

Owocem pracy autora jest opracowanie optymalnej struktury wewnętrznej głównego płata nośnego bezzałogowego statku powietrznego TS17 (Twin Stratos 1:7) oraz wypracowanie czteroetapowego sposobu projektowania oraz prowadzenia analiz dla statków powietrznych typu HALE UAV. W ramach pracy autor przedstawił także mapę wyników optymalizacji uzyskiwanych dla opracowanej struktury wewnętrznej w zależności od położenia głównego dźwigara nośnego oraz ilości warstw usztywniających konstrukcję.

Przeprowadzone badania optymalizacyjne posłużyły do określenia położenia głównego dźwigara nośnego wzdłuż cięciwy odniesienia oraz określenia sposobu rozmieszczenia warstw rowingu usztywniających dźwigar wzdłuż rozpiętości optymalizowanego skrzydła. Wyniki zostały uzyskane na podstawie numerycznych analiz modelu badanego obiektu uwzględniającego grubości poszczególnych warstw kompozytu, parametrów materiałów dobranych na podstawie założeń projektowych, dokładnego kierunku ułożenia włókien struktur kompozytowych zastosowanych. Analizy były prowadzone w oparciu o stały układ mocowań analizowanego obiektu odwzorowujący nietypowy układ kadłubów. Optymalny kształt badanej struktury został określony na podstawie parametrów maksymalnego przemieszczenia, maksymalnego naprężenia wewnątrz strukturalnego oraz kryterium zniszczenia Tsai-Wu.

List of used acronyms

AR	Aspect Ratio
AoA	Angle of attack
BSL	Baseline model
BSL EARSM	Explicit Algebraic Reynolds Stress Models – Baseline model
BSP	Bezzałogowy Statek Powietrzny
CAA	Civil Aviation Authority
CAD	Computer Aided Design
CD	Drag Coefficient
CFD	Computational Fluid Dynamics
CG	Centre of Gravity
CL	Lift Coefficient
Din	Inducted drag
Dop	Drag of aerofoil
EASA	European Union Aviation Safety Agency
FEM	Finite Element Method
GEKO	Generalised k-Omega turbulence model
HALE	High Altitude Long Endurance
HAPS	High-Altitude Pseudo-Satellite
high-AR	High Aspect Ratio
$k - \epsilon$	K-Epsilon turbulence model
$k - \omega$	k-Omega turbulence model
MAC	Mean Aerodynamic Chord
MRF	Moving Reference Frame
MS Excel	Microsoft Excel
NASA	National Aeronautics and Space Administration
NFZ	No-Fly Zone
N-S	Navier-Stokes equations
NSTS	National Standard Scenario
RANS	Reynolds-Averaged Navier-Stokes equations
RPA(S)	Remotely Piloted Aircraft (System)
Si	Silcon
SoD	Sum of drag
STS	Standard Scenario
TS	Twin Stratos (a HALE UAV)
TS11	Twin Stratos (a 1 to 1 scale UAV)
TS12	Twin Stratos (a 1 to 2 scale UAV)
TS17	Twin Stratos (a 1 to 7 scale UAV)
TS18	Twin Stratos (a 1 to 8 scale UAV)
UA	Unmanned Aircraft
UAS	Unmanned Aerial System
UAV	Unmanned Aerial Vehicle
UAVs	Unmanned Aerial Vehicles

List of used symbols

Xi	"i" component centre of gravity distance from the origin along the "X" axis
Yi	"i" component centre of gravity distance from the origin along the "Y" axis
Zi	"i" component centre of gravity distance from the origin along the "Z" axis
mi	"i" component mass
g	gravitational acceleration
Qi	"i" component weight
Xcg	The distance of the resultant centre of gravity to the "X" axis of the adopted coordinate system
Ycg	The distance of the resultant centre of gravity to the "Y" axis of the adopted coordinate system
Zcg	The distance of the resultant centre of gravity to the "Z" axis of the adopted coordinate system
Xmac	Distance from aircraft nose to leading edge MAC
Xlo	Location of the centre of gravity along the MAC measured from the leading edge
lo	Mean aerodynamic chord (MAC)
$\overline{Xlo}$	centre of gravity in percent along mac
X0	The distance of the resultant centre of gravity to the "X" axis of the adopted coordinate system after translation coordinate system to centre of gravity
Y0	The distance of the resultant centre of gravity to the "Y" axis of the adopted coordinate system after translation coordinate system to centre of gravity
Z0	The distance of the resultant centre of gravity to the "Z" axis of the adopted coordinate system after translation coordinate system to centre of gravity
Rxi	The distance of mass "i" from the axis "X" of the new coordinate system
Ryi	The distance of mass "i" from the axis "Y" of the new coordinate system
Rzi	The distance of mass "i" from the axis "Z" of the new coordinate system
Jx	Moments of inertia of the UAV about the "X" axis
Jy	Moments of inertia of the UAV about the "Y" axis
Jz	Moments of inertia of the UAV about the "Z" axis
Jox	Moments of inertia of the "i" component about the "X" axis of its own coordinate system
Joy	Moments of inertia of the "i" component about the "Y" axis of its own coordinate system
Joz	Moments of inertia of the "i" component about the "Z" axis of its own coordinate system
b	Wing span
ly	Chord, defined as a function of span
λ	Elongation, given by the equation
S	Surface of the main wing
ylo	Distance of the mean aerodynamic chord from the airplane symmetry plane
d	Offset from the perpendicular to the plane of symmetry by the last chord of the trapezoidal part of the wing
Xc	Offset the leading edge from the straight line perpendicular to the plane of symmetry of the analysed wing

H	Distance of the last chord of the analysed wing from determined reference plane
l_{Htu}	Rudder chord, from the axis of rotation to the trailing edge
l_{Htuc}	Horizontal tail chord
τ_H	Stabiliser depth
V	Velocity of fluid flow
l	Aerofoil chord length
v	Kinematic viscosity coefficient of the fluid
Re	Reynolds number
α	Angle of attack
ρ	Fluid density
Cl	Lift force coefficient
Cd	Drag coefficient
Cm	Moment coefficient
yi	Location of part "i" of the analysed wing along the span
Δy_i	Width of part "i" of the analysed wing along the span
Cli	Lift force coefficient of "i" wing crossection
A1	Constants used in the calculations
A2	Constants used in the calculations
A3	Constants used in the calculations
FWz	Wing lift force
FWx	Wing drag force
MW	Wing pitching moment
FTUz	Tail unit lift force
FTUx	Tail unit drag force
MTU	Tail unit pitching moment
Fsz	Elevator lift force
Fsx	Elevator drag force
Ms	Elevator pitching moment
L1	Main wing aerodynamic centre to gravity centre distance along "x" axis
L2	Tail unit aerodynamic centre to gravity centre distance along "x" axis
L3	Elevator aerodynamic centre to gravity centre distance along "x" axis
H1	Main wing aerodynamic centre to gravity centre distance along "z" axis
H2	Tail unit aerodynamic centre to gravity centre distance along "z" axis
H3	Elevator aerodynamic centre to gravity centre distance along "z" axis
μ	Dynamic viscosity
P	Pressure
t	Temperature
MACv	Mean aerodynamic chord for vertical tail unit
MACh	Mean aerodynamic chord for horizontal tail unit